An-Najah National University

Faculty of Graduate Studies

THE EFFECT OF BEAM ECCENTRICITY ON THE LOAD CARRYING CAPACITY OF REINFORCED CONCRETE WIDE BEAM-COLUMN JOINT

By

Suliman Ghazi Omar

Supervisors

Dr. Mahmoud Dwaikat

Dr. Monther Dwaikat

This Thesis is Submitted in Partial Fulfillment of the Requirements for the Degree of Master of Structural Engineering, Faculty of Graduate Studies, An-Najah National University, Nablus - Palestine.

2022

THE EFFECT OF BEAM ECCENTRICITY ON THE LOAD CARRYING CAPACITY OF REINFORCED CONCRETE WIDE-BEAM COLUMN JOINT

By

Suliman Ghazi Omar

This Thesis was Defended Successfully on 28/8/2022 and approved by

Dr. Mahmoud Dwaikat Supervisor	Signature
Dr. Monther Dwaikat Co-Supervisor	Signature
Dr. Rabab AL Louzi External Examiner	Signature
Dr. Monther Diab Internal Examiner	Signature

Dedication

This thesis is dedicated to my parents for their infinite support, as well as to my whole family and friends.

With respect and love

Acknowledgements

I would like to express my sincere gratitude to my supervisor Dr. Mahmoud Dwaikat and Dr. Monther Dwaikat for their helpful gaudiness and efforts. And to Dr, Rabab AL Louzi and Dr. Monther Diab.

Declaration

I, the undersigned, declare that I submitted the thesis entitled:

THE EFFECT OF BEAM ECCENTRICITY ON THE LOAD CARRYING CAPACITY OF REINFORCED CONCRETE WIDE BEAM-COLUMN JOINT

I declare that the work provided in this thesis, unless otherwise referenced, is the researcher's own work, and has not been submitted elsewhere for any other degree or qualification.

Student's Name: Suliman Ghazi Omar

Signature: Sulimans

Date: 28/8/2022

List of Contents

List of Tables

List of Figures

THE EFFECT OF BEAM ECCENTRICITY ON THE LOAD CARRYING CAPACITY OF REINFORCED CONCRETE WIDE BEAM-COLUMN JOINT

By
Suliman Ghazi Omar
Supervisors
Dr. Mahmoud Dwaikat
Dr. Monther Dwaikat

Abstract

Background: The beam-column joints of reinforced concrete (RC) are one of the elements in RC structures that have significant influence on the load transfer path. Buildings use two types of RC joints based on beam width: conventional joints and wide beam-column joints.

Objective: The advantages of the wide and shallow RC beam-column joints in frame system are more economical, easier to build, provide a flexible space and less obstruction. This system is most used in Middle Eastern countries and hence is selected to be the subject of this study. The system consists of a one-way monolithic ribbed slab that is supported by concealed and wide beams. In some cases, the wide beam-column joint has eccentricity due to architectural considerations, where the center of the wide beam does not coincide with the center of the column.

Methodology: The structural behaviour of eccentric wide beam-column joint is not fully understood due to the limited experimental research compared to those of conventional frame structures. This research concentrates on the effect of eccentricity on the load carrying capacity of RC edge wide beam-column joint within moment resisting frame (MRF). Finite Element (FE) analysis using (ABAQUS) is conducted to investigate the moment capacity of RC wide beam-column joint. The model is validated based on available experimental results.

Results: and the results are further used to compare the change in bending moment capacity of the beam with and without eccentricity where the present of eccentricity produce additional torsion on wide beam and therefore reduce the bending moment capacity.

Conclusion: An analytical approach is developed to predict the torsional moment on wide beam and use it to find the bending moment capacity. The proposed approach is derived based on principles of mechanics and equilibrium. The results from the approach are found to be consistent with the FE results.

Keywords: eccentricity, wide beam, edge beam, wide beam column joint, eccentric wide beam-column joint, bending capacity, torsional moment on edge beam.

Chapter One

Introduction

1.1 General

In reinforced concrete moment resisting frames (RCMRFs) two types of reinforced concrete (RC) joints are used according to the width of beam: conventional joint and wide beam-column joint. In conventional joint, the width of a beam does not exceed the width of the column; while the wide beam-column joint, the beam is wider than the column.

Architects generally prefer wide beam-column joints as a gravity load carrying system due to the flexibility they provide in the definition of spaces, and their effectiveness in reducing the formwork. The main disadvantages of RC wide beam-column joints are their low flexural stiffness and poor transmission of bending moments from wide beams to columns. These drawbacks are caused by the fact that portion of the wide beam longitudinal reinforcement steel passes through or is anchored in transverse beams rather than the column core. (Benavent-Climent, 2007 and Gomez-Martinez et al., 2016)

Several studies have been conducted on beam-column joints because of their significance in RC buildings. In case of conventional beam, many parameters have been studied experimentally or numerically (Lee et al., 2009, Alva et al., 2013 and Wong and Kuang, 2014). Moreover, previous researches have demonstrated the effects of beam eccentricity on joint behaviour. (Vollum and Newman 1999, JAMES et al. 2005 and Wong et al. 2019). However, these studies concentrated on the eccentricity of conventional beams. Eccentricity in wide beam-column joints has not been studied experimentally or numerically yet. This study focuses on the effect of wide beam eccentricity on the moment bending capacity of the wide beam.

1.2 Problem statement

Despite the many advantages of the wide beam-column frame system that make it commonly used in the Middle East countries, it has a major drawback in that the bending moments are not transmitted properly from wide beam to column. This drawback is primarily due to the partial passage of wide beam longitudinal steel through or anchorage

in the transverse beams rather than in the column core (Benavent-Climent, 2007 and Gomez-Martinez et al., 2016)

The effect of this drawback increases when the centre of beam does not coincide with the centre of column. This case appears especially at edge and exterior beams because architects use narrower columns to blend within the block walls. These columns section have an aspect ratio between 2 and 4 (A.M. Elsouri and M.H. Harajli, 2015). The designers generally ignore the effect of this eccentricity when using finite element programs to simplify modeling and analysis of the structures. Such choice of neglecting this eccentricity produces unreal results in design of buildings. Moreover, the ACI 352R-02 exclude this case from its recommendation because of the lack of research. So, this study focuses on the effect of eccentricity on the moment capacity in edge wide beam-column joints through modelling a frame that consists of a one-way monolithic ribbed slab that is supported over shallow and wide beams, where beams depth equals to that of the slab as shown in Figure (1.B)/ Appendix (B)

1.3 Research objective and scope

The primary objective of this research is to determine how eccentricity affects the moment carrying capacity of an RC edge wide beam-column joint. To achieve this main goal, the following tasks are performed:

1 Investigate the available literature on the RC wide beam-column connections and the key parameters that influence their behaviour. This is presented in next chapter.
2 Develop a non-linear 3-D finite element model for RC wide beam-column joint. The model includes material and geometric nonlinearities. The commercial ABAQUS FE. oriented software is used to create a generic parametric model of an RC edge wide beam-column joint with and without beam eccentricity. Materials, geometry, and required input data used to develop the model are obtained from the literature. The modelling process and related assumptions are explained in detail in Chapter 2.
3 Calibrate the model by comparing its results with the published experimental outcomes. Sensitivity analysis and parametric studies are carried out in order to identify the significant parameters that influence the moment bending capacity of the wide beam-column joint. This is presented in Chapter 3.

4 Develop an equation for engineering use that predicts the torsion on wide beam-column connection and determine the bending capacity of beam in RC edge wide beam-column joint and compare its results with the results obtained from the F.E. models. This is explained in Chapter 4.

5 The results summary, conclusions and recommendations of future work on the effect of eccentricity on wide beam-column joint are discussed in Chapter 5.

Chapter Two

Literature Review

2.1 Overview

Moment-resisting reinforced concrete frames with wide beams have several benefits over traditional structure framing system. They increase the ceiling height, more economical, easy to construct, reduce reinforcement steel congestion in the joint region to make concrete vibration easier and preferred by interior designers and architects as they are less obstructing and the narrow column allows the columns to be embedded into infill blocks walls, creating more usable space. (Pakzad and Khanmohammadi, 2020). In Middle Eastern countries, the most common reinforced concrete structural system is (RCMRFs), which consists of a one-way ribbed slab supported by shallow wide beams with width larger than column width (Elsouri and Harajli, 2013). Some longitudinal reinforcement bars in the beam are anchored outside the column core in wide beam-column joints. This makes the distribution of stress and load transfer mechanism much more complicated compared to that in conventional beam column joints where the forces of wide beam transmitted to the column cause torsion at the joint region, resulting in increased joint shear stress. (Behnam et al., 2017 and Fadwa et al., 2014). This chapter gives brief information collected from codes, studies and papers, dealing with the behaviour of RC wide beam-column joint.

2.2 Types of joints

According to ACI 352R-02, various types of framed joints exist in typical structures, such as: interior joint, roof interior joint, exterior joint, roof exterior joint, corner joint and roof corner joint as illustrated in Figure (2.B)/ Appendix (B).

Because of differences in internal stresses acting on the joint, each type of these joints exhibits a different type of behavior. As flexural and shear stresses act simultaneously within the joint region in a complex combination, these stresses cause a compressive stress and internal diagonal tensile. If the diagonal stress is high enough, it can cause crushing (in compression) of the concrete or diagonal cracking (in tension) (Siva and Thirugnanam, 2012)

The ACI 352R-02 classifies the joints based on the type of design loads and deformations to two categories:

Category 1: joints used for normal wind and gravity loads. which are designed for strength without the ductility considering.

Category 2: joints used to resist lateral loads such as earthquake and cyclonic winds. which are designed for sustained strength under reversal deformations in the inelastic range.

2.3 Code provisions

ACI 318-19, NZS3101, and Eurocode 8 are codes for structural reinforced concrete design that have provided distinct suggestions on using wide beam-column systems, such as geometric limits, unique anchorage requirements, and special reinforcing details. The recommendations are primarily intended to prevent beams from failing prematurely before flexural yielding by reducing shear lag in the creation of wide beam plastic hinges. The primary design approaches for wide beam-column joints are close to those for conventional beam column joints in various codes of practice, but the additional design requirements shown in Table 2.1 should be followed. Different practice design codes have different criteria for designing wide beam-column joints, as can be observed. ACI 318-19 offers the widest beam width while having the smallest effective joint width.

Table 2.1

Provisions for design of the wide beams in different codes of practice

Design code	**Design approach**	**Additional requirements**		
		Limitation of beam width (b_w)	**Limitation of joint width (b_j)**	**Design of spandrel beam for torsion**
ACI 318-19	Follow the conventional beam-column joints design	min (b_c + 1.5h_c: 3b_c)	b_c	Yes
NZS 3101		min (b_c + 0.5h_c: 2b_c)	min (b_c + 0.5h_c: 2b_c)	No
Eurocode 8		min (b_c + h_b: 2b_c)	min (b_c + 0.5h_c: 2b_c)	No

b_c, h_c and h_b are the column width, column height and beam thickness, respectively

ACI 318-19 and ACI 352R-02 connection design parameters

The following are the five primary design parameters for a wide and conventional beam-column joints addressed by ACI 352R-02 and ACI 318-19:

1- The columns and beams framing flexural strengths into a joint must meet Section 18.7.3 of ACI 318-19 in order to generate flexural hinges in the beams instead of the columns.

$$\sum M_{n,c} \geq 1.2 \sum M_{n,b} \tag{2.4.1}$$

where $\sum M_{n,c}$ and $1.2 \sum M_{n,b}$ are the sum of the columns and beams flexural strengths, measured at the joint face respectively. ACI 318-19 Section 18.6.2 specifies that the maximum width of beam (b_w) should be the lower of $b_c + 1.5h_c$ and $3b_c$ as shown in Figure (3.B)/ Appendix (B). Moreover, ACI 352R-02 requires that at least one-third of wide beam top longitudinal steel reinforcement be anchored inside the core of column.

2- To prohibit the joint from shear failure before beam hinging the joint nominal shear strength (V_n) determined on horizontal plane at the joint should meet.

$$\emptyset V_n \geq V_u \tag{2.4.2}$$

$$V_n = 0.083\gamma\sqrt{f'_c} b_j h_c \tag{2.4.3}$$

$$V_u = A_s f_y - V_{col} \tag{2.4.4}$$

where V_u is the applied shear force, $\emptyset$ represent the factor of strength reduction; γ represent the shear strength factor of joint, whose value is determined by the ACI 352R-02 joint classification as shown in table 2.2, f'_c is compression strength of concrete; b_j is the effective width of the joint which equal to width of the column ($b_j = b_c$) according to ACI; A_s is the top beam reinforcement bars; f_y is the yield strength of beam bars and V_{col}: the column shear in equilibrium.

Table 2.2

Values of $\boldsymbol{\gamma}$ for beam-column connections

Classification	**Connection type**	
	1	2
A- Joints with a continuous column		
A.1- joints effectively confined on all four vertical faces	24	20
A.2- joints effectively confined on three vertical faces or on two opposite vertical faces	20	15
A.3- other cases	15	12
B- Joints with discontinuous column		
B.1- joints effectively confined on all four vertical faces	20	15
B.2- joints effectively confined on three vertical faces or on two opposite vertical faces	15	12
B.3- other cases	12	8

3- Section 18.8.5.1 of ACI 318-19 is used to determine the minimum longitudinal beam bars development length l_{dh} anchored in the joint with standard hooks.

$$l_{dh} = \frac{f_y d_b}{5.4\sqrt{f'_c}} \tag{2.4.5}$$

where d_b is the diameter of beam bars.

Furthermore, ACI 352R-02 suggests that the depth of beam to column reinforcement steel ratio be larger than 20 and $20f_y/420$ in section 4.5.5.

4- For exterior wide beam connections, according to ACI 352R-02 Section 3.3.3, the transverse beam should be designed for full equilibrium torsion from the slab and beam bars and satisfy the section 22.7 of ACI 318-19. Eq. (2.4.6) must be satisfied while designing for torsion:

$$T_u \leq \emptyset T_n, \;\; T_n = \frac{2A_o A_t f_y}{s}\cot\theta \tag{2.4.6}$$

where T_u is the sectional factored torsional moment; T_n: the nominal strength of torsional moment; A_o: the area encloses by the path of shear flow, which can be calculated as $0.85A_{oh}$, where A_{oh} denotes the area bounded by the outer closed transverse torsion reinforcement centreline; The concrete compression diagonals are assumed to have a 45^o angle (θ). Torsion reinforcement spacing in transverse beam should not be greater than

the smaller of 300 mm and $P_h/8$, where P_h: the outer closed transverse torsion reinforcement perimeter of the beam. Moreover, according to ACI 352R-02 hooked bars in beams terminating outside core of column should anchored with close hoop spacing in a confined transverse beam core.

The current ACI 318-19 and ACI 352R-02 design approaches define the factor of strength reduction (∅) as 0.75 for torsion and 0.85 for joint shear strength. The term "design strength" of a member in these codes refers to the nominal strength multiply by a factor of strength reduction that is always less than one (∅< 1.0).

It is noted that ACI 352R-02 suggested areas of research need. Eccentric connections in wide beam-column (where the wide beam center does not coincide with the column center) with beam bars that pass outside core of the column are one of these areas.

2.4 Experimental and numerical studies

Over the last three decades, extensive research on conventional beam column connections has been carried out, and the effect of many parameters influencing joint behaviour has been studied experimentally or numerically. (Lee et al., 2009, Alva et al., 2013 and Wong and Kuang, 2014). However, the beams and columns width are chosen to be the same for ease of construction. Wide beam in RC structures, on the other hand, have become the norm due to structural constraints. As a result, RC wide beam-column connections have attracted the attention of researchers, and some researches have been conducted to better understand their performance. (Dabiri et al., 2019). The following is a summary of studies on wide beam-column joints.

Siah et al. (2003) investigated an interior wide beam-column joint without reinforcement steel in the transverse beams, torsion cracking was observed in the transverse beams of the specimen, preventing the joint from reaching its full capacity. They noticed that some of reinforcement in the beam that extends beyond the column can transfer load to the joint via forming a concrete strut-and-tie mechanism. Hence suggested that moment is transferred from beam to the joint core through two loads paths. The initial path called “inside beam portion” depends on the longitudinal reinforcement of the wide beam anchored directly within core of the column and the portion of the longitudinal reinforcement of the wide beam passing outside the column as shown in Figure (4.B)/

Appendix (B). Strut-and-tie modelling can be used to determine the angle θ. The second path which located at lateral region known as "outside beam portions" where the moment of wide beam is transferred partially through torsion to the column. Moreover, they suggested a detailing strategy depend on debonding of longitudinal bars of wide beam to prevent torsional failure in transverse beam.

Benavent-Climent (2007) studied the behaviour of RC exterior and interior wide beam-column connection with shallow transverse beam having fewer amount of reinforcement torsion. The joint was designed and detailed in accordance with construction practices in the Mediterranean region when seismicity is moderate. He found that the wide beam did not reach their full capacity when compared to the forming a full width plastic hinge in which the moment is transmitted from the wide beam to column through two loads paths as illustrate in Figure (5.B) and (6.B)/ Appendix (B).

The first path "inside beam portion" transfer the moment directly to the column within strut and tie mechanism where the width equal to width of column h_c and portion of the longitudinal bars of wide beams crossing the column core with a x distance on each side, and there must be some transverse steel in the wide beam to act as a tie to form this strut and tie mechanism. Hence if the transverse steel exists, they suggested taking $x=0.25h_c$ or else x=0. In the second path, "outside beam portions" the moment is partially transferred in the transverse beams through torsion. Therefore, they suggest simple approach for predicting the maximum bending moments capacity for wide beam, which is

$$M_{fub,pred} = M_{fubi} + 2 * \min\{M_{fubo}, M_T\} \quad (2.5.1)$$

Where $M_{fub,pred}$: nominal moment design capacity of the wide beam

M_{fubi}: is the transferred moment over the first load path called "inside beam portion."

The term $2 * \min\{M_{fubo}, M_T\}$ refers to the transferred moment over the second loads path by the two "outside beam portions" of wide beam. In Eq (2.5.1), ''min'' denotes the smallest value to be taken between the bending moment capacity of each ''outside beam portion'' M_{fubo} and the capacity of spandrel beam for torsion M_T.

Elsouri and Harajli (2013) tested four exterior beam column specimens that were subjected to quasi-static cyclic loading to explore the seismic performance and the potential of improving the same joint without major changes in the construction practices and design. According to local design and construction practice, two of the joints were designed and detailed for gravity loads. with the difference being the column orientation as shown in Figure (7.B)/ Appendix (B). The other two joints were designed with gravity loads in mind as well, moreover their reinforcement steel detailing was enhanced to meet a portion of the ACI 318-08 recommendations and ASCE 352-02 requirements for seismic-resistant structure. During early lateral drift, the as-built joints developed shear failure in the core of the joint while it was noted that the "earthquake-resistant" joint performed significantly better through avoiding the development of joint shear failure. The earthquake resistant joints had considerably deformations, greater lateral loads, and energy dissipation capacity than the as-built joints. The authors complete their studies on interior wide beam-column joints where the same behaviour occurs. (Elsouri and Harajli, 2015).

Masi et al. (2014) used two identical specimens with different axial loads on the column to investigate the influence of low and high axial loads on the seismic behaviour of wide beam-column joints. The test results highlight that the axial loads value has a significant impact on the ductility behaviour and deformation capacities. The axial load reduced the effects of slippage on the beam bars in the column core and delayed vertical cracking at the interface of the beam column. The results showed that the strength capacity in the two specimens is substantially constant as shown in Figure (8.B)/ Appendix (B).

Fadwa et al. (2014) used quasi-static cyclic loads to compare the behaviour of two interior and exterior RC wide beam-column joints with transverse beam that were also wider than the columns and two interior and exterior conventional beam column joints. The effectiveness of lateral reinforcement for transverse beams in wide beam-column joints in ductile RC frame was investigated. The results of tests show that for wide beams column connection the hysteresis response at the same level of lateral drift display a remarkable improvement compared to that of conventional beam column connection, in contrast conventional beam dissipated more energy than wide beam. However, at the end of the experiment, wide beam-column joint crashed at a larger value of lateral drift than conventional joint as shown in Figure (9.B)/ Appendix (B). Hence, the total dissipated

energy in wide beam-column connection specimen was greater than that in the conventional beam column connections.

Mirzabagheri et al. (2016) compared the behavior of two interior beam column connections with discontinuous columns, one with wide beam and the other with conventional beam, under quasi-static cyclic loading. According to the findings, the energy dissipation capacity of both specimens was nearly equal, and that the conventional beam column connection met its capacity expectations, whereas the wide beam-column connection did not. Furthermore, the wide beam-column connection provided adequate joint shear strength because the joint effective area was bigger than the column section also flexural beams and column cracks were the most common cracks in wide beam-column specimens. As a result, the joint shear requirements for wide beam-column joint may be relaxed.

Behnam et al. (2016) conducted an experimental and numerical investigation to study the impact of the reinforcement presence in transverse beam on the overall behaviour of wide beam-column connections of two exterior RC wide beam-column connections. The specimens have the same dimensions and reinforcement detailing, except for the reinforcement detail in transverse beam. The results from both experimental and numerical investigation indicated that the failure mode in the specimen with reinforcement was ductile with beam flexural hinging followed by joint and transverse beam torsional failure, while it changed to the brittle transverse beam torsional failure in the other specimen. According to the results of the test and numerical analysis, providing both transverse and longitudinal reinforcement within the transverse beam is required for adequate seismic performance. Therefore, it is suggested to design the transverse beam for full equilibrium torsion.

Etemadi and Fallahnezhad (2017) the effect of wide beam geometry on mechanical properties, crack patterns and types, plastic dissipation energy of the joint, and length of the plastic hinge through steel reinforcements was numerically investigated. It is possible to conclude that increasing the width of the wide beam can improve beam resistance to crack type A (caused by tensile stress). However, such an increase can adversely reduce the resistance of the structure against crack types B and C (caused by shear stress). Figure (10.B)/ Appendix (B) shows types and patterns of these cracks. Changing the dimension

of the beam in wide beam-column joint can have a significant influence on the plastic dissipation energy capacity of the structure. Thus, structures with small beam width have higher values of the plastic dissipation energy. Moreover, increasing beam width will reduce the length of plastic hinge.

As shown in Figure (10.B)/ Appendix (B) four types of crack as follow: Crack Type A: which are distributed on the top and bottom surface through the length of beam. Crack Type B: started from the column corner with the approximate angle of 45º. Crack Type C: formed on the outer part of wide beam close to column sides. Narrow flexural cracks developed at the column face, Crack type D.

Behnam et al. (2017) performed reverse cyclic loading tests on four large-scale exterior reinforced concrete beam column connections. They concentrated on the influence of the width of beam to column width ratio and the ratio of joint shear stress on the seismic behaviour of exterior beam column connections. The results indicated that wide beam-column connections with 1 and 1.5 beam width ratios have no significant crack at the joint region where beam plastic hinges can form completely. In contrast, specimens with 2 and 2.5 beam width ratios showed major damage in the core of joint as shown in Figure (11.B)/ Appendix (B). for the transverse beam the torsion failure was also observed in a 2.5 width ratio specimen. Furthermore, Behnam, Kuang, and Samali (2018) used the three-dimensional FEA software ABAQUS to predict the behaviour of these specimens. The element results, including lateral loads-displacement behaviour, patterns of cracks, reinforcement yielding, and the modes of failure, agree well with the test results.

Kuang et al. (2017) and Behnam et al. (2017) created a theoretical formula for beam width limitation for interior and exterior wide beam-column joints respectively. The effective width of wide beam was obtained by utilizing the principle of joint rotational stiffness equivalence and equivalent frame model. The suggested effective width model considers the influence of flexural and torsion at the joint region and can simulate various practical cases. This theoretical formula is explained as follows:

When a horizontal lateral load is applied to the column, the wide beam-column joints rotate, causing the inside portion of transverse beam to bend and twist, resulting in bending of the outside portions. The inside and outside load paths are depicted in Figure (12.B)/ Appendix (B).

The total wide beam-column connection rotational stiffness which shown in Figure (13.B)/ Appendix (B) can be evaluated by

$$K_{total} = K_i + 2K_o \tag{2.5.2}$$

where K_i is the inside portion rotation stiffness and K_o is the rotation stiffness of the overall outside portion, which contains the transverse beam.

By substituting and simplifying the equations, the proposed effective beam width for interior and exterior wide beam-column joint as follows:

$$b_w = b_c + \beta h_c \tag{2.5.3}$$

Where β for interior wide beam-column joint

$$\beta = 0.125 \left[\frac{(\lambda-1)^3 \left(\eta - \frac{0.63 h_b}{h_c}\right)}{\lambda^2} \right]^{0.5} * \left(1 + \left[1 + \frac{16\left(\frac{b_c}{h_c}\right)}{(\lambda-1)^{1.5}\left(\eta - \frac{0.63 h_b}{h_c}\right)^{0.5}} \right]^{0.5} \right) \tag{2.5.4}$$

and β for exterior wide beam =

$$\beta = 0.175 \left[(\lambda - 1)\left(\eta - \frac{0.63 h_b}{h_c}\right) \right]^{0.5} * \left(1 + \left[1 + \frac{11\left(\frac{b_c}{h_c}\right)}{(\lambda-1)\left(\eta - \frac{0.63 h_b}{h_c}\right)^{0.5}} \right]^{0.5} \right) \tag{2.5.5}$$

Where $\lambda = \frac{L}{h_c}$ and $\eta = \frac{b_t}{h_c}$

It is noted that the suggested method provides a good explanation of how design parameters affect beam width restriction, such as beam length, size of transverse beam and column and beam dimensions.

Pakzad and Khanmohammadi (2020) studied the behaviour of RC exterior wide beam-column joints designed in accordance with ACI 352R-02 and ACI 318-14. Four wide beam-column joint specimens were subjected under constant axial and lateral quasi-static cyclic load. The specimens used various transverse beam types, such as wide and conventional beams, as well as three-column geometry (rectangular, square, and circular). Lower energy dissipation and higher displacement ductility were observed in the circular column specimen compared to the square column specimen. The transverse beam type was the most important factor influencing crack patterns and load transfer mechanisms

of longitudinal steel bars of wide beam anchored in transverse beams. During the tests, on the bottom, top and side faces of wide transverse beams, inclined cracks developed extensively.

2.5 Summary

RC frames with wide beams have several benefits over traditional structure framing systems, the most important of which is ease of construction and cost effectiveness. Current codes of practice design wide beam-column joints similar to the conventional beam column joints, but have additional recommendations to prevent wide beam-column joint from premature failure.

To study the behaviour of wide beam-column joint, various investigations have been carried out. The main focus of studying wide beam is some of the longitudinal steel bars of beam are anchored out of the core of column, the wide beam transfer moment to the joint core over two loads baths directly and as torsion as shown in literature review. While the other studies compare the behaviour between conventional beam column joints and wide beam-column joints and study the effect of various parameters to develop the capacity of wide beam-column such as present of transverse beam, reinforcement in transverse beam and confinement of the joint.

It is noted that the previous research was concerned with the concentric wide beam-column joints, where no specific data is available for eccentricity of wide beam-column joints. Moreover, ACI 352R-02 suggested more research. One of these areas is eccentric connections in wide beam-column joint with beam longitudinal bars that passes outside column core where this type is excluded from the code recommendation (add the year). This research focuses on the influence of the beam eccentricity on the bending moment capacity of RC edge wide beam-column joints.

Chapter Three

Finite Element Simulation

3.1 General

Real specimen testing is not always possible due to the cost and time constraints. As a result, finite element analyses are a popular computer-based technique for dealing with a wide variety of boundary problems. It excels modelling by defining the mechanic properties, boundary condition, interfaces between part of model and loads. Moreover, it gives accurate results for deflections, propagation and formation of cracks, and possible RC elements failure mechanisms. As a result, the commercial software ABAQUS is used to develop a 3-D non-linear finite element model of wide beam-column joints.

This chapter illustrates the details of RC wide beam-column joint modelling, which includes; the definition of materials, creation of parts, modelling of interfaces, selection of analysis type, loading setup, boundary conditions and mesh selection.

3.2 Constitutive models

The most difficult part of finite element modelling of concrete structures is the proper constitutive model of concrete in tension, compression. Selected constitutive models of concrete and steel are presented in this section.

3.2.1 Concrete

Various concrete constitutive models have been improved and used in FEA software over years. These models were primarily based on elastic theory, concrete-damage theory, plasticity theory, and coupled elasticity and plasticity theory. Each model's popularity and attractiveness are determined by its degree of practicality, accuracy, and simplicity (Grassl et al., 2013).

In order to simulate concrete in RC members, ABAQUS includes three models: brittle crack, concrete smeared crack, and concrete damaged plasticity (CDP) (ABAQUS User Manual, 2014).

1. **The brittle crack** model is only applicable to linear-elastic material with tensile crack. As a result, it cannot represent real concrete in terms of compression and tension behaviour.

2. In **the smeared crack** model, the cracks forms wherever the stresses in concrete reach beyond the failure surfaces, whether in the area of biaxial tension or the area of combined tension and compression. The presence of crack is determined by how the crack affect material stiffness and stress. The model's main limitations are mesh size dependence, stress locking due to stress distribution across widely open crack, and loading instability at late stage. (Behnam et al., 2017)

3. Due to friction and sliding of the micro-cracks, after loading and unloading permanent strain remain in concrete material. Inelastic deformations and stiffness degradation are associated with the confined concrete failure mechanism in tension and compression. **The CDP model** was created to capture these concrete properties. As a result, in this study, the CDP was used to represent concrete.

The CDP model is based on plastic flow theory and are a continuous, damage model and plasticity-based. The damage in concrete is described by combined scalar damaged elasticity and non-associate multi hardening plasticity in the model. The model suggests two failure mechanism: concrete compressive crushing and tensile cracking (ABAQUS User Manual, 2014). Furthermore, the CDP model is adequate for modeling RC structures subjected to cyclic and static loads for each ABAQUS/Standard and ABAQUS/Explicit.

The main features of CDP models are described as:

1- Decomposition of additive strain rate

For the rate independent model, Eq. 2.1 assumes an additive rate of strain decomposition.

$$\dot{\varepsilon} = \dot{\varepsilon}^{el} + \dot{\varepsilon}^{pl} \tag{3.1}$$

where $\dot{\varepsilon}$ is total rate of strains, $\dot{\varepsilon}^{el}$ is elastic rate of strains, and $\dot{\varepsilon}^{pl}$ is rate of plastic strains.

2- The stress-strain relationship

The stiffness degradation in the CDP model is modeled by specifying the relation between the effective stresses and strains, where stress-strain is based on a basic model that gives plasticity-damage coupling via effective stress and scalar damage, as shown in Eq. 3.2. (Lubliner et al. 1989).

$$\sigma = (1-d)D_0^{el}:\left(\varepsilon - \varepsilon^{pl}\right) = (1-d)\overline{\sigma} : D^{el} = (1-d)D_0^{el} \qquad (3.2)$$

where σ is Cauchy stress; D_0^{el}: the initial (undamaged) elastic stiffness; $D^{el} = (1-d)D_0^{el}$: is the elastic stiffness that has degraded; ε: total strain; ε^{pl}: plastic strain, d is the stiffness damage scalar variable, which can range from zero (undamaged concrete materials) to one (full damage concrete materials). The plastic yield function is expressed in the form of effective stress $\overline{\sigma}$, according to concept of the effective stress.

3- Variables for hardening

Damaged states are considered in compression and tension by assigning two hardening variables, $\tilde{\varepsilon}_c^{pl}$ and $\tilde{\varepsilon}_t^{pl}$ which refer to equivalent plastic strains in compression and tension, respectively. Increasing the values of hardening variables represents micro-cracking in concrete (Najafgholipour et al., 2017).

4- Yield criterion

The yield surface function depends on the model suggested by Lubliner et al. (1989) model with adjustments by Lee and Fenves (1998) as shown in Figure 3.1. The yield functions take the effective stress space from following

$$F = \frac{1}{1-\alpha}\left(\overline{q} - 3\alpha\overline{p} + \beta\left(\tilde{\varepsilon}^{pl}\right)\langle\overline{\sigma}_{max}\rangle - \gamma\langle\overline{\sigma}_{max}\rangle\right) - \overline{\sigma}_c\left(\tilde{\varepsilon}_c^{pl}\right) \leq 0 \qquad (3.3)$$

where $\overline{p}$: the effective pressure of hydrostatic; $\overline{q}$: the equivalent stress of von Mises; $\langle x\rangle = 0.5(x + |x|)$: the Macauley bracket; $\overline{\sigma}_{max}$: the tensor's algebraically greatest eigenvalue, $\overline{\sigma}_c, \alpha, \beta, \gamma$ are dimensionless constants that should be defined in Eqs. 3.4– 3.6, respectively

$$\alpha = \frac{(\sigma_{b0}/\sigma_{co})-1}{2(\sigma_{b0}/\sigma_{co})-1}; 0 \leq \alpha \leq 0.5 \qquad (3.4)$$

$$\beta\left(\tilde{\varepsilon}^{pl}\right) = \frac{\bar{\sigma}_c\left(\tilde{\varepsilon}_c^{pl}\right)}{\bar{\sigma}_t\left(\tilde{\varepsilon}_t^{pl}\right)}(1-\alpha) - (1+\alpha) \tag{3.5}$$

$$\gamma = \frac{3(1-K_c)}{2K_c-1} \tag{3.6}$$

where $(\sigma_{b0}/\sigma_{co})$ is the biaxial compressive yield stress to yield stress ratio of uniaxial compressive that has an effect on the yield surface in a plane stress condition. Typical experiment value of $(\sigma_{b0}/\sigma_{co})$ ratio range from 1.10 to 1.16, resulting in value of α between 0.08 and 0.12; $\bar{\sigma}_c\left(\tilde{\varepsilon}_c^{pl}\right)$ and $\bar{\sigma}_t\left(\tilde{\varepsilon}_t^{pl}\right)$ are compression and tension effective cohesion stress, respectively. The factor γ can be calculated by comparing the yield conditions along the compressive and tensile meridians where this factor only appears for triaxial compression stress states. As shown in Figure (14.B)/ Appendix (B) the coefficient K_c determines the deviatoric cross-section shape.

5- Flow rule

The flow rule connects the surface yield and stress-strain of concrete relationships. For the flow potential function, G, the CDP models suggest a non-associated Drucker-Prager hyperbolic function, as given by Eq. 3.7. (ABAQUS User Manual, 2014).

$$G = \sqrt{(\xi\sigma_{t0}\tan\psi)^2 + \tilde{q}^2} - \tilde{p}\tan\psi \tag{3.7}$$

where ξ: the eccentricity of flow; ψ: the dilation angle and σ_{t0}: the uniaxial tensile stress.

6- Visco-plastic regularisation

Materials with stiffness reduction and softening behaviour may cause convergence issues. To overcome some of these convergence issues, the constitutive concrete material model with visco-plastic regularisation was used. According to the generalisations of the Devaut-Lions strategy, the CDP models can be regularised using visco-plastic regularisation. To derive the plastic strain tensor in the CDP models with viscous parameters, an extra viscosity parameter called as the relaxation time (μ) must be defined (Lubarda et al., 1994).

In general, two series of uniaxial data, two series of damage parameters, and five extra parameters should be defined in order to utilize the CDP models in ABAQUS:

1- The concrete uniaxial compressive stress-strain relationship:

$$\varepsilon_0 = 2f_c'/E_c \tag{3.8}$$

Figure (15.B)/ Appendix (B) depicts the three phases of the concrete stress-strain behaviour under compression. The equations for the assuming compression stress-strain curve are shown in Eq. 3.9. which denotes the linear-elastic branch, where ε_c is a variable that range from zero to a $0.4f'_c/E_c$, and E_c is elasticity modulus at initial stage. The linear branch terminates at $0.4f'_c$ stress value. In the descending branch, Eq. 3.10 shows the second branch up to 0.0035 strain value. At peak stress, the corresponding strain value is defined as $\varepsilon_0 = 2f_c'/E_c$, η_c is the material constant. For Eqs. 3.9 and 3.10 at the strain level of $\varepsilon_c = 0.4f_c'/E_c$, the stress and strain are compatible which gives the value of η_c. The third and descending branch is described by Eq 3.11; where λ_c is concrete constant crushing energy. The value of λ_c can be calculated at the strain level of $\varepsilon_c = 0.0035$ where the stress and strain are compatible, for Eqs. 3.10 and 3.11. To prevent any numerical problems, the concrete ultimate strain ε_u was specified to a large value of 0.035. (Jankowiak and Lodygowski, 2005).

$$\sigma_{c,1} = E_c\varepsilon_c, \varepsilon_c \leq 0.4f_c'/E_c \tag{3.9}$$

$$\sigma_{c,2} = \frac{\eta_c\frac{\varepsilon_c}{\varepsilon_0}-\left(\frac{\varepsilon_c}{\varepsilon_0}\right)^2}{1+(\eta_c-2)\frac{\varepsilon_c}{\varepsilon_0}} f_c', \frac{0.4f_c'}{E_c} \leq \varepsilon_c \leq 0.0035 \tag{3.10}$$

$$\sigma_{c,3} = \left(\frac{2+\lambda_c f_c'\varepsilon_0}{2f_c'} - \lambda_c\varepsilon_0 + \frac{\lambda_c\varepsilon_c^2}{2\varepsilon_0}\right)^{-1}, 0.0035 \leq \varepsilon_c \leq 0.03 \tag{3.11}$$

(ABAQUS) requires data in the form of inelastic strain, $\tilde{\varepsilon}_c^{in}$ which corresponding to the undamaged material as the total strains minus the elastic strains. Inelastic strain values are automatically converted to plastic strain values by ABAQUS through using $\tilde{\varepsilon}_c^{in} = \varepsilon_c - \sigma_c/E_c$, as shown in Figure 3.2. (ABAQUS User Manual, 2014).

2- Uniaxial concrete tensile stress-crack width relationship

Figure (16.B)/ Appendix (B) represents the stress crack displacement response of concrete in tension, where f_t denotes the max tensile strength and G_f is the fracture energy of concrete, which denotes the region inside the tensile stress-crack diagram. The use of stress crack width displacement depending on fracture energy can assist to improve numerical convergence and avoid mesh-sensitivity. The concrete fracture energy G_f (N/mm) for standard concrete can be determined from Eq. 3.12 (Behnam et al., 2018).

$$G_f = G_{f0}\left(\frac{f'_c+8}{f_{cmo}}\right)^{0.7} \tag{3.12}$$

Where G_{f0}: the base fracture energy that based on max size of aggregate and f_{cmo} = 10 MPa.

3- Tension and compression damage parameters

According to Figure (17.B)/ Appendix (B), damage parameters were included into the CPD models in compression and tension. The concrete damages were expected to occur only in the softening area for both compression and tension. In compression, the damage values are shown after the maximum load associated with the strain value, ε_0. It was also assumed that when the strength drops to 80%, the damage parameter will reach a value of 0.8, and the max value for the damage parameter was set at 0.95, corresponding to a 95% decrease in stiffness. (Genikomsou and Polak, 2015).

4- Additional parameter

The values for the additional five parameters are used to conclude the surface yield.(σ_{b0}/σ_{c0} and K_c), the potential flow (ξ and ψ) and the viscoplastic regularization (μ) where the default values are assumed as shown in Table 3.1 (ABAQUS User Manual, 2014).

Table 3.1

CDP input parameter

Parameter	σ_{b0}/σ_{co}	K_c	ψ	ξ	μ
Value	1.16	0.667	35	0.1	0

3.2.2 Steel

For reinforcement steel bars, typical stress-strain diagrams used in RC structure are obtained from monotonic tension test on steel bars as represents in Figure (18.B)/ Appendix (B). The curves indicate a linear elastic part at initial stage, a yield area in which strain rises with minimal or little stress increase, a strain-hardening region where the stress rises with strain again, and final stage when fracture occurs the stress drops off (Park and Paulay, 1975).

The elastic modulus of reinforcing steel is defined by the slope of the linear elastic part of the curve, which is commonly taken to be 200GPa. The stress at the yield region is known as the yield strength, and it is a critical feature of reinforcement steel.

In design, the stress-strain curve shape should be idealized. Generally, the curve is idealized as two straight lines as shown in Figure (19.B)/ Appendix (B). The ACI-318 code assumes this stress-strain curve for reinforcement steel while neglecting the higher yield point and the stress increase due to strain hardening, which is known as the elastic perfectly plastic curve.

The reinforcement's uniaxial stress-strain data was modeled in ABAQUS as elastic perfectly plastic with Poisson's ratio (v), Young's modulus (Es), and yield strength (f_y) of 0.3, 200GPa and 420MPa, respectively.

3.3 Modelling of interfaces

Modelling beam-column joints requires interface modelling in RC elements. ABAQUS has several options for modeling concrete and reinforcement interfaces. These interfaces are called constraints such as tie constraint between parts of beam and column or between loading plate and beam used to connect two surfaces so that there is no relative motion between them. The coupling constraint restricts the motion of a surface to the motion of a single point. This constraint is used when defining support or boundary condition. Also, to define the contact between reinforcement steel and concrete the embedded region constraint is used. Perfect bond surfaces with no slip of the reinforcement is assumed in concrete.

3.4 Analysis type, boundary conditions and loading.

In order to avoid the convergence problem, a dynamic analysis in ABAQUS/Explicit was performed to obtain the whole behaviour of the model, the loads are applied in very large time step to converge to the static solution. To evaluate whether the results from an ABAQUS/Explicit simulation reflect a quasi-static solution the kinetic energy of the deforming material should not exceed a small fraction of its internal energy throughout the majority of a quasi-static analysis where the small fraction typically means 1–5%. In ABAQUS/Explicit, these models were solved using a full Newton solver with default matrix storage. An automated incremental with a short time step size and a high maximum number of increments was utilized to improve the convergence rate.

To reduce running time, part of the full model is modelled using symmetric boundary conditions at X and Z directions where in these directions the x-translation and the z-translation is restricted, respectively. Figure 3.1 shows full model and reduced model. Pinned support was used at inflection point of column located at upper and lower half of column. The load was applied as a uniformly distributed load on slab and beam. Also, axial load is applied on columns.

Figure. 3.1

Shows types of model

Figure. 3.1.a

Full model

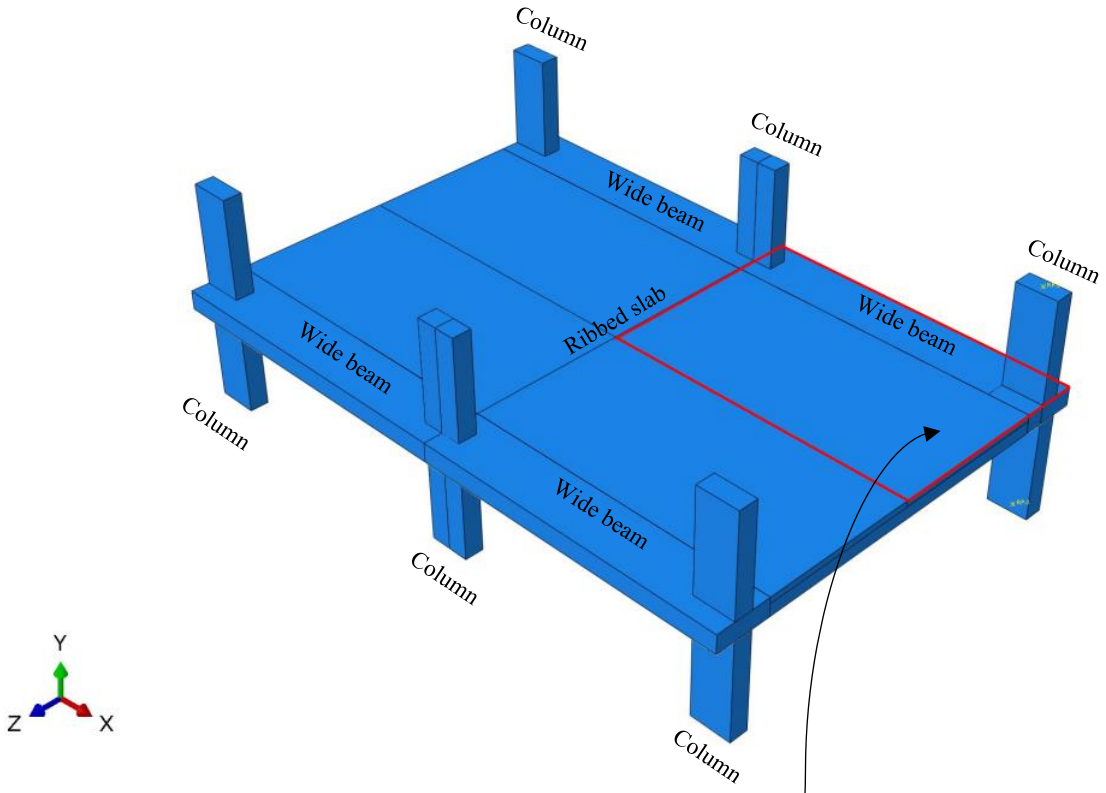

Figure. 3.1.b

Reduced model

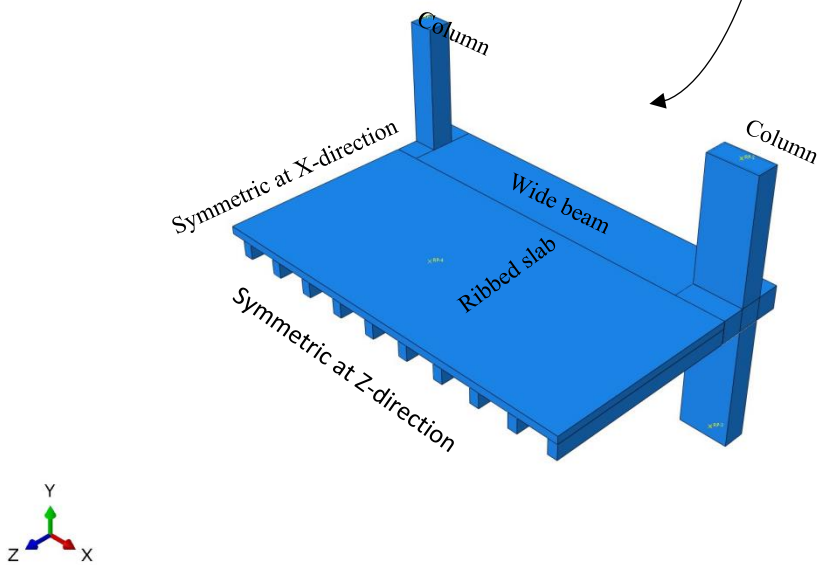

3.5 Mesh type

In this finite element model, global mesh was used instead of meshing part by part. To model a solid element (concrete), a linear eight-nodded brick element (C3D8R) is used. The reduced integration method is used to avoid the result of locking behaviour from the first-order elements and the enhanced hourglass control, the 2-node linear 3D truss element (T3D2) is used to model the longitudinal reinforcing bars and stirrups to reduce the computational running time expect the longitudinal bars in wide beam while it is modelled as 2-node linear beam in space element (B31). This is to facilities computations the moment over the cross section. Figure (20.B)/ Appendix (B) shows the three types of elements with degree of freedom for translation (U_n) and rotation (θ_n).

Chapter Four

Parametric and Analytical Investigations

4.1 Overview

Before starting the parametric study, the finite element model is validated using experimental tests available in literature. The experimental work of Fadwa et al. (2014) is selected for verification. After that a parametric study is carried out to explore the bending moment capacity of RC edge wide beam-column joints under different parameters.

4.2 Sensitivity Study and Validation

A sensitivity study was carried out to validate the effect of mesh size, materials and boundary conditions from finite element model on the results obtained and validated by experimental study of Fadwa et al. (2014).

The details of the test specimens and materials properties used for verifying numerical models are shown in Figures (21.B)/ Appendix (B) and Table 4.1.

Table 4.1

Measured material properties

concrete			
f_c' (MPa)	f_{ct}(MPa)	E_c(MPa)	
28.50	2.86	19940	
Reinforcement steel diameter	f_{sy}(MPa)	E_s(MPa)	ε_{sy}
ϕ8	346.84	195733	0.00177
ϕ14	345.38	202405	0.00171
ϕ16	497.64	201738	0.00247
ϕ18	494.62	224503	0.00220
ϕ20	436.10	198108	0.00220

The material properties and boundary conditions of numerical models are assumed to be the same as those of experimental models. For verification, the force–displacement curve for the column's top surface was used. The mesh size in FE Analysis can have a significant impact on the results. The finer the mesh size, in general, the more precise the solution. This is because it improves the distributions of strain and stress precision in structure. A

balance between the computation time and the desired accuracy is selected. Mesh sensitivity analysis is commonly performed in finite element solutions by starting with a coarse mesh and tracking the convergence of one of the variables as the mesh is optimized until an appropriate mesh size is attained. Concrete is the material most sensitive to mesh size in the current model due to high nonlinearity in its behaviour due to cracking and stiffness degradation. The mesh size effect is investigated in this study using three sizes: 60 mm, 50 mm, and 40mm. Figure 4.1.a illustrates the numerical model force–displacement curves and the envelope curve of the force–displacement hysteresis curve in experimental study. It can be shown in Figure 4.1.a that the mesh size of 40 mm and 50 mm gave almost the same result when compare to the other mesh; so, the mesh size of the rest of models is considered 50 mm to reduce computation time. Moreover, to validate the explicit dynamic analysis result the result are compared to those from with static analysis as shown in Figure 4.1.b. This figure illustrates that the dynamic and static analysis result is almost the same.

Figure. 4.1

Validation result

Figure. 4.1.a

Comparison between the experimental test result and different mesh sizes

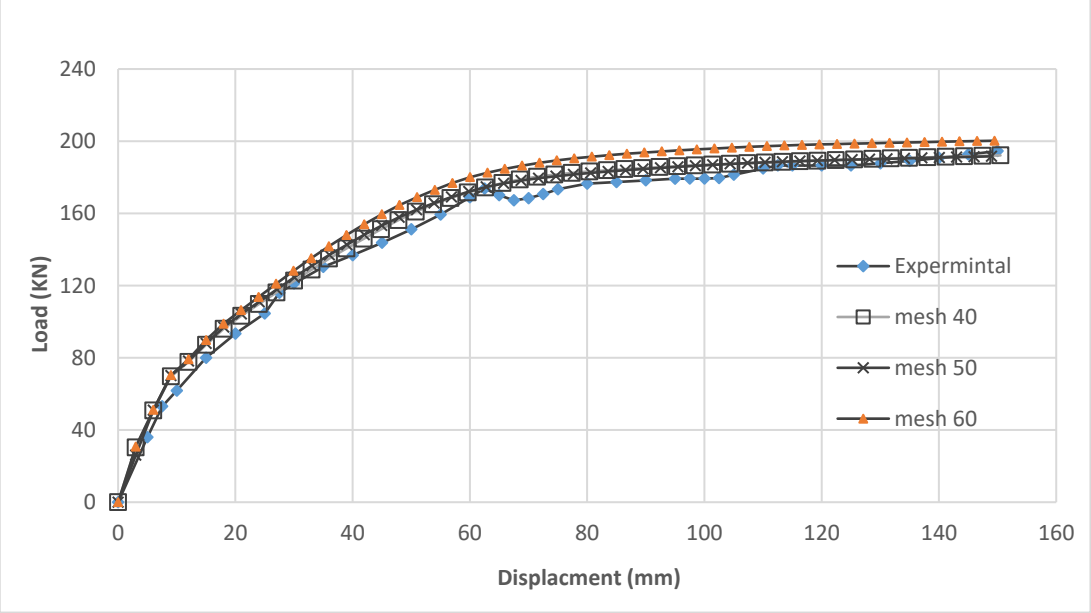

Figure. 4.1.b

Comparison between dynamic and static analysis result

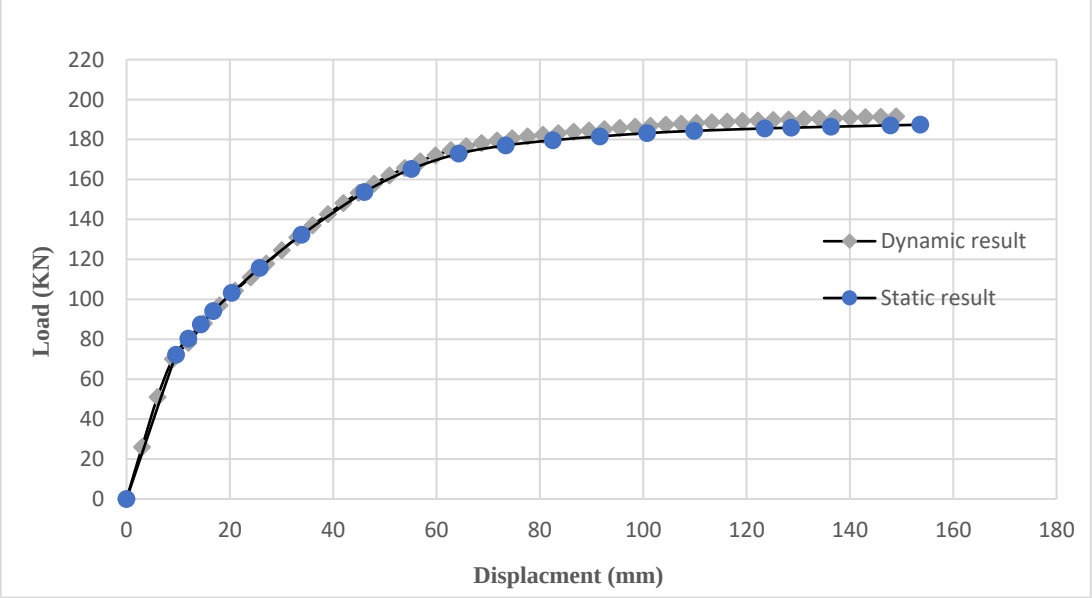

4.3 Parametric study

4.3.1 General

Parametric study is carried out to explore the moment capacity of edge RC wide beam-column connection. Due to time and computational limitations, this study focuses on four main parameters: eccentricity ratio of wide beam (ER), beam width (b_w), slab width (l_s) and absence and presence of transverse beam (TB). The comparison is made based on the influence of these parameters on the moment capacity of RC edge wide beam-column connection.

4.3.2 Parameter range

Total of 54 nonlinear simulations have been conducted on RC edge wide beam-column joint with and without eccentricity. The parameters are varied according to Table (1.A)/ Appendix (A). The beam width is assumed to vary as 900 mm, 750mm and 600mm. The beam width to column width is taken to be equal and less than maximum wide beam width according to ACI 318 ($b_w \leq 3b_c$) and is varied as 3, 2.5 and 2. Eccentricity ratio (ER) which means the offset distance of centerline of wide beam from center of column (E) to half of wide beam width (b_w) minus column width (b_c) as shown in Equation 4.1.

$$ER = \frac{2*E}{(b_w - b_c)} \tag{4.3.1}$$

Where the value of eccentricity ratio is set to be 0, 0.5 and 1 to include the state of wide beam with and without eccentricity. For slab width (l_s) also 3 values are taken which are 4m, 5m and 6m to simulate the common slab width. The last parameter is absence and presence of transverse beam where the reinforcement of this transverse beam is set to be minimum according to ACI 318 code. Figure (22.B)/ Appendix (B) show the generic model with its boundary condition. However, constant properties and dimensions of wide beam-column joint and reinforcement detailed are summarized in Table 4.2 and Figure 4.2 respectively.

To simulate the service axial loads, a five story is assumed and analysis to generate the value of axial loads as real structure, a compressive force of 1100 kN is applied on edge column and 550 kN is applied on exterior column ($0.23\,A_g f'_c$) where A_g: the column gross sectional area and f'_c: the concrete compression strength.

Each simulation is given a representative name. Generally, the first symbol denotes the wide beam width, while the second symbol denotes the eccentricity ratio, the third symbol denotes the slab width; the final symbol denotes the absence and presence of transverse beam. For instance, simulation (B900-ER0-S4-No TB) means first wide beam width (900mm) with zero eccentricity ratio and slab width (4m) without transverse beam. Another example is simulation (B750-ER1-S6-TB) means 750 mm wide beam width with eccentricity ratio (1) and (6m) slab width with transverse beam.

Table 4.2

Constant dimensions of wide beam-column joint

Dimension name	**Value**
Column width	300 mm
Column depth	650 mm
Column height	3200 mm
Beam depth	300 mm
Beam length	5050 mm
Yield strength of steel (f_y)	420MPa
Compression strength of concrete (f'_c)	24MPa

Figure. 4.2

Dimensions and reinforcement details of models

Figure. 4.2.a

Beam-slab section without transverse beam

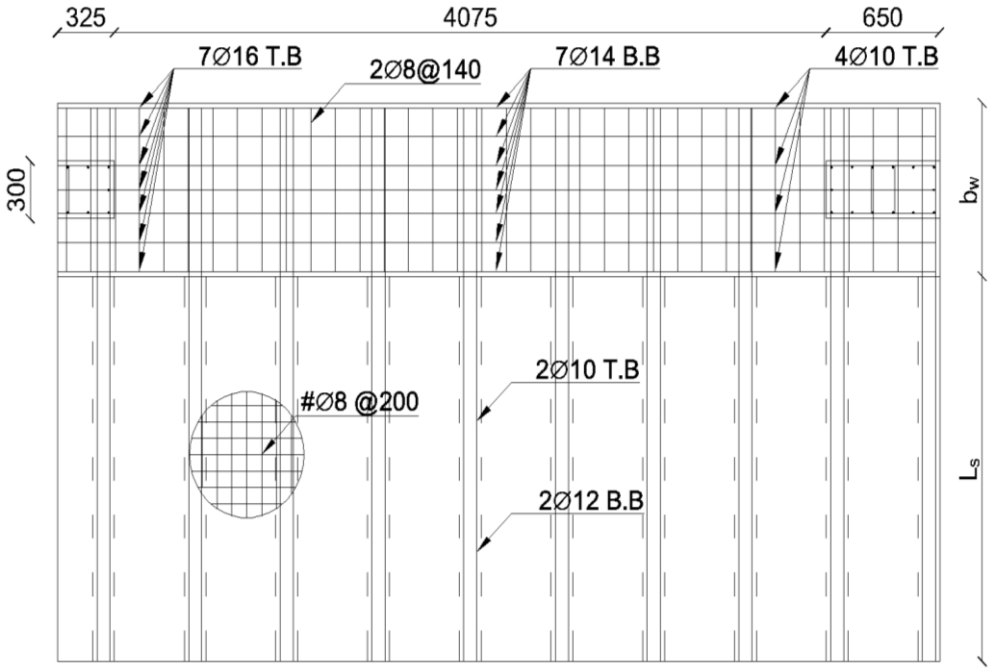

Figure. 4.2.b

Beam-slab section with transverse beam

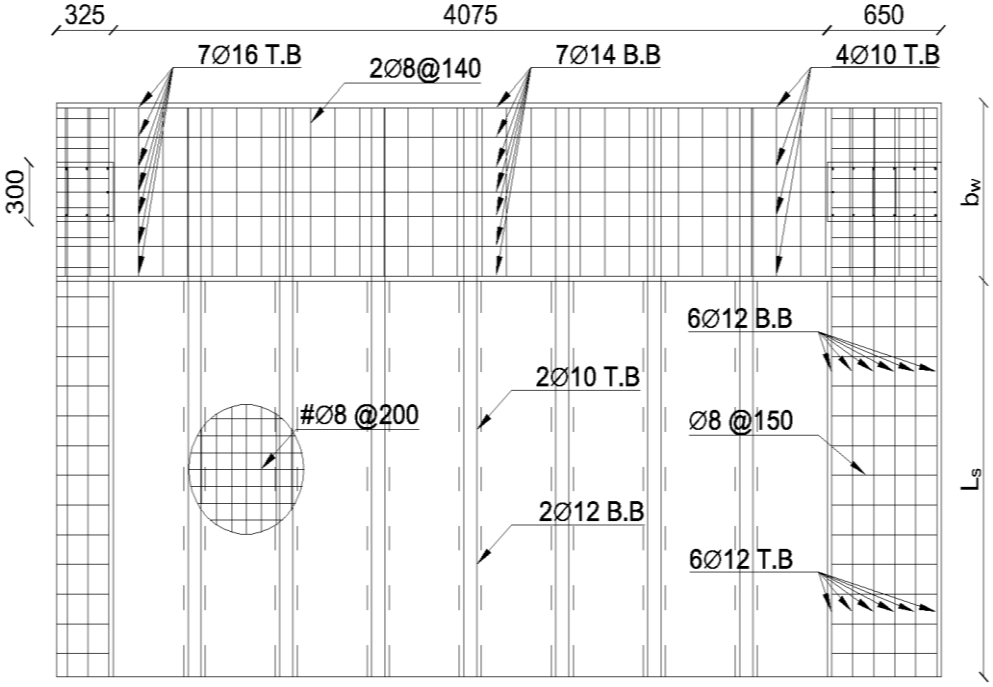

Figure. 4.2.c

Beam section

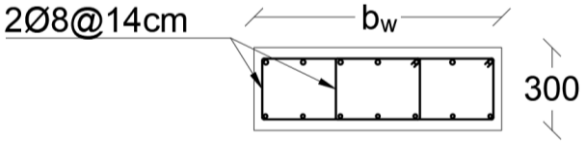

Figure. 4.2.d

Beam-column section

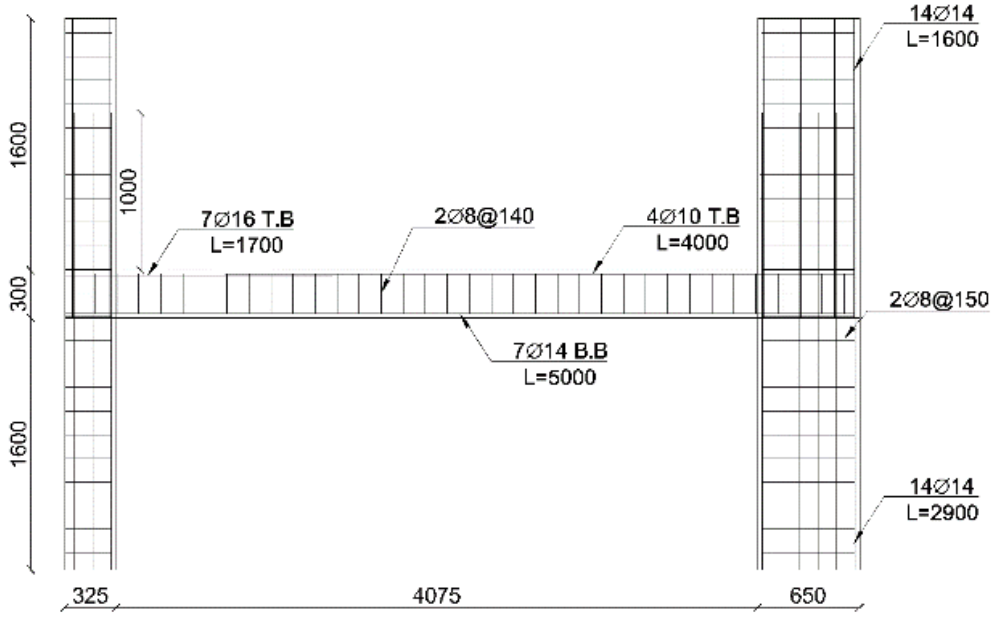

Figure. 4.2.e

Slab section

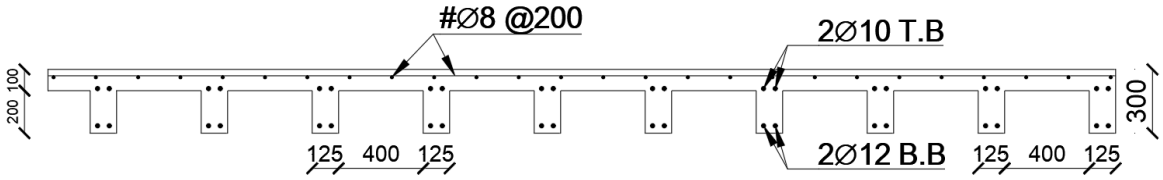

4.4 Result and discussion

4.4.1 General

This section presents the main findings of all developed models. Moment-deflection curves for all cases are shown and discussed, and are used to estimate the moment capacity of beam. All values are used to produce design guidelines through simple

practical equations to determine the beam's moment capacity. The results of the 54 simulations are given in the following section.

3.4.2 Behaviour

Figure 4.3 shown the general shape of deflection for all model. In figure 4.4a display the deflection shape at early stage of loads where the shape of deflection for models be as usual without effect of torsion. Then when the loads increase the effect of torsion will appear and causing a change in deflection shape as shown in figure 4.4b and 4.4c. Moreover, in figure 4.4 shows the cracks pattern at failure using tension damage parameters for different value of eccentricity. This shape of cracks demonstrates the presence of torsion on wide beam.

Figure 4.3

General deflection shape of models

Figure 4.3.a

Deflection shape at early stage

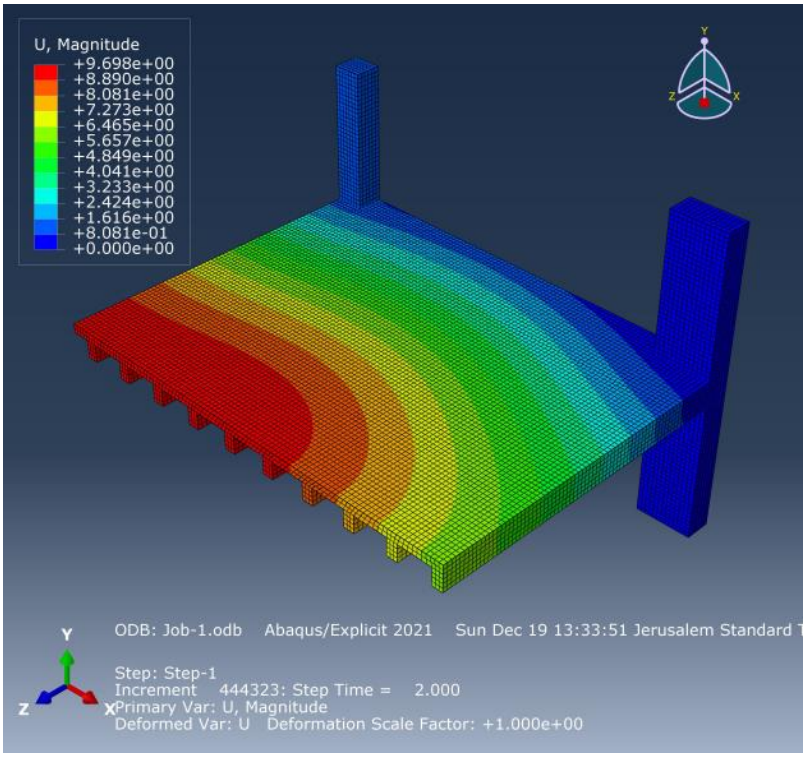

.

Figure 4.3.b

Deflection shape at middle stage

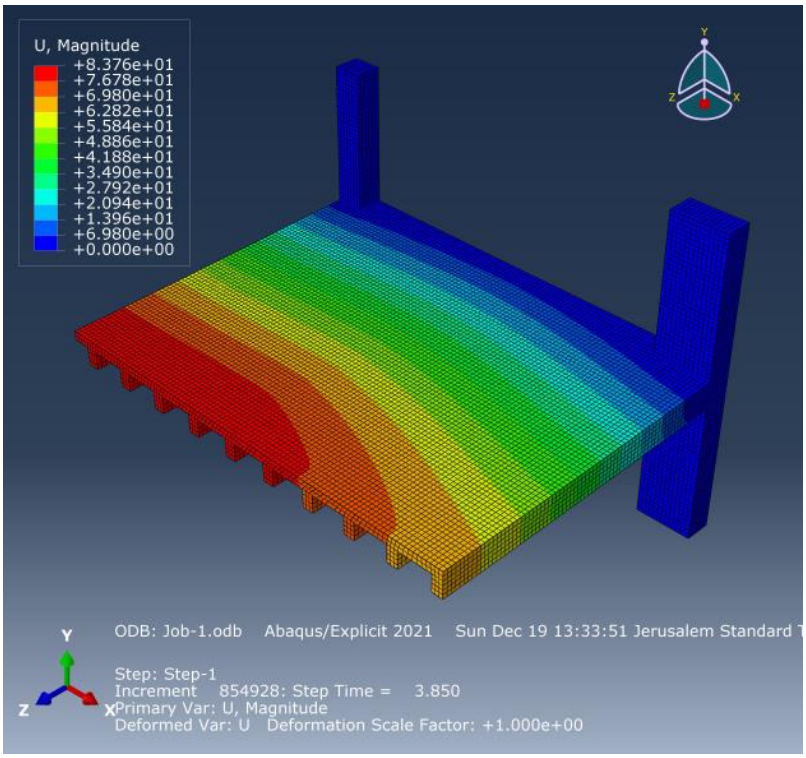

Figure 4.3.c

Deflection shape at final stage

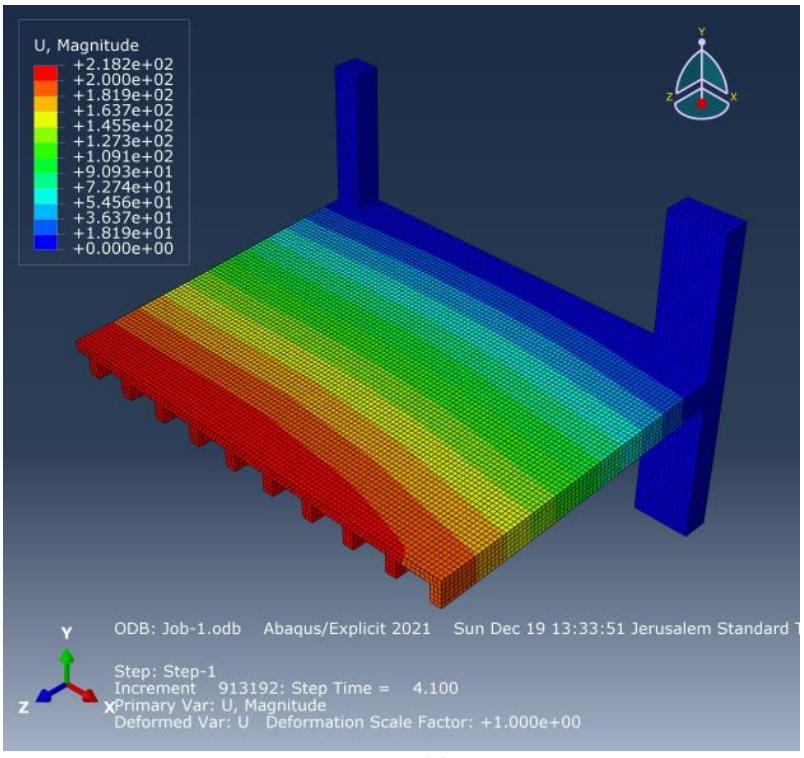

(c)

Figure. 4.4

Tension damage of models

Figure. 4.4.a

Tension damage for 0-eccentricty ratio

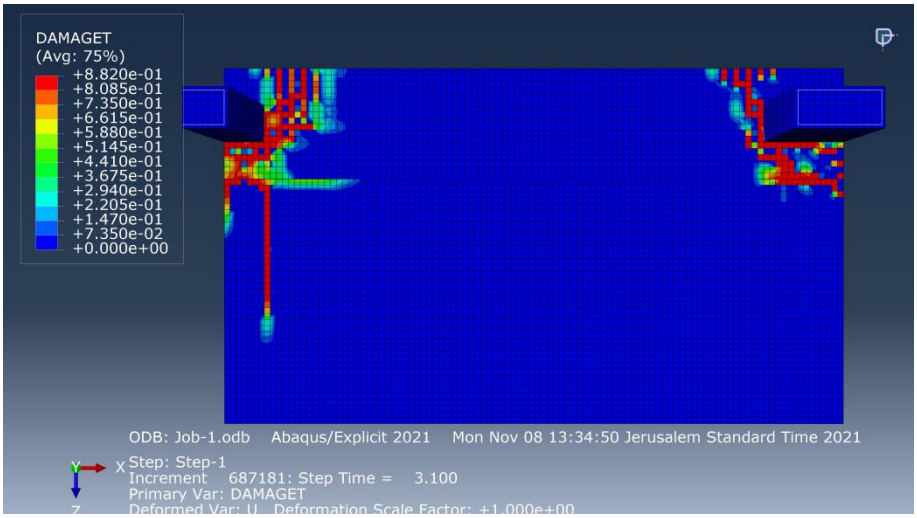

Figure. 4.4.b

Tension damage for 0.5-eccentricty ratio

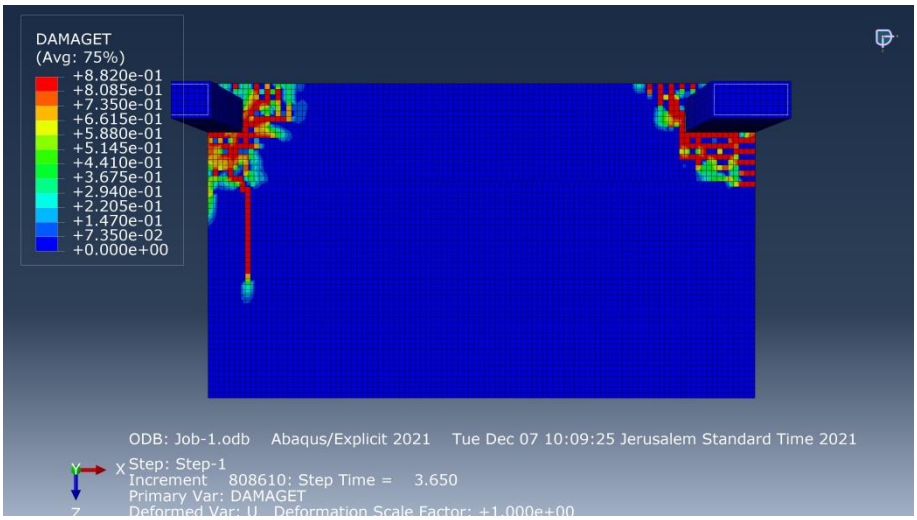

Figure. 4.4.c

Tension damage for 1-eccentricty ratio

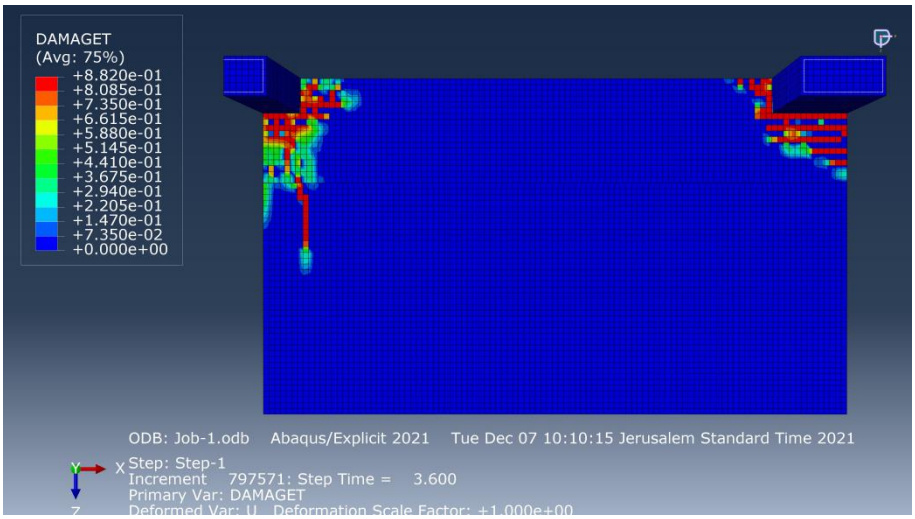

3.4.3 Moment-deflection curves

Moment-deflection curves of edge beams are generated for all models. The moment is taken at the interior column face and deflection is taken at centre of the slab to make the curve visible. Then the peak point of each curve represents the bending capacity of wide beam. In figure 4.5 shows the moment-deflection curves for beam width 900mm. The other curve for beam width 750mm and 600mm shown in Figure (23.B)/ Appendix (B).

Figure. 4.5

Moment-deflection curves for all models

Figure. 4.5.a

Beam width 900mm and slab width 4m without transverse beam

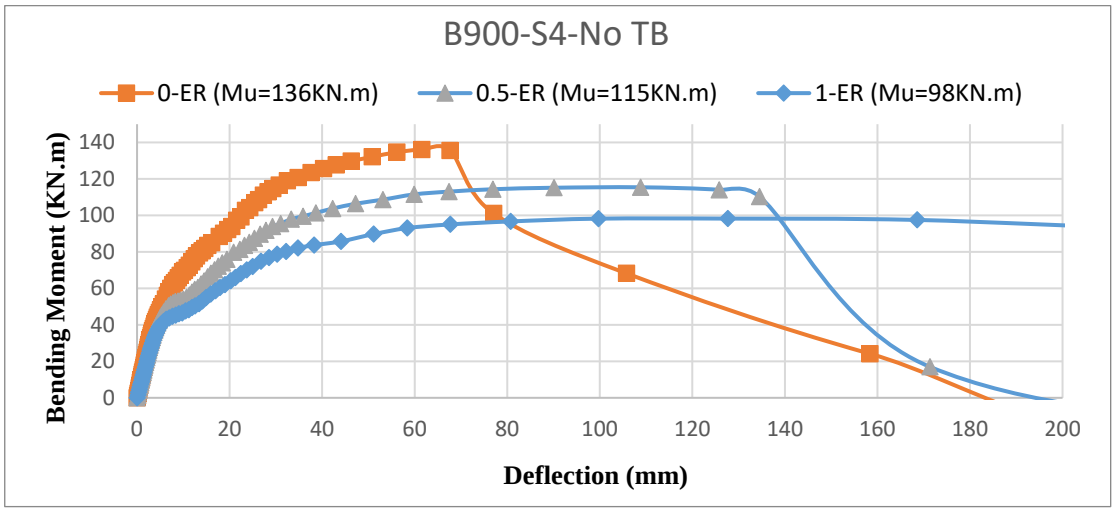

Figure. 4.5.b

Beam width 900mm and slab width 5m without transverse beam

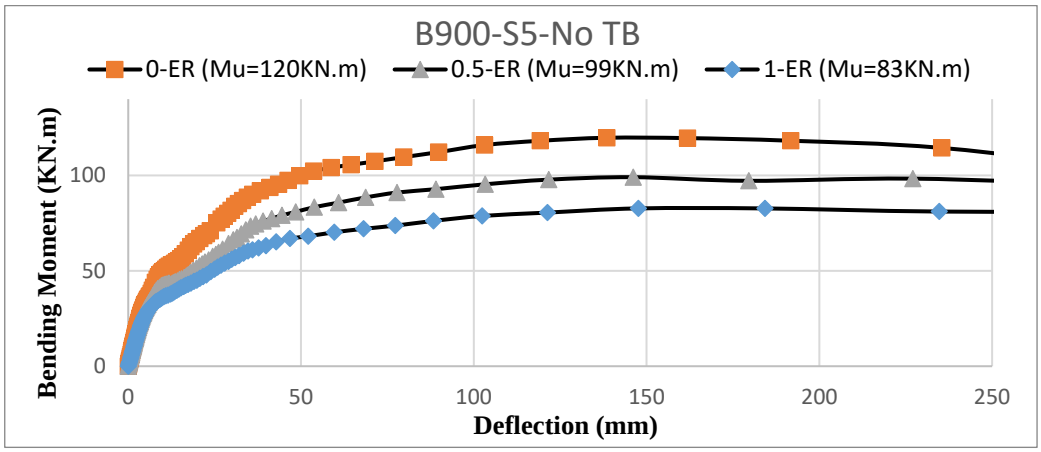

Figure. 4.5.c

Beam width 900mm and slab width 6m without transverse beam

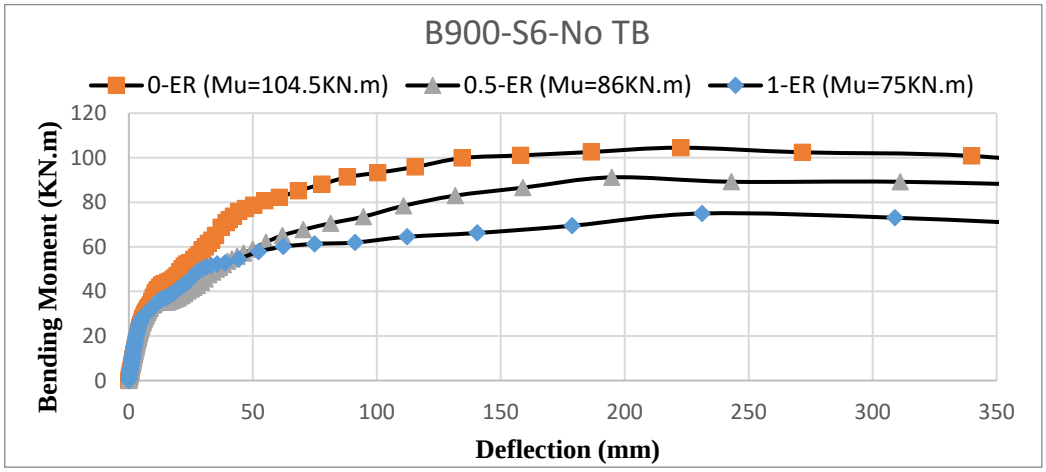

Figure. 4.5.d

Beam width 900mm and slab width 4m with transverse beam

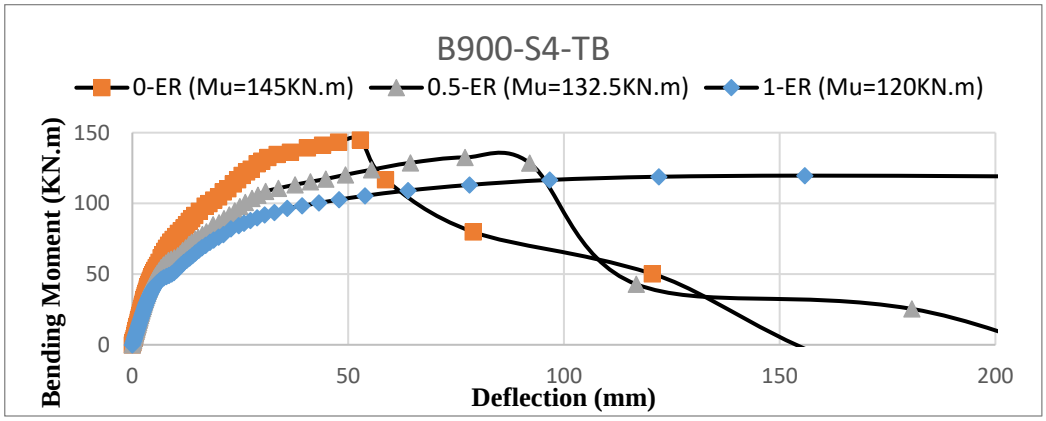

Figure. 4.5.e

Beam width 900mm and slab width 5m without transverse beam

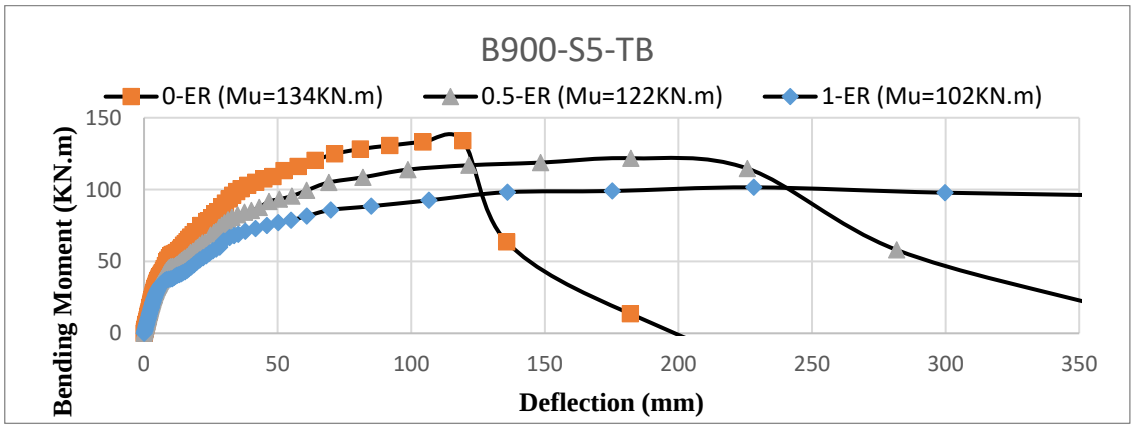

Figure. 4.5.f

Beam width 900mm and slab width 6m without transverse beam

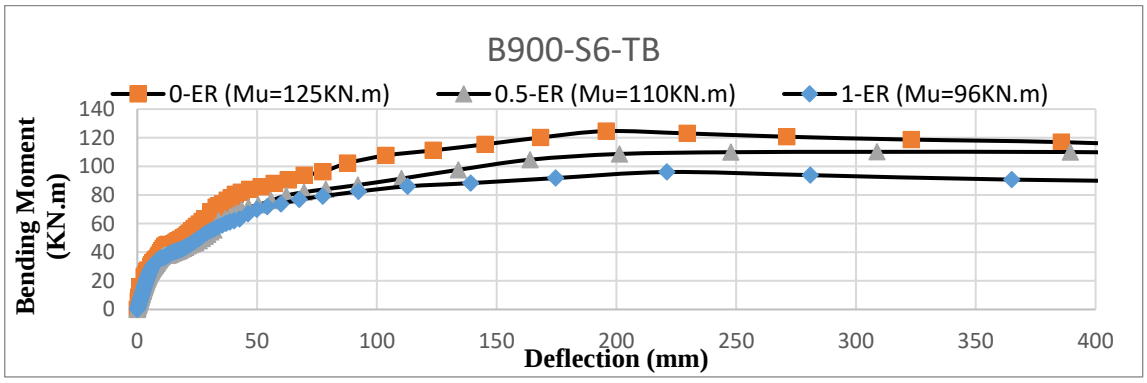

These curves are used to determine the moment capacity of the beam in each case which is considered as the peak of the curve.

4.4.3 Effect of eccentricity

The maximum bending moment for each case without transverse beam are given in Figure 4.6.a which shows the effect of eccentricity on moment capacity with beam width equals 900mm, 750mm and 600mm, respectively. The results indicate that when the eccentricity increases, the bending capacity decrease. This is because the eccentricity causes additional torsion on a beam in addition the torsion from the slab. This increases the stress in the longitudinal reinforcement due to torsion which reduces the bending stress and thus the bending capacity of the beam. The same behaviour is noticed for models with transverse beam as shown in Figures 4.6.b.

Figure. 4.6

Effect of eccentricity on bending moment

Figure. 4.6.a

Effect of eccentricity on bending moment for beam width 900 without transverse beam

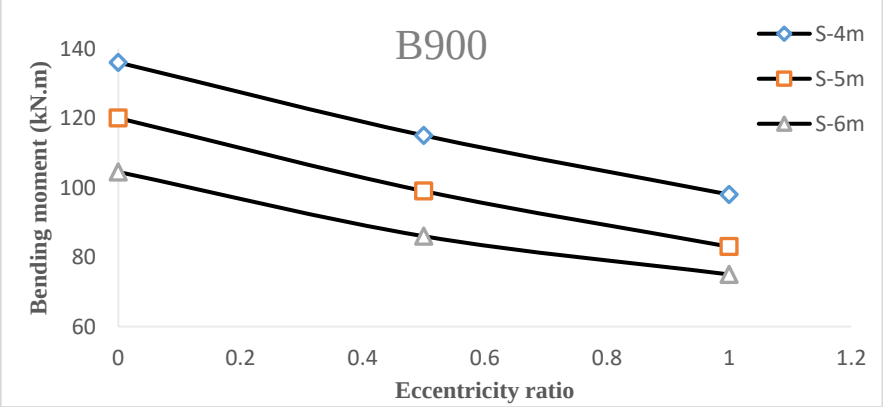

Figure. 4.6.b

Effect of eccentricity on bending moment for beam width 750 without transverse beam

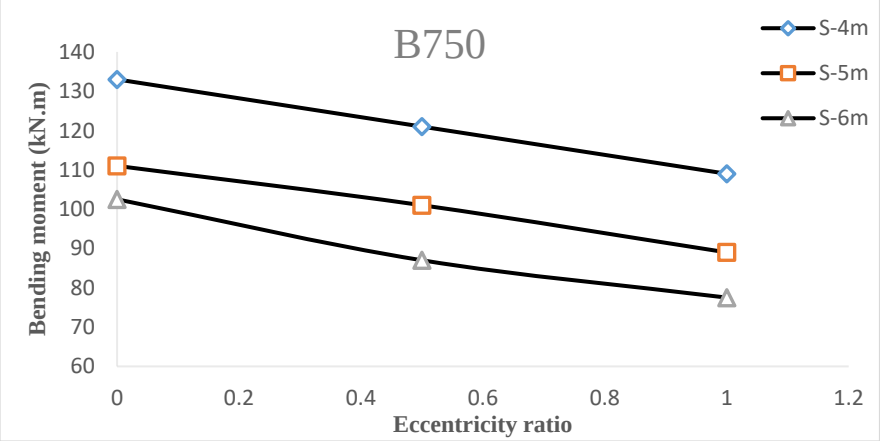

Figure. 4.6.c

Effect of eccentricity on bending moment for beam width 600 without transverse beam

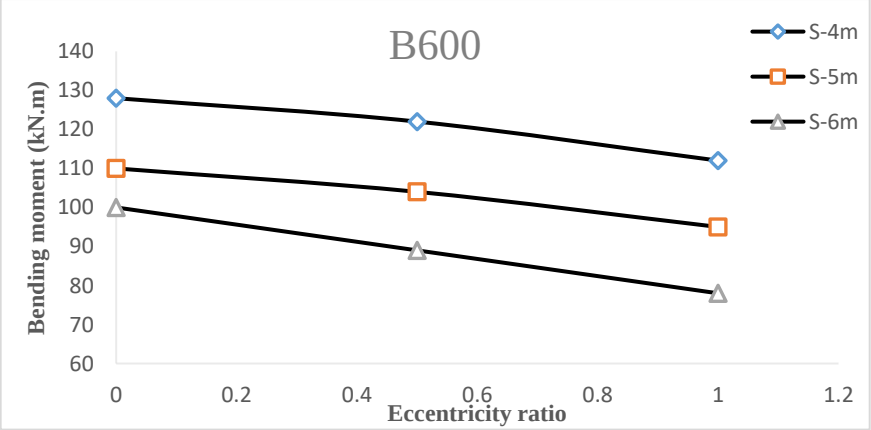

Figure. 4.6.d

Effect of eccentricity on bending moment for beam width 900 with transverse beam

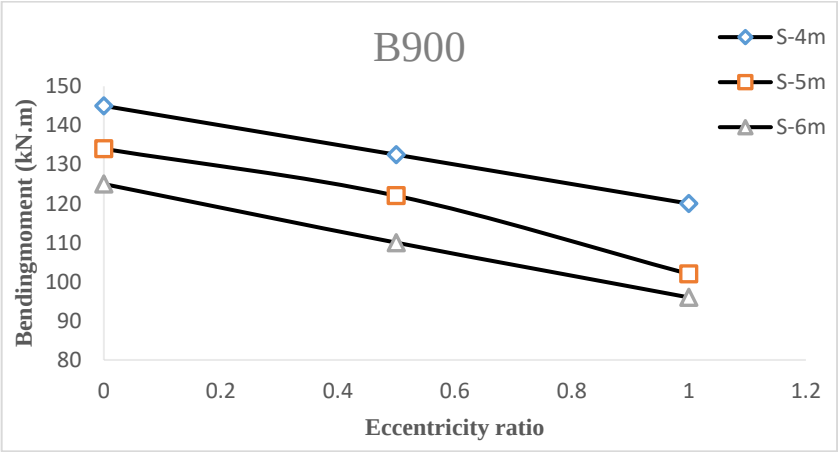

Figure. 4.6.e

Effect of eccentricity on bending moment for beam width 750 without transverse beam

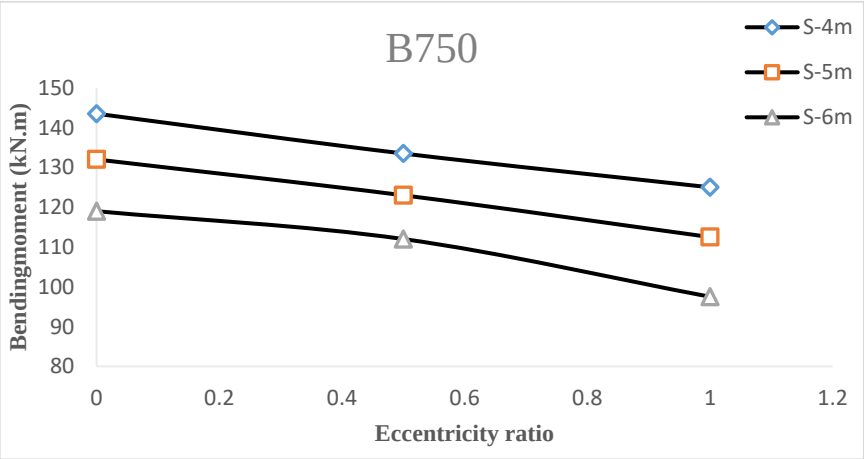

Figure. 4.6.f

Effect of eccentricity on bending moment for beam width 600 without transverse beam

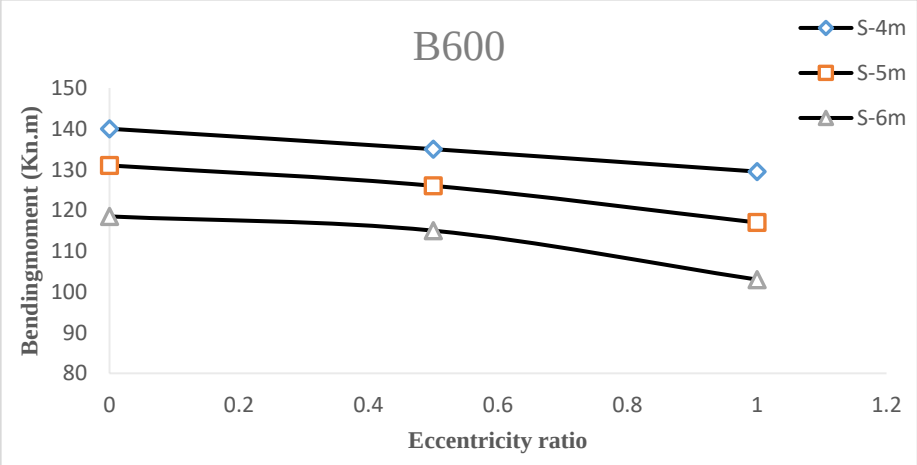

4.4.4 Effect of slab width

The effect of slab width on moment capacity is shown in Figures 4.7.a without transverse beam. Results show that, when the slab width increases the bending capacity decreases. This is because the torsion on beam increases with increase of slab width. The same behaviour occurs in cases with transverse beam as shown in Figures 4.7.b.

Figure. 4.7

Effect of slab width on bending moment

Figure. 4.7.a

Effect of slab width on bending moment for beam width 900 without transverse beam

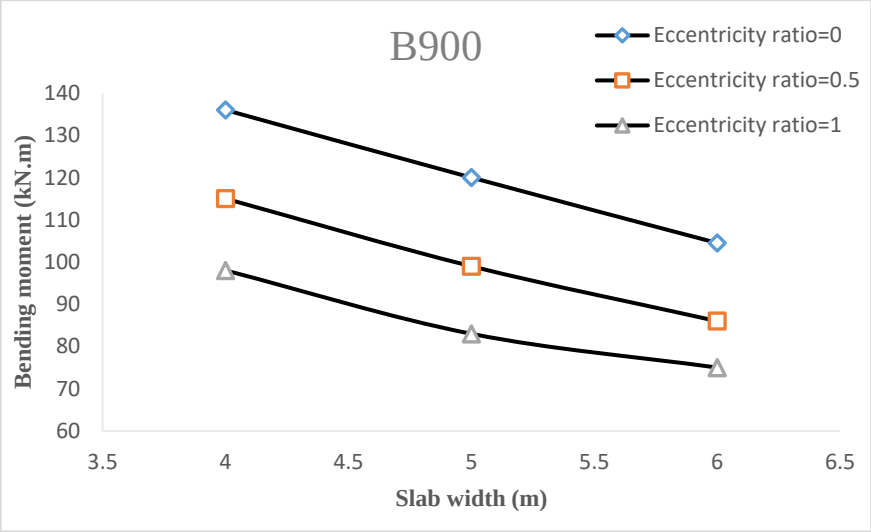

Figure. 4.7.b

Effect of slab width on bending moment for beam width 750 without transverse beam

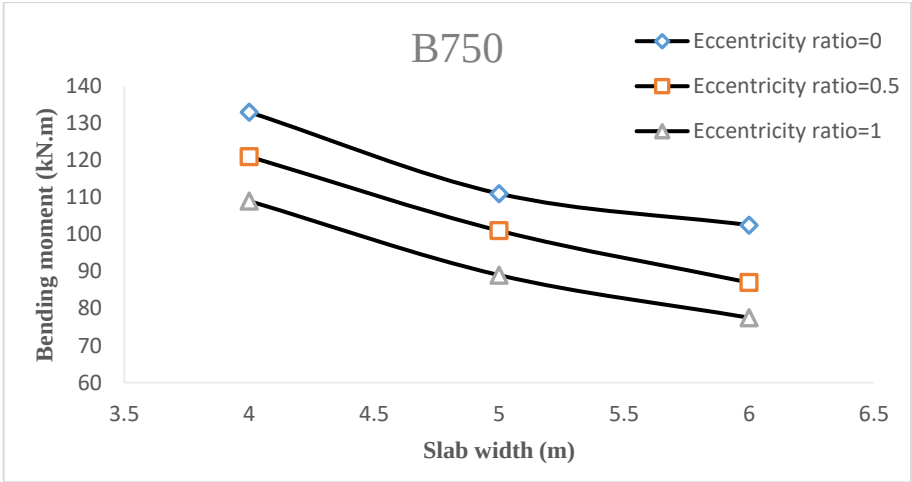

Figure. 4.7.c

Effect of slab width on bending moment for beam width 600 without transverse beam

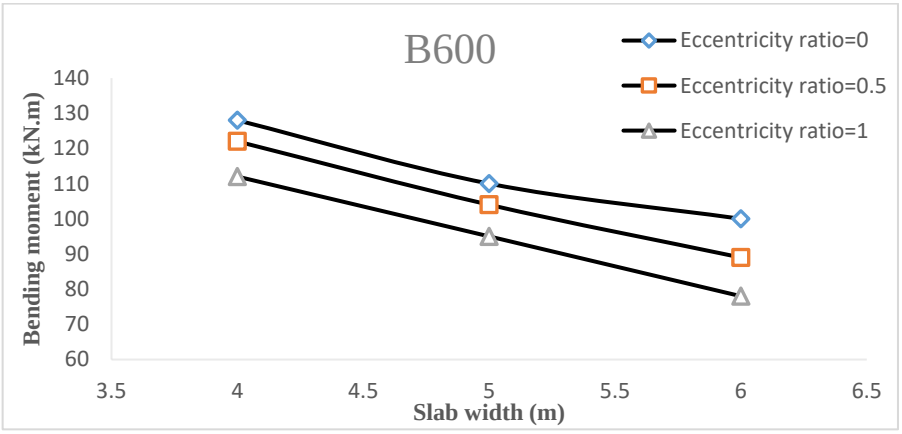

Figure. 4.7.d

Effect of slab width on bending moment for beam width 900 with transverse beam

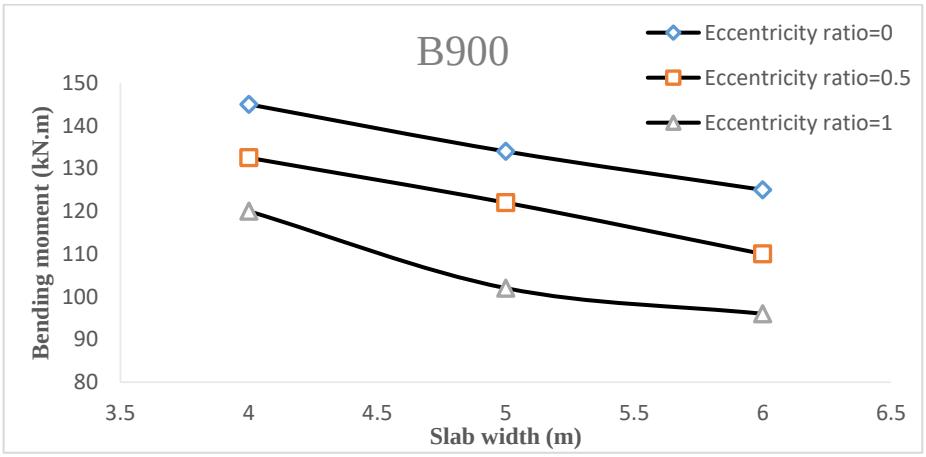

Figure. 4.7.e

Effect of slab width on bending moment for beam width 750 with transverse beam

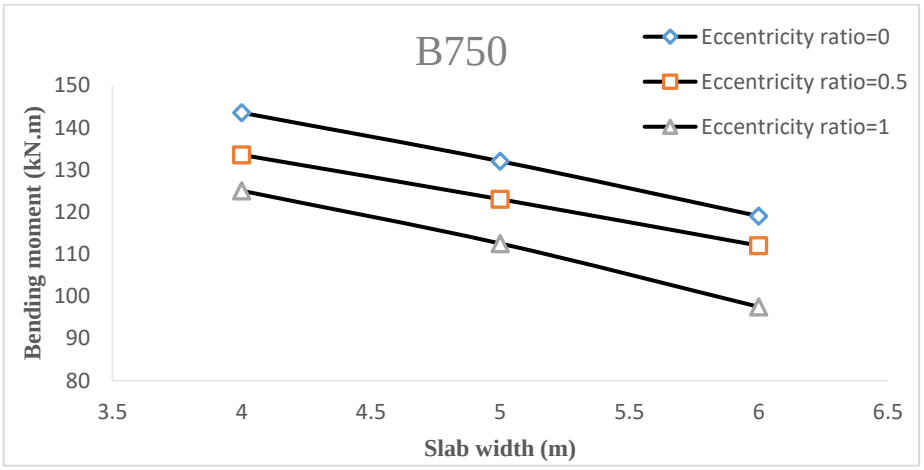

Figure. 4.7.f

Effect of slab width on bending moment for beam width 600 with transverse beam

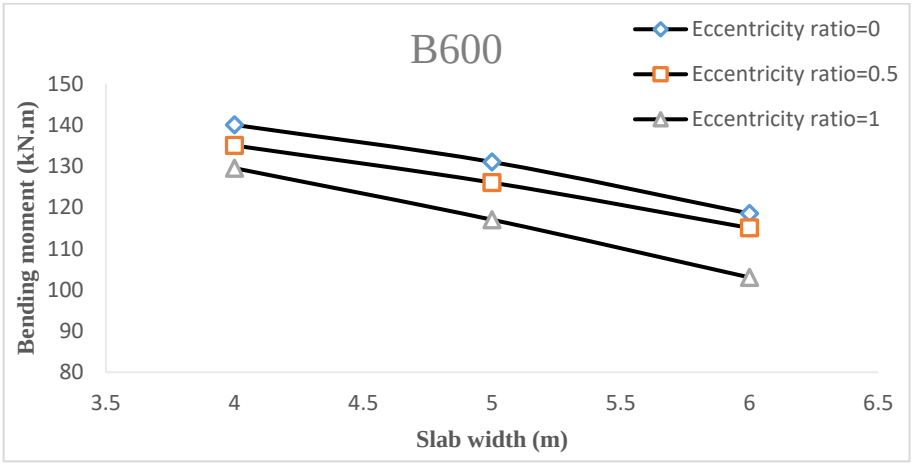

4.4.5 Effect of beam width

The influence of beam width on the moment capacity of wide beam with various eccentricity ratios and slab widths is shown in Figure 4.8.a. Results show that in cases without eccentricity the increases of beam width beam increase a little in the moment capacity of the wide beam-column joints while in cases with eccentricity the increasing of beam width decreases the moment capacity of wide beam-column joints. The same behaviour is noticed for models with transverse beam as shown in Figures 4.8.b.

Figure. 4.8

Effect of beam width on bending moment

Figure. 4.8.a

Effect of beam width on bending moment for slab width 4 without transverse beam

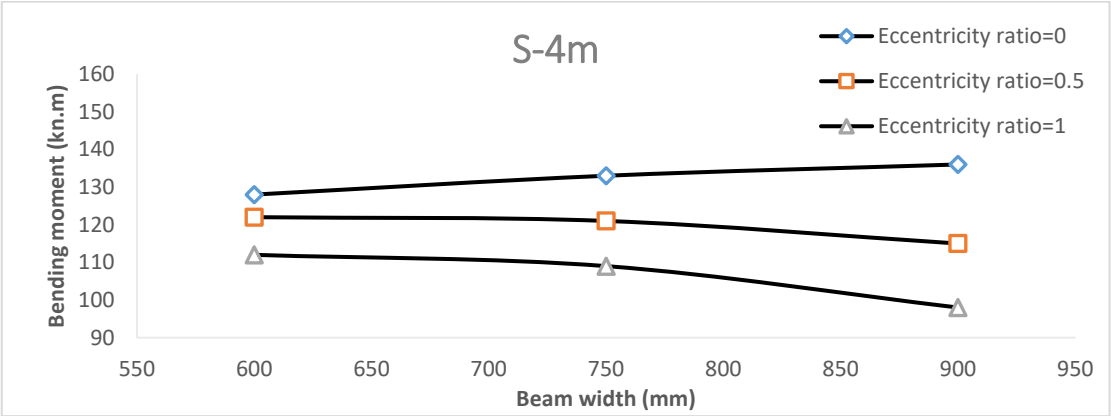

Figure. 4.8.b

Effect of beam width on bending moment for slab width 5 without transverse beam

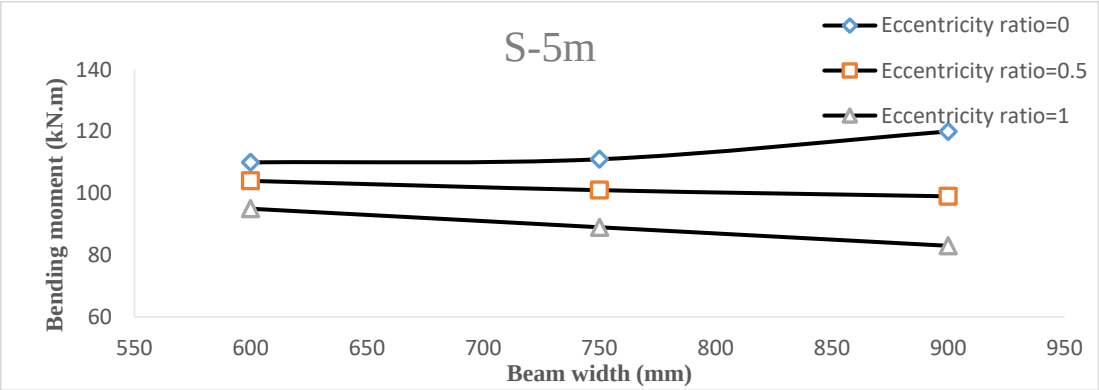

Figure. 4.8.c

Effect of beam width on bending moment for slab width 6 without transverse beam

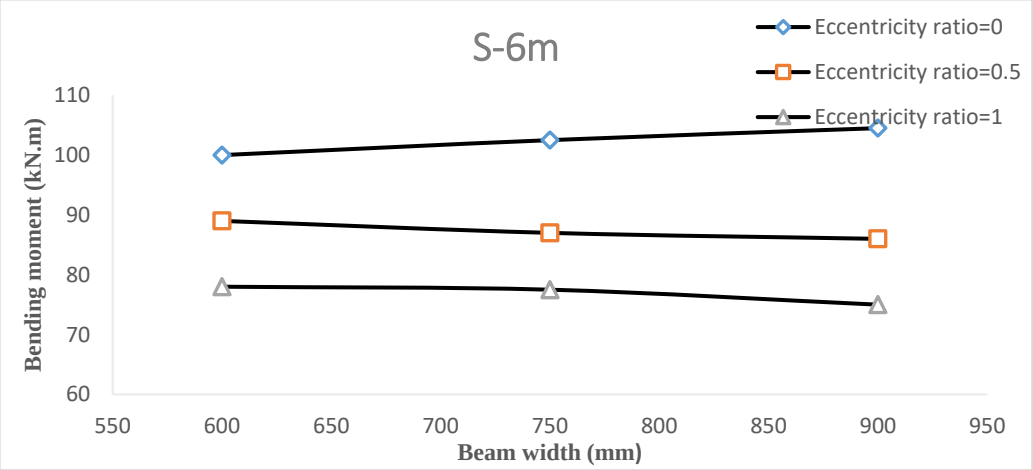

Figure. 4.8.d

Effect of beam width on bending moment for slab width 4 with transverse beam

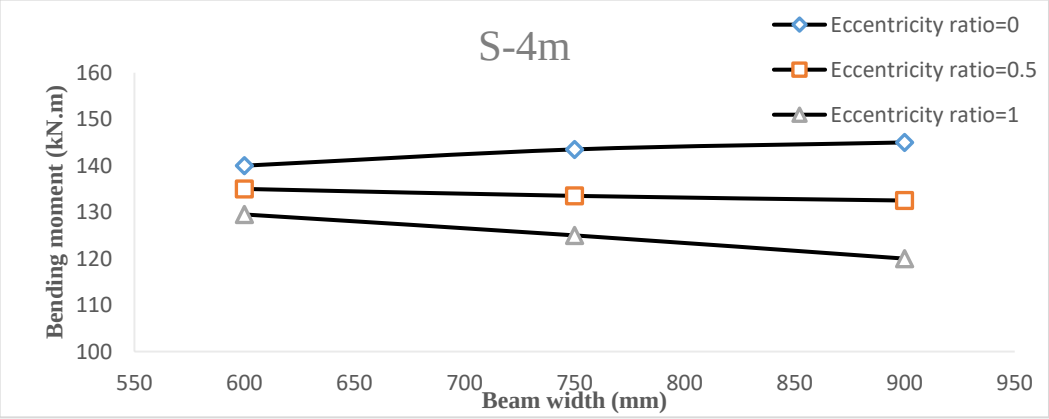

Figure. 4.8.e

Effect of beam width on bending moment for slab width 5 without transverse beam

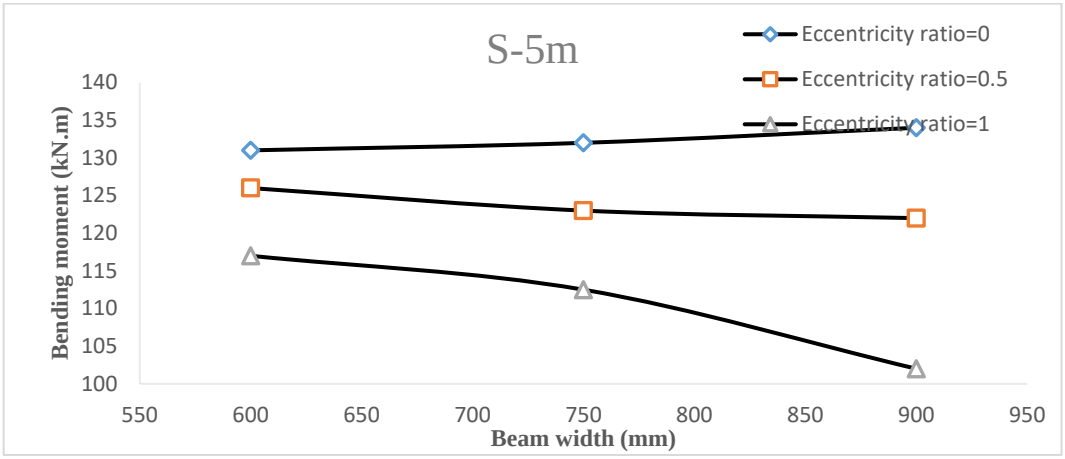

Figure. 4.8.f

Effect of beam width on bending moment for slab width 6 without transverse beam

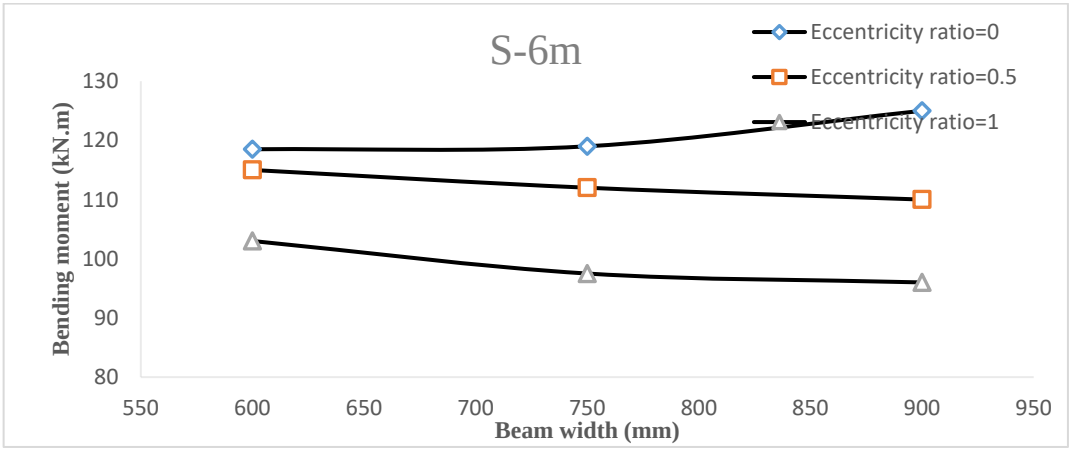

4.4.6 Effect of Transverse Beam

The maximum bending moment from each curve for cases with and without transverse beam are displayed in Table (2.A)/ Appendix (A). The results show that the presence of transverse beam increases in the bending capacity of edge beam. This behaviour is explained by the fact that the transverse beam resist part of torsion that acts on the edge beam.

4.5 Analytical study

After conducting the computer simulations and confirming the reasonability of the results, the target is to develop an equation or method for predicting the bending capacity of an

edge RC wide beam-column joint with and without eccentricity. Mechanics and moment distribution principles are used to develop a method to determine the required bending capacity in the beam through calculate the value of torsion on beam then the interaction between bending moment capacity and torsion is then used to estimate the moment capacity as follow:

4.5.1 Torsion on beam

Torsion on edge wide beam is produced from slab load and eccentricity between centreline of beam and centreline of column as follows.

4.5.1.1 Torsion from slab load

When the distributed load (w) acts on the slab as shown in Figure 4.9.a it will create a negative bending moment at the end of the slab due to the torsional restraint of the edge beam.

If we separate the slab from the edge beam, as shown in Figure 4.9.b, the negative distributed moment (designated as m) act on the end of the slab produces distributed torsion on beam. The reaction of this torsion generates an internal torsion (T) at the end of the beam. The torsion T is equal to $ml_b/2$. The moment m will be called the joint moment and can be determined from the compatibility of rotation at the joint while neglecting the vertical deflection of the edge beam (Thomas and Mo, 2010). Thus,

$$m = \frac{\frac{1}{12}wl_s^2}{1+\frac{K_s}{4K_{tb}}} \tag{4.5.1}$$

Where $\frac{1}{12}wl_s^2$ is taken from assumed connection between slab and edge beam and the other end as fixed.

w: distributed load (kN/m^2)

l_s: clear slab width (m)

K_s: flexural stiffness of the slab = $4EI/l_s$ where E: concrete elastic modulus and I: moment of inertia of slab.

K_{tb}: torsional stiffness of edge beam = CG/l_b, where C: St. Venant's torsional constant = $C = \frac{h_b^3 b_w}{3}(1 - 0.63\frac{h_b}{b_w})$, G is shear modulus of concrete.

$l_b, b_w \; and \; h_b$ are length, width and thickness of beam, respectively.

4.5.1.2 Torsion from eccentricity

To calculate the torsion produced by eccentricity on edge wide beam we need to find vertical reaction at support (P) and multiply it by eccentricity value as shown in Figure 4.9.c.

$$T_E = P * E \tag{4.5.2}$$

Figure. 4.9

Analytical analysis

Figure. 4.9.a

Space frame showing the test model

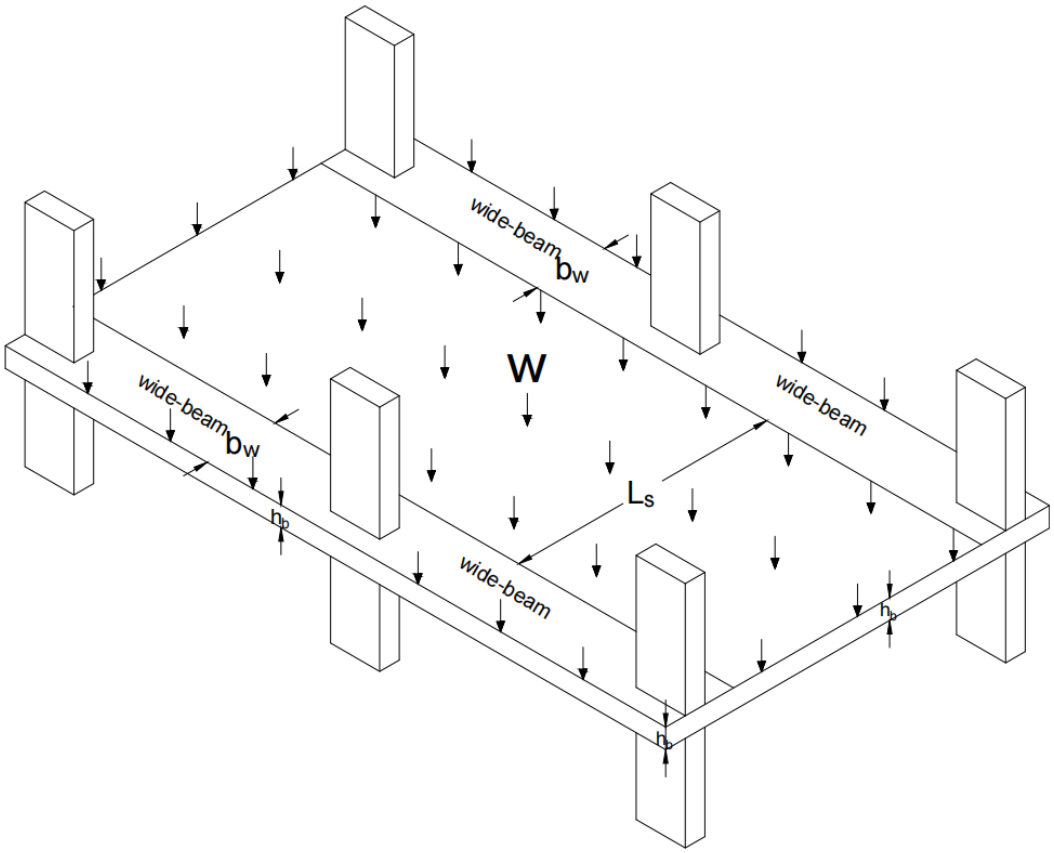

Figure. 4.9.b

Separated test model

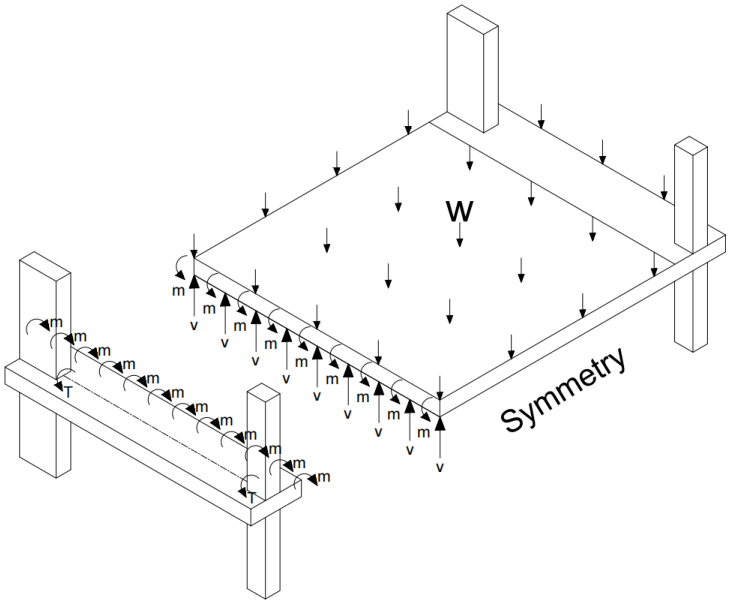

Figure. 4.9.c

Eccentric wide beam-column

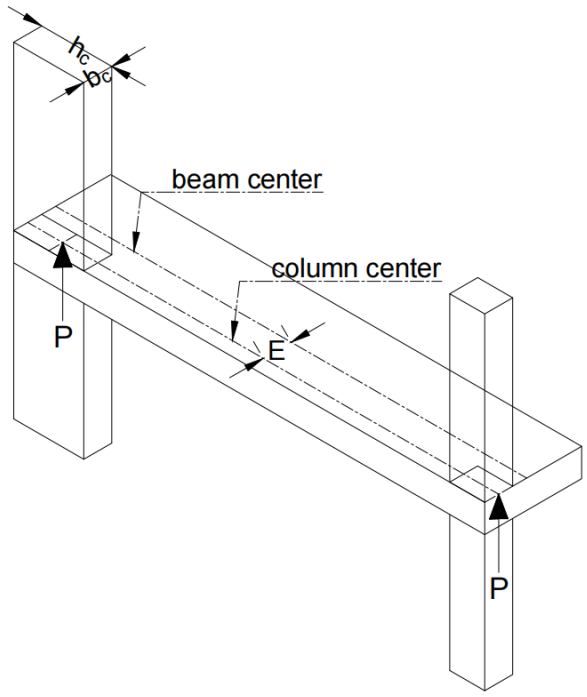

4.5.1.3 Total torsion

According to ACI 318, the critical design section of torsion is at distance d from the column face. However, the total torsion at column centre is:

at column centre

$$T = \frac{ml_b}{2} + T_E - M_{u,T.B} \tag{4.5.3}$$

And thus, at distance d from face of column, the Torsion is:

$$T = \left(\frac{ml_b}{2} + T_E - M_{u,T.B}\right) * \frac{\frac{l_b}{2} - \left(d + \frac{h_c}{2}\right)}{\frac{l_b}{2}} \tag{4.5.4}$$

Where $M_{u,T.B}$: flexural capacity of transverse beam, d: depth of beam, h_c: column height and l_b: beam length.

4.5.2 Interaction between combined bending and torsion

Generally, the bending and torsion capacity of section depend on longitudinal reinforcement steel. When the torsion is calculated according to the previous section the bending moment capacity can be determined. The interaction between bending moment and torsion is considered as per Lampert and Collins (1972). Their method depends on the space truss and skew bending theory. The internal lever arm is considered to be constant through the prismatic member and independent of the reinforcement amount used when calculating the flexural capacity. The obtained interaction relation assumes that in bending, the beams fail in combination of flexure and torsion along an inclined plane. For each inclined plane, the capacity of such a beam could be defined in terms of moment capacity in the transverse and longitudinal directions. A parabolic interaction between torsion and flexure was discovered in both the skew bending theory and the truss analogy approaches. Therefore, Lampert and Collins (1972) suggested an interpolated parabolic interaction relation for pure flexure and pure torsion as shown in Figure (24.B)/ Appendix (B). They noticed that these relationships agree well with experiments.

The interaction curve is as follows if the longitudinal reinforcement steel bars yield on the flexural tension side:

$$\left(\frac{T_u}{T_{uo}}\right)^2 = r\left(1 - \frac{M_u}{M_{uo}}\right) \tag{4.5.5}$$

The interaction curve is as follows if the longitudinal reinforcement steel bars yield on the flexural compression side:

$$\left(\frac{T_u}{T_{uo}}\right)^2 = 1 + r\frac{M_u}{M_{uo}} \quad (4.5.6)$$

Where

T_u, M_u: the ultimate torque and bending moment, respectively;

T_{uo}: pure ultimate torsional capacity of the section which equal =$2A_o f_y\sqrt{\frac{A_t}{s}\frac{A_l}{P_o}}$, if r=1

A_o: enclosed region defined by the connecting lines between the longitudinal bar's centers which equal x_o*y_o as shown in Figure (25.B)/ Appendix (B).

P_o: perimeter formed by the same set of lines

A_l: longitudinal bars total area (tension and compression)

At: area of one leg of stirrups

S: spacing between stirrups

f_y: yield stress of steel

M_{uo}: The section's pure ultimate flexural capacity which equal = $A_s f_y\left(d - \frac{a}{2}\right)$

r: the tensile reinforcement bars' yield force divided by the compressive reinforcement bars' yield force given as follow:

$$r = \frac{A_s f_y}{A'_s f'_y} \quad (4.5.7)$$

4.6 Proposed method results

Bending capacity for all cases was calculated using previous method through determining the total torsion acts on the beam from slab loads and beam eccentricity using Equation 4.5.4. Then, the value of pure torsion is calculated and pure bending capacity is substituted in interaction equation to find the bending capacity. The results are compared to bending capacity from ABAQUS as shown in Table (3.A)/ Appendix (A). The largest relative error between result from ABAQUS and proposed method is 7.7% while the

smallest relative error is 0.08% while the average error is3.29% as shown in Figure (26.B)/Appendix (B).

4.8 Summary

In this chapter the effect of eccentricity of wide beam-column joint on moment capacity of beam studied for typical wide beam-column-slab. The parameters that are predicted to have significant impact on the moment capacity in addition to eccentricity include the slab width, beam width and presence and absence of transverse beam.

As a result, it is noticed that the increase of eccentricity of wide beam decrease the load carrying capacity of beam due to produce additional torsion on wide beam. where the increase of slab width will decrease the load carrying capacity because of increase the value of torsion. For the increases of beam width beam without eccentricity the wide beam-column joint moment capacity increases a little while in cases with eccentricity the increasing of beam width decreases the moment capacity of wide beam-column joint. Finally, the presence of transverse beam will increase the capacity of edge beam to resist torsion.

By taking the effect of all parameters. A design guideline suggested by simple approach to predict the value of torsion on edge wide beam and calculate the area of longitudinal steel bars through interaction relationship between bending and torsion in the next chapter.

Chapter Five

Conclusions and Recommendations

5.1 Overview

The moment capacity of a three-dimensional (3-D) finite element (F.E.) non-linear models of an edge RC wide beam-column joints are studied under various parameters in this thesis. In addition, a simplified method for predicting the reduced bending capacity of wide beams are proposed. The main findings and results of the study are summarized in the following sections.

5.2 Research finding

Based on this thesis results, the following conclusions are stated:

1. Eccentricity of wide beam column produced additional torsion on edge wide beam. Hence when the value of eccentricity increases the capacity of wide beam to resist bending moment decreases.

2. Increasing the width of slab will increase the value of torsion that effect on wide beam and therefore decrease the bending moment capacity of wide beam.

3. The width of the beam has small effect on the moment capacity if the eccentricity is maintained

4. In cases where the transverse beam is present, the load carrying capacity of edge beam increases because the transverse beam resist part of torsion exposed on edge beam which equal approximately to its bending capacity.

5.3 Design guidelines

According to the proposed approach designer can follow the following steps:

- Assume slab width (l_s), beam length (l_b), distributed load (w), ultimate moment (M_u), stress of steel (f_y) and concrete (f'_c) are given.

- Assume dimensions of edge beam (b_w and h_b), area of stirrups leg (A_t) and spacing between stirrups (s).

- Calculate the joint moment from (Thomas and Mo, 2010) equation with modifications to suit our case as follow: $m = \frac{\frac{1}{12}wl_s^2}{1+\frac{K_s}{4K_{tb}}}$,

- Calculate slab flexural stiffness (K_s) and torsion stiffness of edge wide beam (K_{tb}) as follow: $K_s = 4EI/l_s$ and $K_{tb} = CG/l_b$ where E: elastic modulus of concrete, I: moment of inertia of slab, l_s: clear slab width, C: St. Venant's torsional constant $= \frac{h_b^3 b_w}{3}(1 - 0.63\frac{h_b}{b_w})$, G is the shear modulus of concrete. $l_b, b_w \; and \; h_b$ are dimensions of beam length, width and thickness, respectively. Then substitute in joint moment equation.

- Calculate ultimate torsion moment (T_u) at d distance from face of column as follows:

$$T_u = \left(\frac{ml_b}{2} + T_E - M_{u,T.B}\right) * \frac{\frac{l_b}{2} - \left(d + \frac{h_c}{2}\right)}{\frac{l_b}{2}} \qquad (5.7.1)$$

T_E: torsion from eccentricity which equal $T_E = P * E$ where P: reaction at support and E: eccentricity value between column centre and beam centre.

$M_{u,T.B}$: flexural capacity of transverse beam, d: depth of beam, h_c: column width and l_b: beam length.

- Substituted in interaction equation for torsion and bending with assume r=1

$$\left(\frac{T_u}{\emptyset_T T_{uo}}\right)^2 = r\left(1 - \frac{M_u}{\emptyset_B M_{uo}}\right) \qquad (5.7.2)$$

Where $\emptyset_T T_{uo}$: pure ultimate torsional capacity of the section which equal $= 0.75 * 2A_o f_y \sqrt{\frac{A_t}{s}\frac{A_l}{P_o}}$

A_o: enclosed region defined by the connecting lines between the centers of longitudinal bars which equal $x_o * y_o$

P_o: perimeter formed by the same set of lines

A_l: total area of longitudinal bars (tension and compression)

At: area of one leg of stirrups

S: spacing between stirrups

f_y: yield stress of steel

$\emptyset_B M_{uo}$: pure ultimate flexural capacity of the section which equal = 0.9*$A_s f_y jd$

A_s: area of longitudinal steel bars

jd: internal lever arm. assume the jd = 0.92d to simplify equation and to avoid the quadratic equation.

After substituted all values in interaction equation we can determine the area of longitudinal steel (A_s)

Example:

Find the steel area required for a rectangular wide beam at point B with a beam width and depth 80cm and 35cm respectively and a span of 6m that is to carry a total factor load = 20kN/m^2 as shown in Figure (27.B)/ Appendix (B) where the ultimate moment = 110kN.m at point B. Material strengths are f'_C = 24MPa and f_y = 420MPa. assume stirrups $\emptyset 10@150mm$

Solution:

Flexural stiffness of slab $K_s = \frac{4EI}{l_s} = \frac{4*23025*(10*925008829.88)}{5250} = 162272977584.66$

torsion stiffness of edge wide beam $K_{tb} = \frac{CG}{l_b}$ where $C = \frac{h_b^3 b_w}{3}\left(1 - 0.63\frac{h_b}{b_w}\right) = \frac{350^3*800}{3}\left(1 - 0.63\frac{350}{800}\right) = 8282020833.33$ so

$K_{tb} = \frac{8282020833.33*(\frac{23025}{2})}{5500} = 17335775426.13$

Calculate the ultimate torsion at d distance from column face where the eccentricity between column centre and wide beam centre =250mm as follow:

$$T_u = \left(\frac{ml_b}{2} + T_E - M_{u,T.B}\right) * \frac{\frac{l_b}{2} - \left(d + \frac{h_c}{2}\right)}{\frac{l_b}{2}}$$

Where $m = \frac{\frac{1}{12} w l_s^2}{1 + \frac{K_s}{4K_{tb}}} = \frac{\frac{1}{12} * 20 * 5.25^2}{1 + \frac{162272977584.66}{4 * 17335775426.13}} = 13.75\ Kn.m/m$

$T_E = P * E = 20 * 3.4 * 2.75 * 0.250 = 46.75\ Kn.m$

$M_{u,T.B} = 0$ where no transverse beam

So $T_u = \left(\frac{13.75 * 5.5}{2} + 46.75 - 0\right) * \frac{\frac{5.5}{2} - \left(0.325 + \frac{0.7}{2}\right)}{\frac{5.5}{2}} = 66\ Kn.m$

Substituted in interaction equation for torsion and bending with assume r=1 and $A_t = 2A_s$

$$\left(\frac{T_u}{\emptyset_T T_{uo}}\right)^2 = r\left(1 - \frac{M_u}{\emptyset_B M_{uo}}\right)$$

Where $\emptyset_T T_{uo} = 0.75 * 2 * 189475 * 420\sqrt{\frac{2A_s}{150}\frac{78.5}{1960}} = 2758472.29\sqrt{A_s}$

$$\emptyset_B M_{uo} = 0.9 * A_s * 420 * 0.92 * 325$$

$$= 113022\ A_s$$

$$\left(\frac{66 * 10^6}{2758472.29\sqrt{A_s}}\right)^2 = 1 * \left(1 - \frac{110 * 10^6}{113022\ A_s}\right)$$

By solution an equation $A_s = 1545.7 mm^2$

Assume using $\emptyset = 16$ for longitudinal steel bars then the number of bars = 8bars.

5.4 Future work

As mentioned before, this thesis focuses on the edge RC wide beam-column joint with distributed load on slab or gravity load, it is recommended to consider the seismic behaviour of edge wide beam with the same parameters and other types of joints in any further studies.

Furthermore, the effect of beam depth and length are not included in this research. It is recommended to study the impact of the beam depth on the load carrying capacity of eccentric edge RC wide beam column joints and other type of joints. Also, the area of needed to research is how to determine the deflection of slab in case of wide beam with and without eccentricity. Finally, the effect of eccentricity on ductility of wide beam column joint.

References

[1] Elsouri, A. M., & Harajli, M. H. (2015). Interior RC wide beam-narrow column joints: Potential for improving seismic resistance. Engineering structures, 99, 42-55.

[2] Lee, J. Y., Kim, J. Y., & Oh, G. J. (2009). Strength deterioration of reinforced concrete beam–column joints subjected to cyclic loading. Engineering Structures, 31(9), 2070-2085.

[3] Alva, G. M. S., & de Cresce El, A. L. H. (2013). Moment–rotation relationship of RC beam-column connections: Experimental tests and analytical model. Engineering Structures, 56, 1427-1438.

[4] Wong, H. F., & Kuang, J. S. (2014). Predicting shear strength of RC interior beam–column joints by modified rotating-angle softened-truss model. Computers & Structures, 133, 12-17.

[5] Vollum, R. L., & Newman, J. B. (1999). Towards the design of reinforced concrete eccentric beam—column joints. Magazine of Concrete Research, 51(6), 397-407.

[6] Wong, H. F., Liu, Y., Luk, S. H., Lee, P. M., & Kwong, W. H. (2019). Effects of eccentricity on seismic behavior of non-seismically designed reinforced concrete beam-column joint.

[7] Lafave, J. M., Bonacci, J. F., Burak, B., & Shin, M. (2005). Eccentric beam-column connections. Concrete international, 27(9), 58-62.

[8] Benavent-Climent, A. (2007). Seismic behavior of RC wide beam-column connections under dynamic loading. Journal of earthquake engineering, 11(4), 493-511.

[9] Gómez-Martínez, F., Alonso-Durá, A., De Luca, F., & Verderame, G. M. (2016). Ductility of wide beam RC frames as lateral resisting system. Bulletin of Earthquake Engineering, 14(6), 1545-1569.

[10] ACI (2002) ACI-ASCE 352: Recommendations for design of beam–column joints in monolithic reinforced concrete structures (ACI352R-02). American Concrete Institute, Farmington Hills, MI, USA.

[11] Fadwa, I., Ali, T. A., Nazih, E., & Sara, M. (2014). Reinforced concrete wide and conventional beam–column connections subjected to lateral load. Engineering Structures, 76, 34-48.

[12] Behnam, H., Kuang, J. S., & Huang, R. Y. (2017). Exterior RC wide beam-column connections: Effect of beam width ratio on seismic behaviour. Engineering Structures, 147, 27-44.

[13] Elsouri, A. M., & Harajli, M. H. (2013). Seismic response of exterior RC wide beam–narrow column joints: earthquake-resistant versus as-built joints. Engineering Structures, 57, 394-405.

[14] Elsouri, A. M., & Harajli, M. H. (2015). Interior RC wide beam-narrow column joints: Potential for improving seismic resistance. Engineering structures, 99, 42-55.

[15] Pakzad, A., & Khanmohammadi, M. (2020). Experimental cyclic behavior of code-conforming exterior wide beam-column connections. Engineering Structures, 214, 110613.

[16] ACI (2019) ACI 318-19: Building code requirements for structural concrete and commentary. American Concrete Institute, Farmington Hills, MI, USA.

[17] Eurocode 8 (2004). "Design of structures for earthquake resistance. European Committee for Standardization".

[18] NZS 3101 (2006). "The design of concrete structures. Wellington, New Zealand: Standards Association of New Zealand".

[19] Dabiri, H., Kheyroddin, A., & Kaviani, A. (2019). A numerical study on the seismic response of RC wide column–beam joints. International Journal of Civil Engineering, 17(3), 377-395.

[20] Siah, W. L., Stehle, J. S., Mendis, P., & Goldsworthy, H. (2003). Interior wide beam connections subjected to lateral earthquake loading. Engineering Structures, 25(3), 281-291.

[21] Benavent-Climent, A., Cahís, X., & Zahran, R. (2009). Exterior wide beam–column connections in existing RC frames subjected to lateral earthquake loads. Engineering Structures, 31(7), 1414-1424.

[22] Benavent-Climent, A., Cahís, X., & Vico, J. M. (2010). Interior wide beam-column connections in existing RC frames subjected to lateral earthquake loading. Bulletin of Earthquake Engineering, 8(2), 401-420.

[23] Masi, A., Santarsiero, G., Mossucca, A., & Nigro, D. (2014). Influence of axial load on the seismic behavior of RC beam-column joints with wide beam. In Applied Mechanics and Materials (Vol. 508, pp. 208-214). Trans Tech Publications Ltd.

[24] Mirzabagheri, S., Tasnimi, A. A., & Mohammadi, M. S. (2016). Behavior of interior RC wide and conventional beam-column roof joints under cyclic load. Engineering structures, 111, 333-344.

[25] Behnam, H., Kuang, J. S., & Abdouka, K. (2016). BEHAVIOUR OF RC SPANDREL BEAM IN EXTERIOR WIDE BEAM-COLUMN CONNECTIONS.

[26] Etemadi, E., & Fallahnezhad, K. (2017). Behavior of reinforced concrete interior wide beam-column connections under lateral loading: A finite element study. International Journal of Engineering and Technology, 9(3), 2559-2570.

[27] Behnam, H., Kuang, J. S., & Samali, B. (2018). Parametric finite element analysis of RC wide beam-column connections. Computers & Structures, 205, 28-44.

[28] Kuang, J. S., Behnam, H., & Huang, Q. (2017). Effective beam width of reinforced-concrete wide beam–column connections. Proceedings of the Institution of Civil Engineers-Structures and Buildings, 170(5), 336-353.

[29] Behnam, H., Kuang, J. S., Wong, H. F., Huang, Q., & Al-Mahaidi, R. (2018). Analysis of laterally loaded exterior wide beam–column connections. Magazine of Concrete Research, 70(10), 500-511.

[30] KR, S. C., & GS, T. (2012). Comparative Study on Behaviour of Reinforced Beam-Column Joints with Reference to Anchorage Detailing.

[31] Grassl, P., Xenos, D., Nyström, U., Rempling, R., & Gylltoft, K. (2013). CDPM2: A damage-plasticity approach to modelling the failure of concrete. International Journal of Solids and Structures, 50(24), 3805-3816.

[32] Lubliner, J., Oliver, J., Oller, S., & Oñate, E. (1989). A plastic-damage model for concrete. International Journal of solids and structures, 25(3), 299-326.

[33] Najafgholipour, M. A., Dehghan, S. M., Dooshabi, A., & Niroomandi, A. (2017). Finite element analysis of reinforced concrete beam-column connections with governing joint shear failure mode. Latin American Journal of Solids and Structures, 14, 1200-1225.

[34] Lee, J., & Fenves, G. L. (1998). Plastic-damage model for cyclic loading of concrete structures. Journal of engineering mechanics, 124(8), 892-900.

[35] Lubarda, V. A., Krajcinovic, D., & Mastilovic, S. (1994). Damage model for brittle elastic solids with unequal tensile and compressive strengths. Engineering Fracture Mechanics, 49(5), 681-697.

[36] Jankowiak, T., & Lodygowski, T. (2005). Identification of parameters of concrete damage plasticity constitutive model. Foundations of civil and environmental engineering, 6(1), 53-69.

[37] Genikomsou, A. S., & Polak, M. A. (2015). Finite element analysis of punching shear of concrete slabs using damaged plasticity model in ABAQUS. Engineering structures, 98, 38-48.

[38] Park, R., & Paulay, T. (1975). Reinforced concrete structures. John Wiley & Sons.

[39] Hsu, T. T., & Mo, Y. L. (2010). Unified theory of concrete structures. John Wiley & Sons.

[40] Lampert, P., & Collins, M. P. (1972, August). Torsion, bending, and confusion-An attempt to establish the facts. In Journal Proceedings (Vol. 69, No. 8, pp. 500-504).

[41] ABAQUS: ABAQUS Analysis User's Manual Version 6.14. (2014). Assault Systems.

Appendices

Appendix A

Tables

Table 1.A

Variable properties for all models

Model	Beam width (b_w)	Eccentricity ratio (ER)	Slab width (l_s)	Transverse beam (TB)
B900-ER0-S4-No TB	900	0	4000	No
B900-ER0-S4-TB	900	0	4000	yes
B900-ER0.5-S4-No TB	900	0.5	4000	no
B900-ER0.5-S4-TB	900	0.5	4000	yes
B900-E1-S4-No TB	900	1	4000	No
B900-ER1-S4-TB	900	1	4000	yes
B900-ER0-S5-No TB	900	0	5000	No
B900-ER0-S5-TB	900	0	5000	yes
B900-ER0.5-S5-No TB	900	0.5	5000	no
B900-ER0.5-S5-TB	900	0.5	5000	yes
B900-ER1-S5-No TB	900	1	5000	No
B900-ER1-S5-TB	900	1	5000	yes
B900-ER0-S6-No TB	900	0	6000	No
B900-ER0-S6-TB	900	0	6000	yes
B900-ER0.5-S6-No TB	900	0.5	6000	no
B900-ER0.5-S6-TB	900	0.5	6000	yes
B900-ER1-S6-No TB	900	1	6000	No
B900-ER1-S6-TB	900	1	6000	yes
B750-ER0-S4-No TB	750	0	4000	No
B750-ER0-S4-TB	750	0	4000	yes
B750-ER0.5-S4-No TB	750	0.5	4000	no
B750-ER0.5-S4-TB	750	0.5	4000	yes
B750-ER1-S4-No TB	750	1	4000	No
B750-ER1-S4-TB	750	1	4000	yes
B750-ER0-S5-No TB	750	0	5000	No
B750-ER0-S5-TB	750	0	5000	yes
B750-ER0.5-S5-No TB	750	0.5	5000	no
B750-ER0.5-S5-TB	750	0.5	5000	yes
B750-ER1-S5-No TB	750	1	5000	No
B750-ER1-S5-TB	750	1	5000	yes
B750-ER0-S6-No TB	750	0	6000	No
B750-ER0-S6-TB	750	0	6000	yes
B750-ER0.5-S6-No TB	750	0.5	6000	no
B750-ER0.5-S6-TB	750	0.5	6000	yes
B750-ER1-S6-No TB	750	1	6000	No
B750-ER1-S6-TB	750	1	6000	yes
B600-ER0-S4-No TB	600	0	4000	No
B600-ER0-S4-TB	600	0	4000	yes
B600-ER0.5-S4-No TB	600	0.5	4000	no
B600-ER0.5-S4-TB	600	0.5	4000	yes
B600-ER1-S4-No TB	600	1	4000	No
B600-ER1-S4-TB	600	1	4000	yes
B600-ER0-S5-No TB	600	0	5000	No
B600-ER0-S5-TB	600	0	5000	yes

B600-ER0.5-S5-No TB	600	0.5	5000	no
B600-ER0.5-S5-TB	600	0.5	5000	yes
B600-ER1-S5-No TB	600	1	5000	No
B600-ER1-S5-TB	600	1	5000	yes
B600-ER0-S6-No TB	600	0	6000	No
B600-ER0-S6-TB	600	0	6000	yes
B600-ER0.5-S6-No TB	600	0.5	6000	no
B600-ER0.5-S6-TB	600	0.5	6000	yes
B600-ER1-S6-No TB	600	1	6000	No
B600-ER1-S6-TB	600	1	6000	yes

Table 2.A

Summary of F.E result

Model	**Beam width (b_w) mm**	**Eccentricity ratio (ER)**	**Eccentricity value (E) mm**	**Slab width (l_s) mm**	**Transverse beam (TB)**	**Distributed load Kn**	**Maximum bending moment (M_u) Kn.m**
B900-ER0-S4-No TB	900	0	0	4000	No	41	136
B900-ER0-S4-TB	900	0	0	4000	Yes	44	145
B900-ER0.5-S4-No TB	900	0.5	150	4000	No	36.5	115
B900-ER0.5-S4-TB	900	0.5	150	4000	Yes	41	132.5
B900-ER1-S4-No TB	900	1	300	4000	No	31	98
B900-ER1-S4-TB	900	1	300	4000	Yes	36	120
B900-ER0-S5-No TB	900	0	0	5000	No	30.7	120
B900-ER0-S5-TB	900	0	0	5000	Yes	34.5	134
B900-ER0.5-S5-No TB	900	0.5	150	5000	No	27	99
B900-ER0.5-S5-TB	900	0.5	150	5000	Yes	30.5	122
B900-ER1-S5-No TB	900	1	300	5000	No	23.6	83
B900-ER1-S5-TB	900	1	300	5000	Yes	27	102
B900-ER0-S6-No TB	900	0	0	6000	No	23.6	104.5
B900-ER0-S6-TB	900	0	0	6000	Yes	27	125
B900-ER0.5-S6-No TB	900	0.5	150	6000	No	20.4	86
B900-ER0.5-S6-TB	900	0.5	150	6000	Yes	24	110
B900-ER1-S6-No TB	900	1	300	6000	No	18	75
B900-ER1-S6-TB	900	1	300	6000	Yes	21	96
B750-ER0-S4-No TB	750	0	0	4000	No	43	133
B750-ER0-S4-TB	750	0	0	4000	Yes	46	143.5
B750-ER0.5-S4-No TB	750	0.5	112.5	4000	No	38	121
B750-ER0.5-S4-TB	750	0.5	112.5	4000	Yes	44	133.5

B750-ER1-S4-No TB	750	1	225	4000	No	32	109
B750-ER1-S4-TB	750	1	225	4000	Yes	39.5	125
B750-ER0-S5-No TB	750	0	0	5000	No	32	111
B750-ER0-S5-TB	750	0	0	5000	Yes	38	132
B750-ER0.5-S5-No TB	750	0.5	112.5	5000	No	28.5	101
B750-ER0.5-S5-TB	750	0.5	112.5	5000	Yes	35	123
B750-ER1-S5-No TB	750	1	225	5000	No	25	89
B750-ER1-S5-TB	750	1	225	5000	Yes	30	112.5
B750-ER0-S6-No TB	750	0	0	6000	No	23	102.5
B750-ER0-S6-TB	750	0	0	6000	Yes	29	119
B750-ER0.5-S6-No TB	750	0.5	112.5	6000	No	22	87
B750-ER0.5-S6-TB	750	0.5	112.5	6000	Yes	26	112
B750-ER1-S6-No TB	750	1	225	6000	No	19	77.5
B750-ER1-S6-TB	750	1	225	6000	Yes	23	97.5
B600-ER0-S4-No TB	600	0	0	4000	No	45	128
B600-ER0-S4-TB	600	0	0	4000	Yes	48	140
B600-ER0.5-S4-No TB	600	0.5	75	4000	No	40	122
B600-ER0.5-S4-TB	600	0.5	75	4000	Yes	45	135
B600-ER1-S4-No TB	600	1	150	4000	No	36	112
B600-ER1-S4-TB	600	1	150	4000	Yes	42.5	129.5
B600-ER0-S5-No TB	600	0	0	5000	No	35.5	110
B600-ER0-S5-TB	600	0	0	5000	Yes	42	131
B600-ER0.5-S5-No TB	600	0.5	75	5000	No	29.4	104
B600-ER0.5-S5-TB	600	0.5	75	5000	Yes	37	126
B600-ER1-S5-No TB	600	1	150	5000	No	27	95
B600-ER1-S5-TB	600	1	150	5000	Yes	33	117
B600-ER0-S6-No TB	600	0	0	6000	No	25	100
B600-ER0-S6-TB	600	0	0	6000	Yes	32	118.5
B600-ER0.5-S6-No TB	600	0.5	75	6000	No	23	89
B600-ER0.5-S6-TB	600	0.5	75	6000	Yes	29	115
B600-ER1-S6-No TB	600	1	150	6000	No	20.7	78
B600-ER1-S6-TB	600	1	150	6000	Yes	25.5	103

Table 3.A

ABAQUS and proposed method results

Status	Model	NUMARICAL RESULT (ABAQUS)	ANALYTICAL PROPSED METHOD RESULT	RELATIVE ERROR= $\frac{M_{u,ABAQUS} - M_{u,P.M}}{M_{u,ABAQUS}} * 100\%$
1	B900-ER0-S4-No TB	136	135.56	0.32
2	B900-ER0-S4-TB	145	150.37	-3.70
3	B900-ER0.5-S4-No TB	115	113.54	1.27
4	B900-ER0.5-S4-TB	132.5	135.38	-2.18
5	B900-ER1-S4-No TB	98	92.72	5.39
6	B900-ER1-S4-TB	120	115.09	4.09
7	B900-ER0-S5-No TB	120	122.51	-2.09
8	B900-ER0-S5-TB	134	141.80	-5.82
9	B900-ER0.5-S5-No TB	99	102.34	-3.37
10	B900-ER0.5-S5-TB	122	126.15	-3.40
11	B900-ER1-S5-No TB	83	82.62	0.46
12	B900-ER1-S5-TB	102	107.59	-5.48
13	B900-ER0-S6-No TB	104.5	108.20	-3.54
14	B900-ER0-S6-TB	125	129.97	-3.98
15	B900-ER0.5-S6-No TB	86	92.63	-7.7
16	B900-ER0.5-S6-TB	110	113.53	-3.21
17	B900-ER1-S6-No TB	75	76.39	-1.86
18	B900-ER1-S6-TB	96	98.94	-3.07
19	B750-ER0-S4-No TB	133	132.90	0.08
20	B750-ER0-S4-TB	143.5	149.19	-3.96
21	B750-ER0.5-S4-No TB	121	116.10	4.05
22	B750-ER0.5-S4-TB	133.5	137.79	-3.21
23	B750-ER1-S4-No TB	109	102.75	5.74
24	B750-ER1-S4-TB	125	122.17	2.26
25	B750-ER0-S5-No TB	111	118.92	-7.13
26	B750-ER0-S5-TB	132	138.60	-5.00
27	B750-ER0.5-S5-No TB	101	102.30	-1.28
28	B750-ER0.5-S5-TB	123	122.21	0.64
29	B750-ER1-S5-No TB	89	87.86	1.28
30	B750-ER1-S5-TB	112.5	110.93	1.40
31	B750-ER0-S6-No TB	102.5	108.90	-6.24
32	B750-ER0-S6-TB	119	126.24	-6.08
33	B750-ER0.5-S6-No TB	87	87.80	-0.93
34	B750-ER0.5-S6-TB	112	112.69	-0.61
35	B750-ER1-S6-No TB	77.5	79.30	-2.32
36	B750-ER1-S6-TB	97.5	101.36	-3.96
37	B600-ER0-S4-No TB	128	131.38	-2.64
38	B600-ER0-S4-TB	140	148.42	-6.02
39	B600-ER0.5-S4-No TB	122	119.84	1.77
40	B600-ER0.5-S4-TB	135	143.45	-6.26
41	B600-ER1-S4-No TB	112	107.31	4.19
42	B600-ER1-S4-TB	129.5	133.75	-3.29
43	B600-ER0-S5-No TB	110	112.78	-2.53
44	B600-ER0-S5-TB	131	137.43	-4.91

45	B600-ER0.5-S5-No TB	104	107.15	-3.03
46	B600-ER0.5-S5-TB	126	129.44	-2.73
47	B600-ER1-S5-No TB	95	94.60	0.42
48	B600-ER1-S5-TB	117	120.95	-3.37
49	B600-ER0-S6-No TB	100	102.11	-2.11
50	B600-ER0-S6-TB	118.5	123.53	-4.25
51	B600-ER0.5-S6-No TB	89	90.27	-1.43
52	B600-ER0.5-S6-TB	115	113.66	1.16
53	B600-ER1-S6-No TB	78	82.10	-5.26
54	B600-ER1-S6-TB	103	108.58	-5.42

Appendix B

Figures

Figure 1.B

Edge beam-column joint with one-way ribbed slab

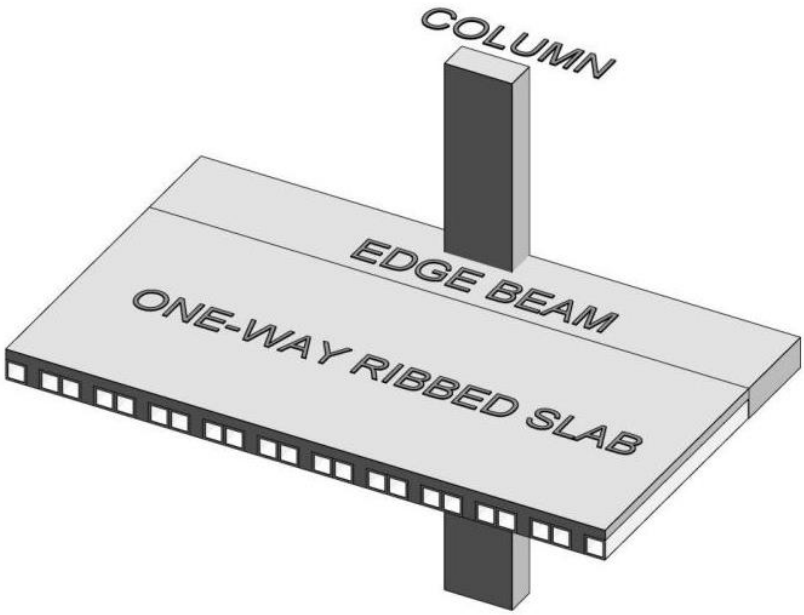

Figure 2.B

Types of joint (ACI 352R-02)

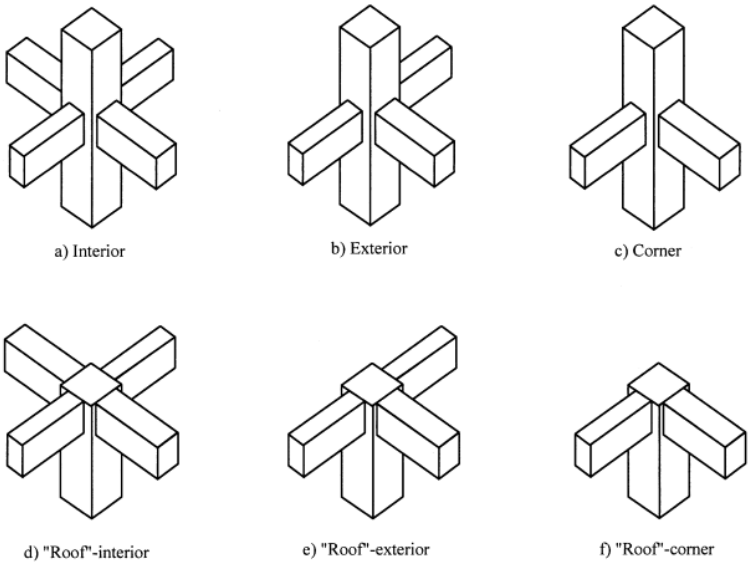

Figure 3.B

Maximum beam width

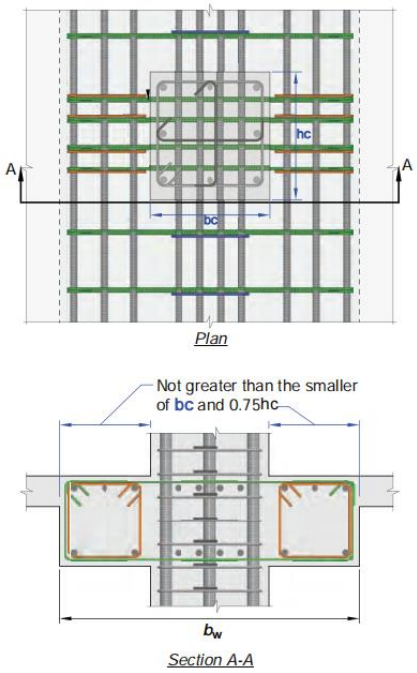

Figure 4.B

Transfer moment at wide beam connection

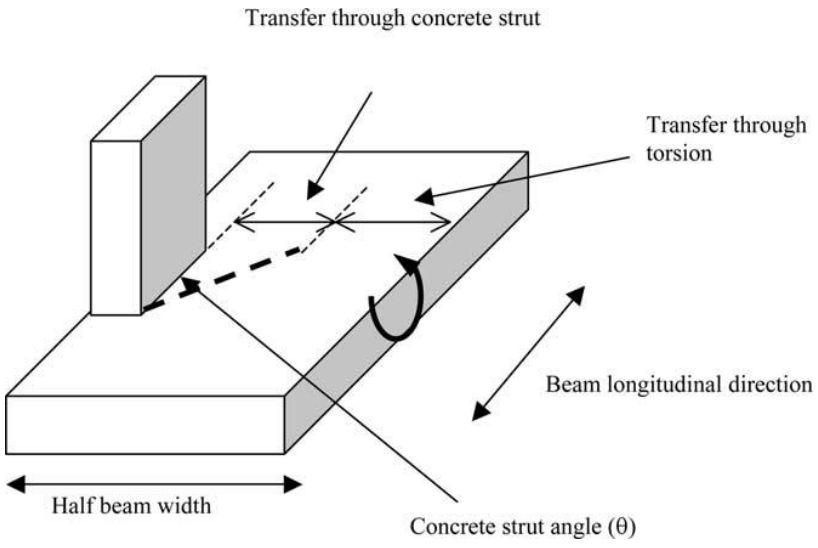

Figure 5.B

Load transfer paths in interior wide beam-column

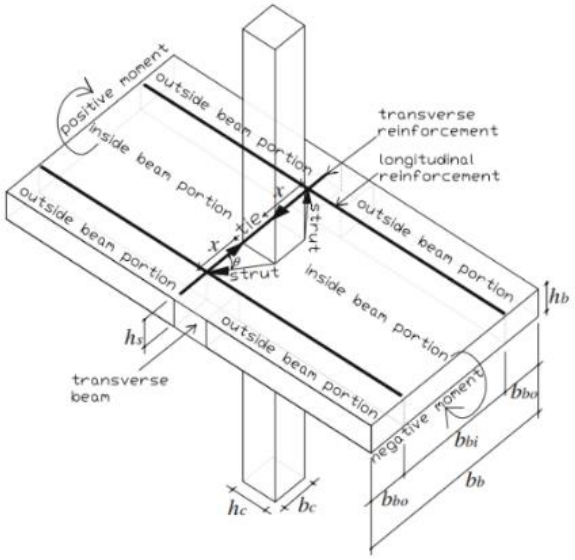

Figure 6.B

Load transfer paths in exterior wide beam-column

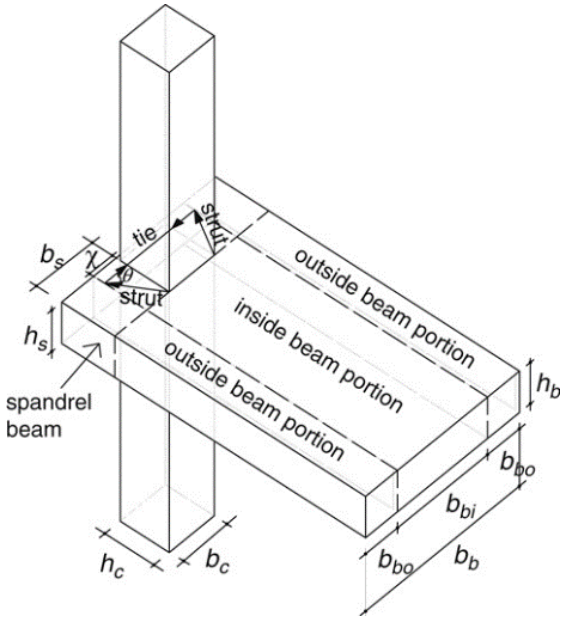

Figure 7.B

Perpendicular and parallel long dimension column in the wide beam-column joint

Figure 7.a.B

Perpendicular long dimension column in the wide beam-column joint

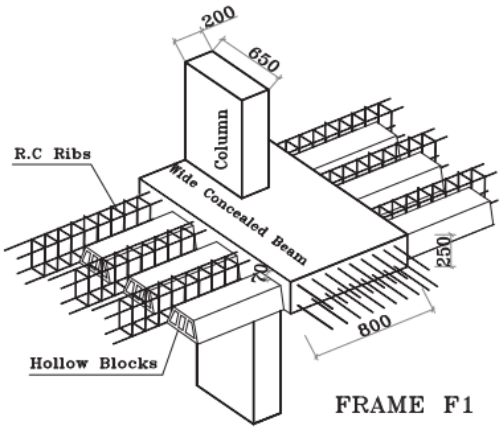

Figure 7.b.B

Parallel long dimension column in the wide beam-column joint

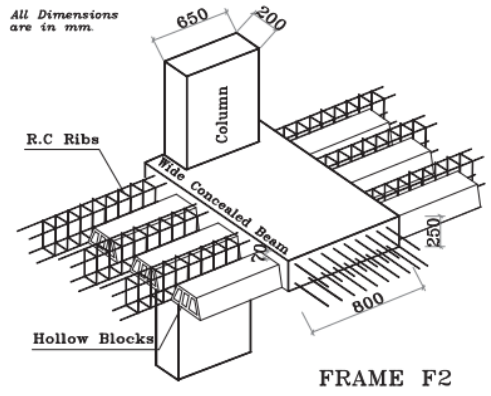

Figure 8.B

Load-deflection curve for specimen with high (NH) and low (NL) axial load

Figure 8.a.B

Load-deflection curve for specimen with high (NH)

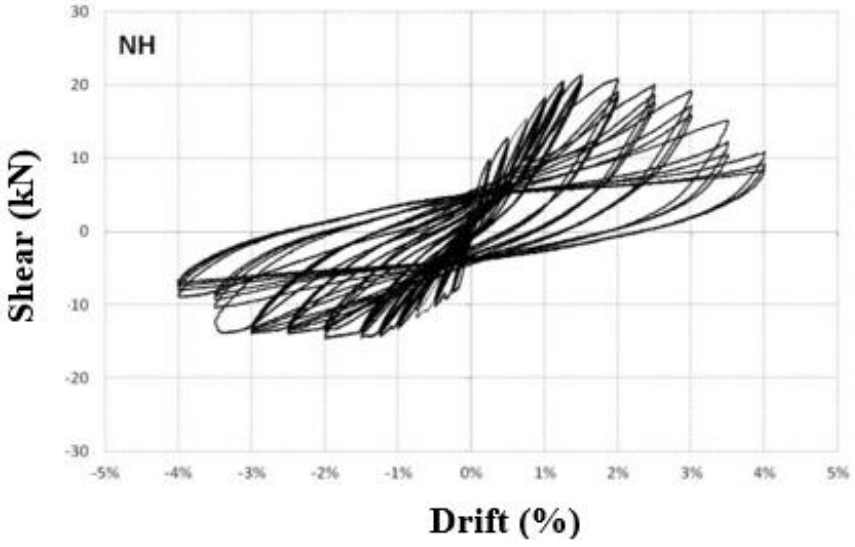

Figure 8.b.B

Load-deflection curve for specimen with low (NL) axial load

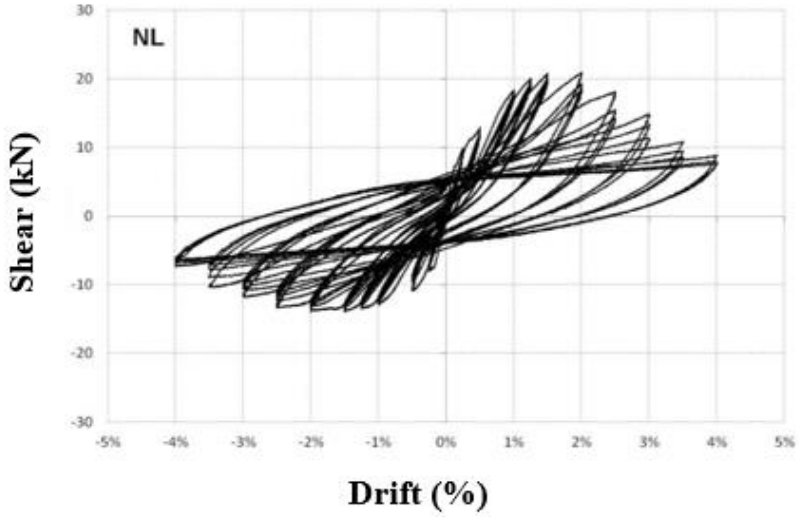

Figure 9.B

Lateral load vs drift for specimen

Figure 9.a.B

IWBCC: interior wide beam column connection

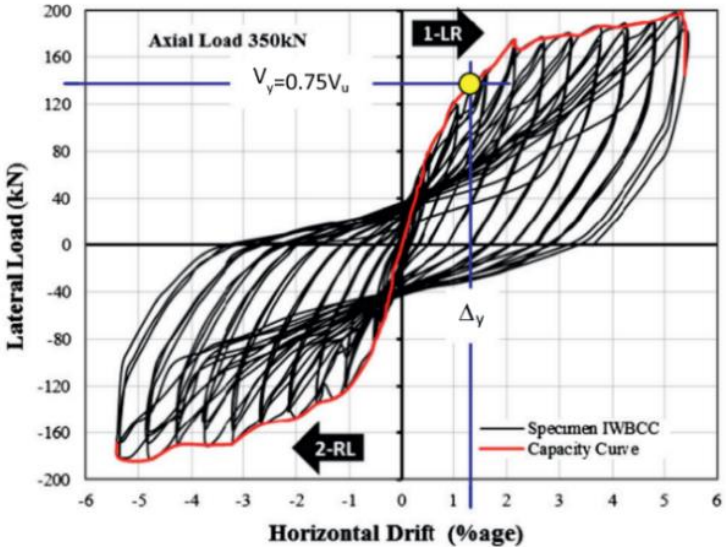

Figure 9.b.B

EWBCC: exterior wide beam column connection

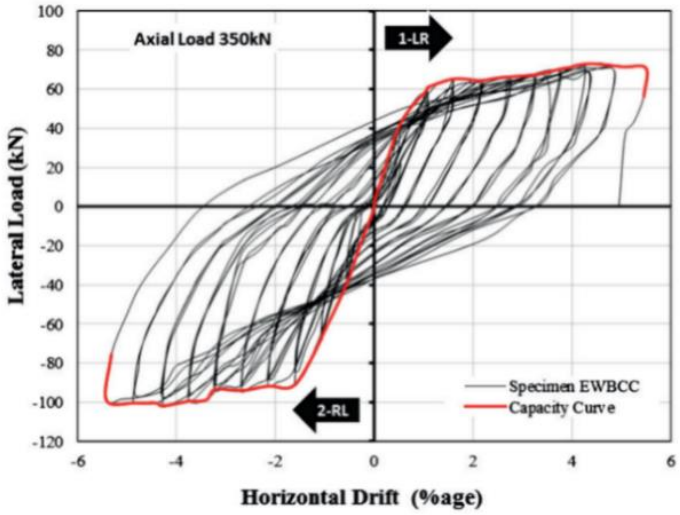

Figure 9.c.B

ICBCC: interior conventional beam column connection

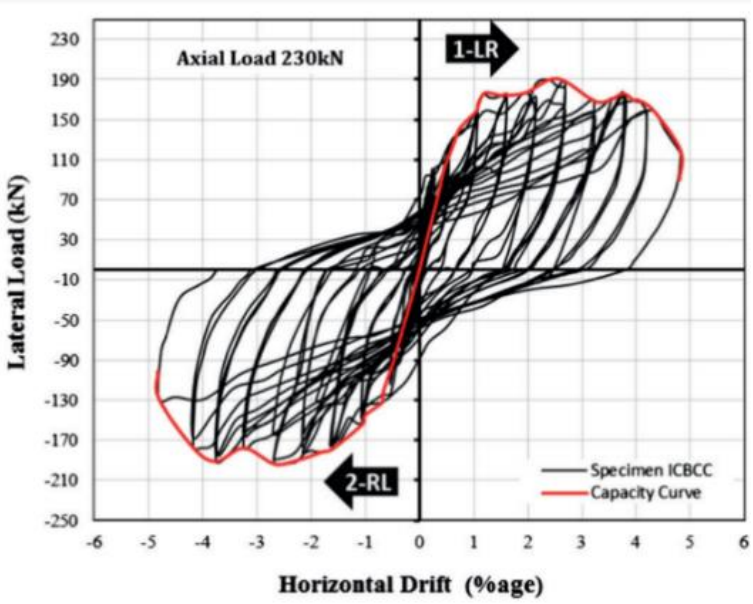

Figure 9.d.B

ECBCC: exterior conventional beam column connection

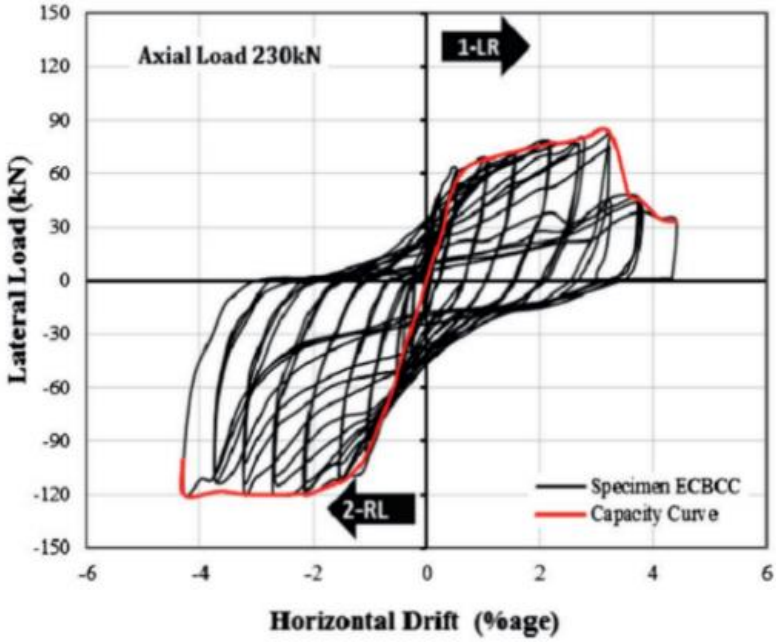

Figure 10.B

Type and patterns of the cracks

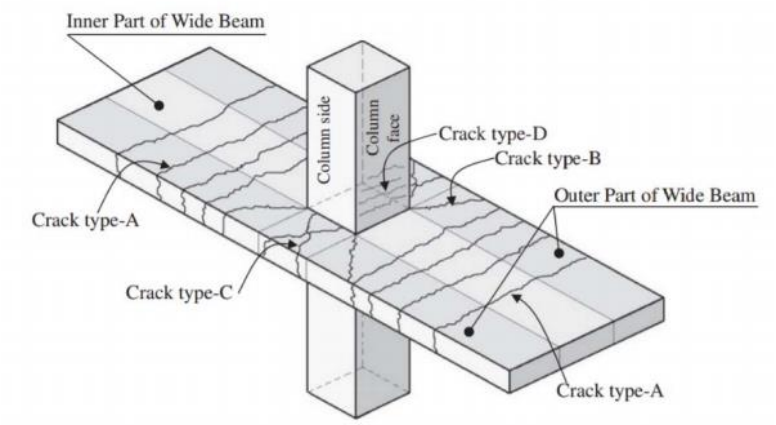

Figure 11.B

Crack patterns of test specimens

Figure 11.a.B

Specimen width ratio=1

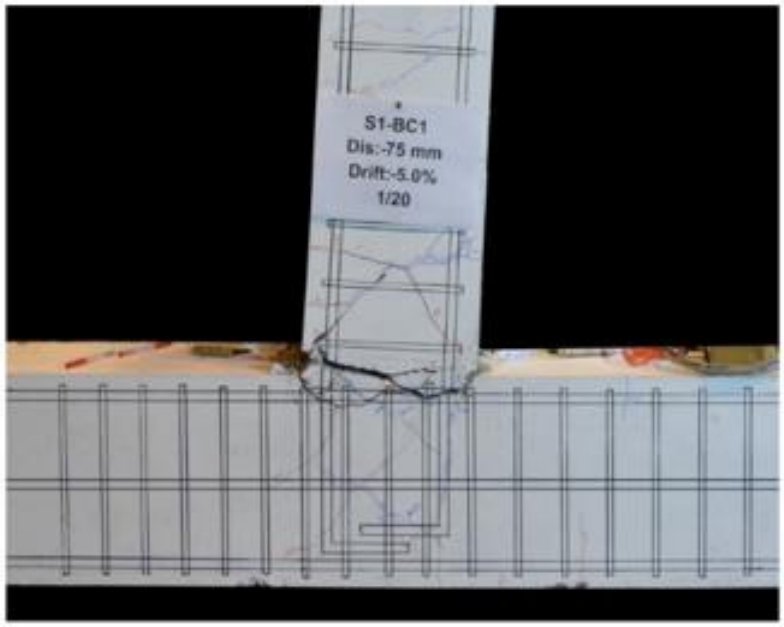

Figure 11.b.B

Specimen width ratio=1.5

Figure 11.c.B

Specimen width ratio=2

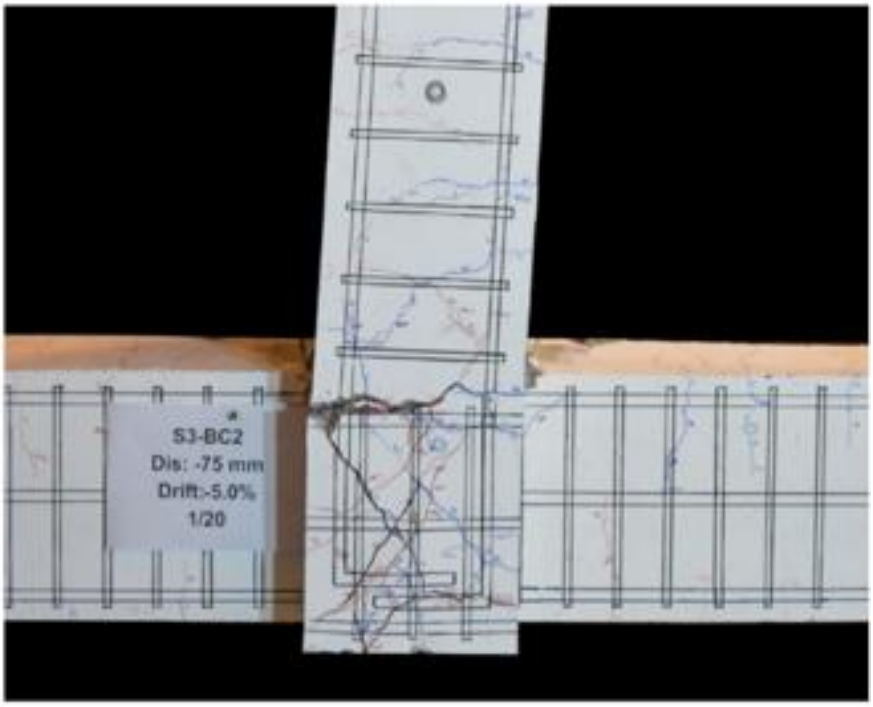

Figure 11.d.B

Specimen width ratio=2.5

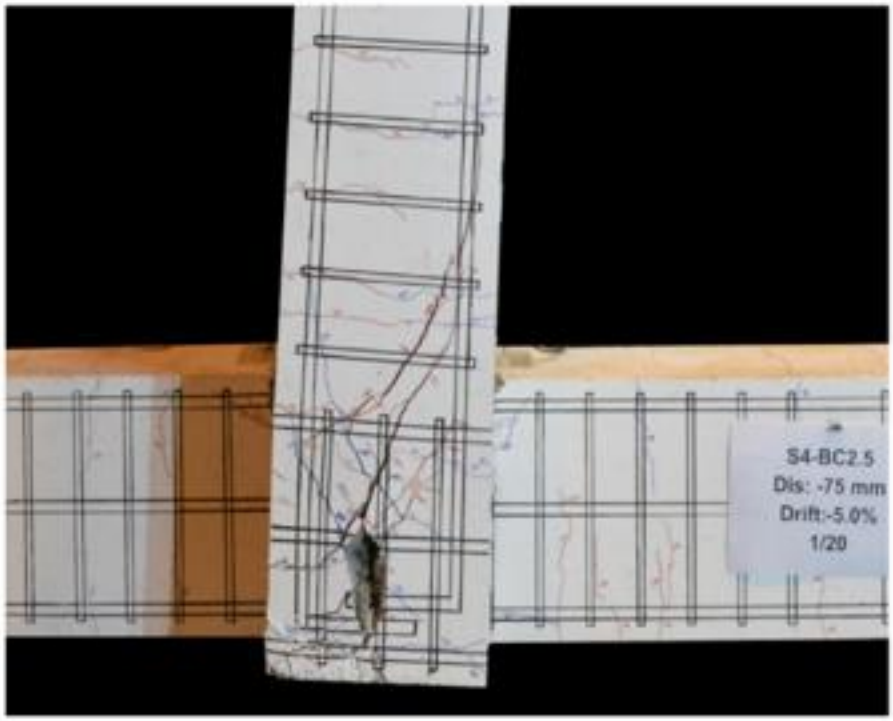

Figure 12.B

Load transfer mechanism proposed for a typical interior and exterior wide beam-column connection

Figure 12.a.B

Interior wide beam-column joint

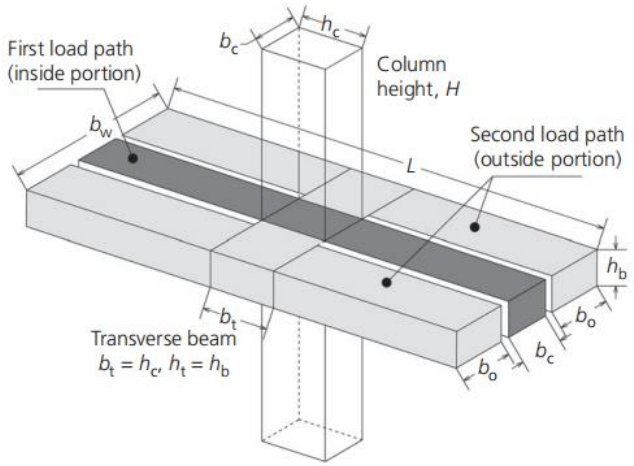

Figure 12.b.B

Exterior wide beam-column joint

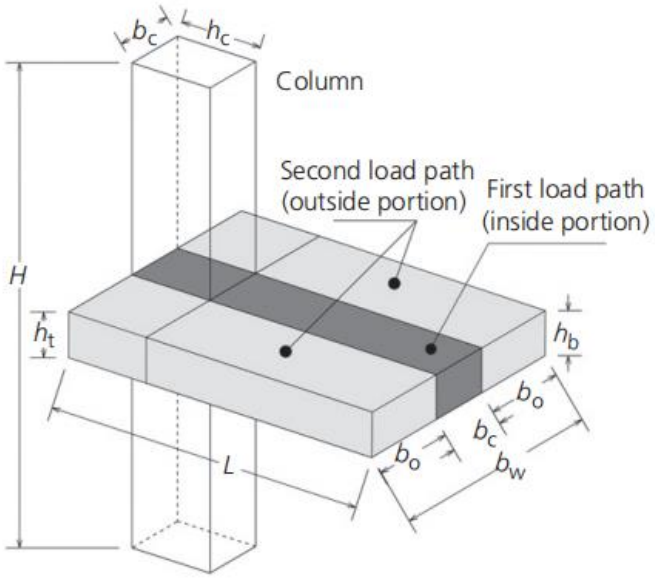

Figure 13.B

Proposed analytical model for wide beam-column joint

Figure 13.a.B

Interior wide beam-column joint

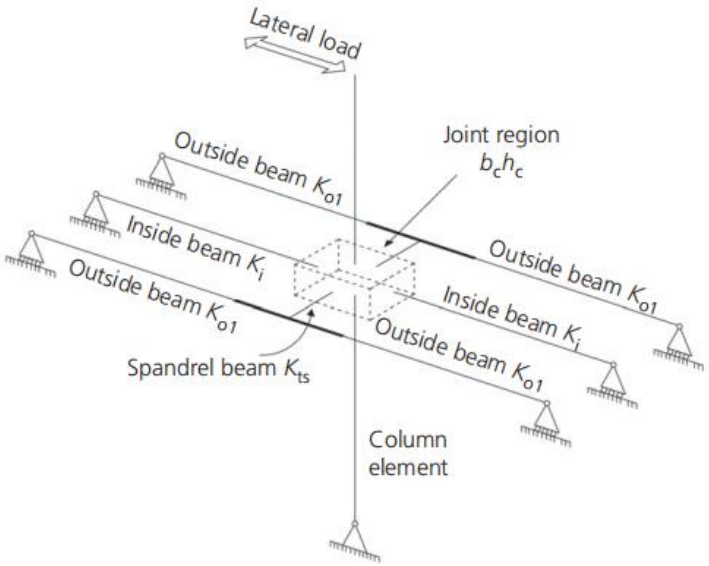

Figure 13.a.B

Exterior wide beam-column joint

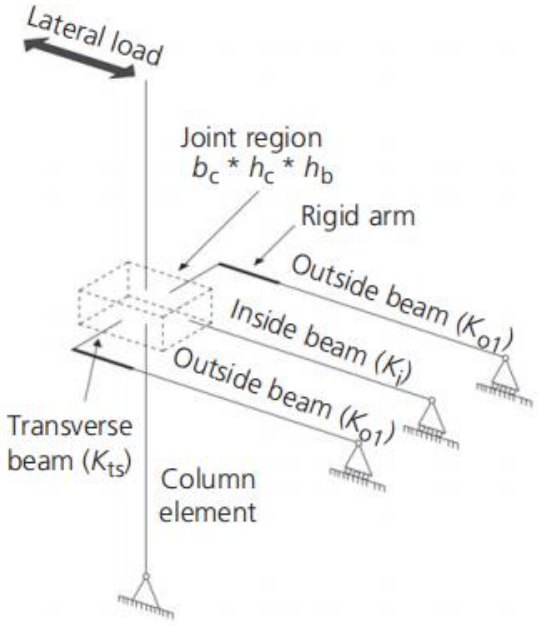

Figure 14.B

models of concrete damage plasticity

Figure 14.a.B

Yield surface in plane stress

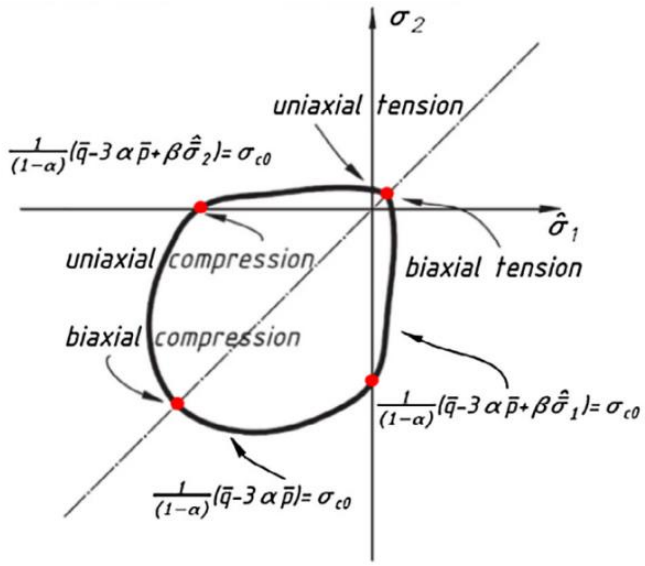

Figure 14.b.B

Yield surface in the deviatoric plane

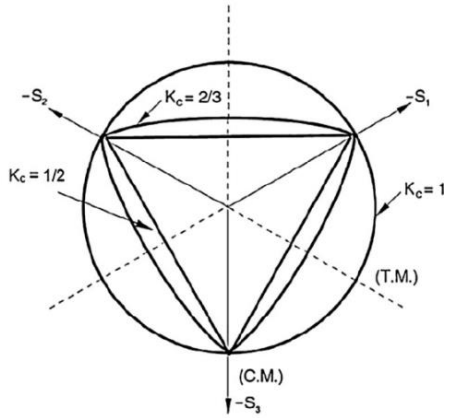

Figure 15.B

The uniaxial compressive stress-strain relationship for concrete

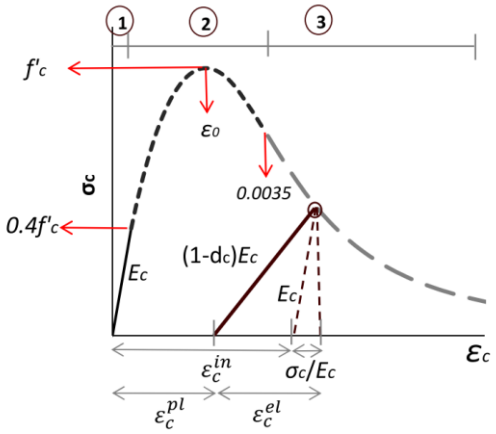

Figure 16.B

Concrete uniaxial tensile stress-crack width relationship

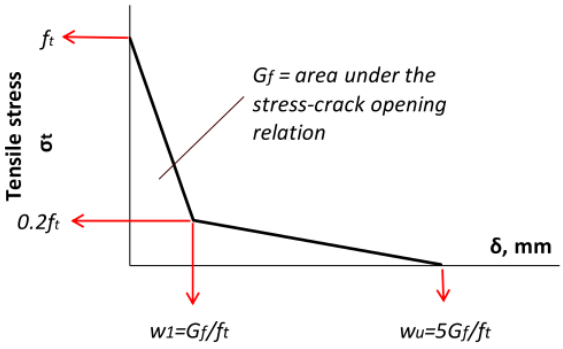

Figure 17.B

Damage parameters in compression and tension

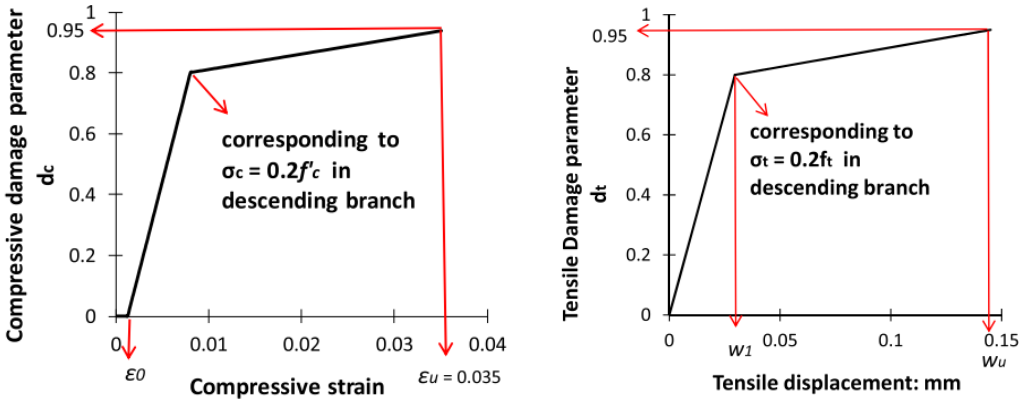

Figure 18.B

Typical stress-strain curve for reinforcement steel

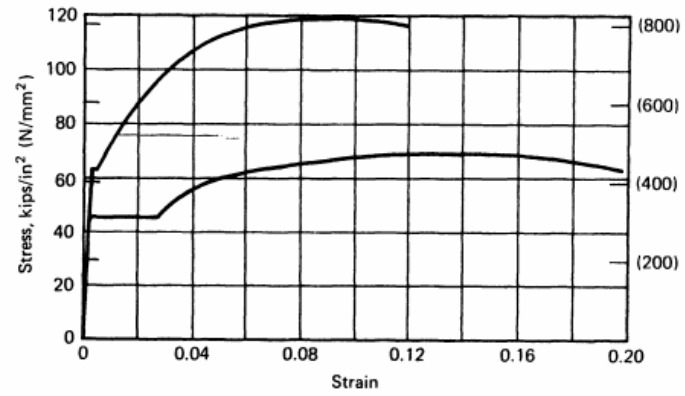

Figure 19.B

Elastic perfectly plastic

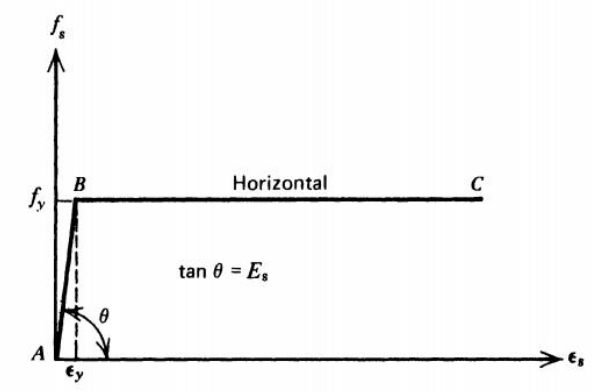

Figure 20.B

Elements used in the finite element model of wide beam-column joint with their degree of freedom

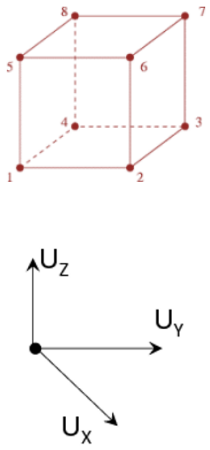	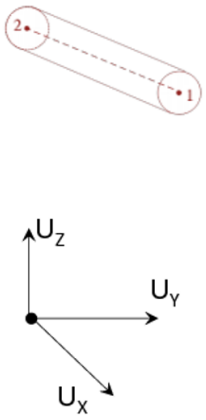	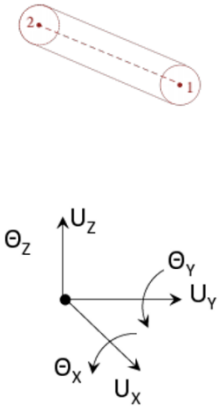
(a) 8-node solid element (C3D8R) for concrete	(b) truss element (T3D2) for reinforcing steel	(c) Beam element (B31) for reinforcing steel

Figure 21.B

Detail of specimen

Figure 21.a.B

Schematic test setup for specimen

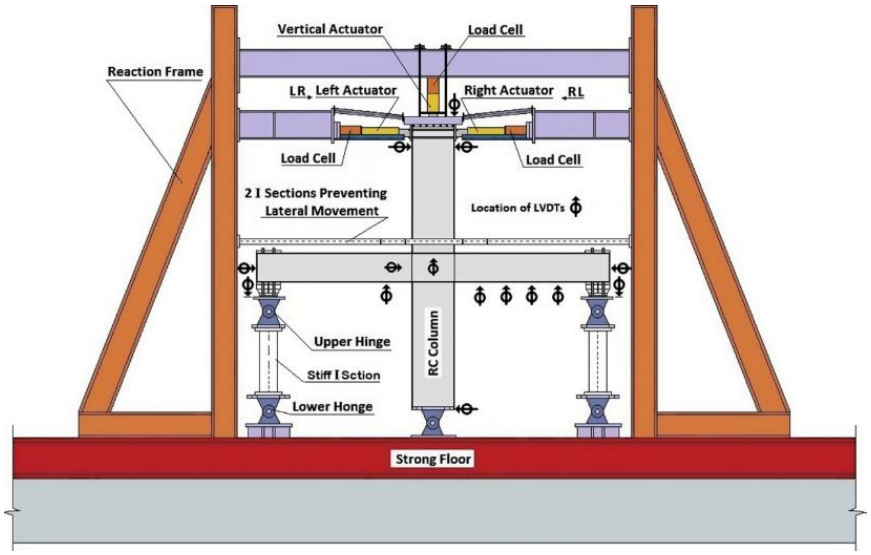

Figure 21.b.B

Dimensions and reinforcement details of specimen

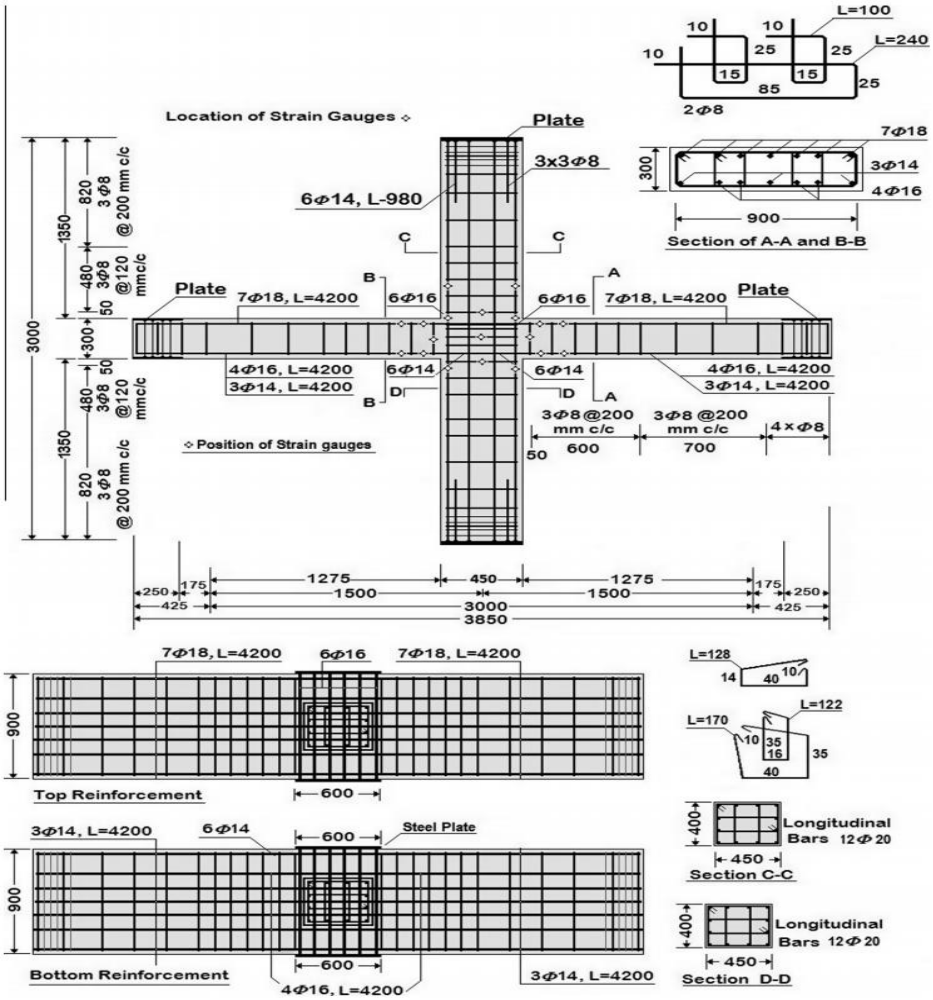

Figure 22.B

Generic model with boundary condition and load location

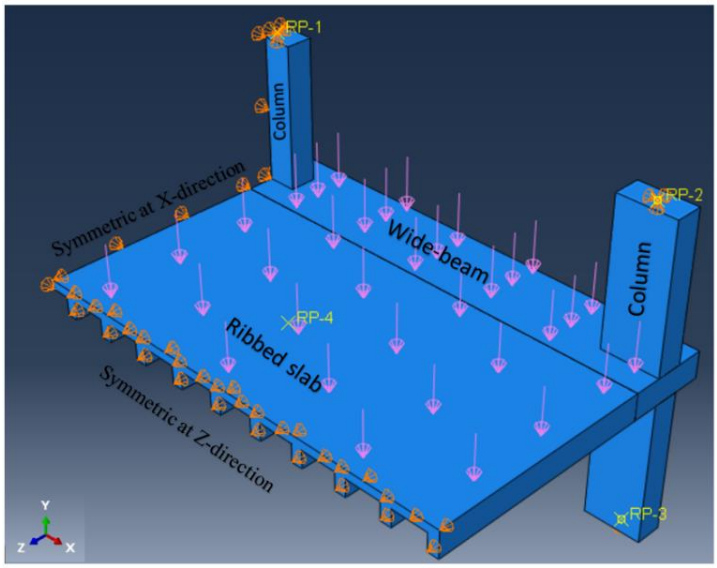

Figure 23.B

Moment-deflection curves for beam width 750 and 600mm models

Figure 23.a.B

Beam width 750mm and slab width 4m without transverse beam

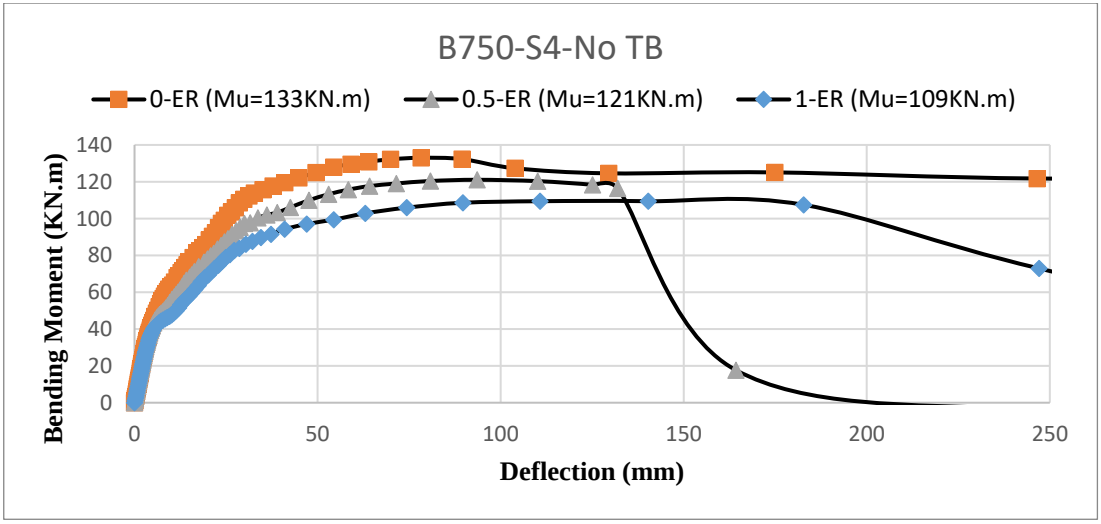

Figure 23.b.B

Beam width 750mm and slab width 5m without transverse beam

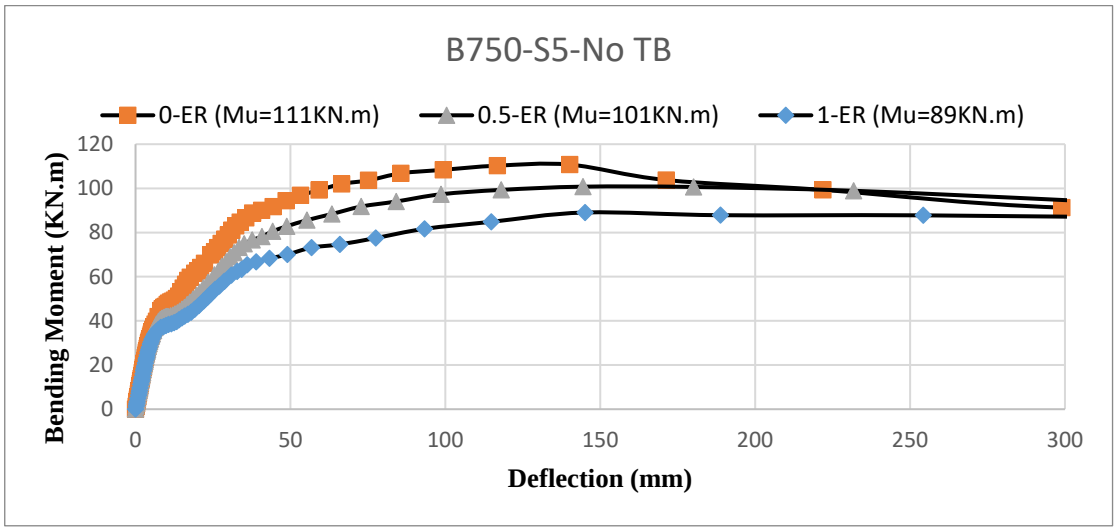

Figure 23.c.B

Beam width 750mm and slab width 6m without transverse beam

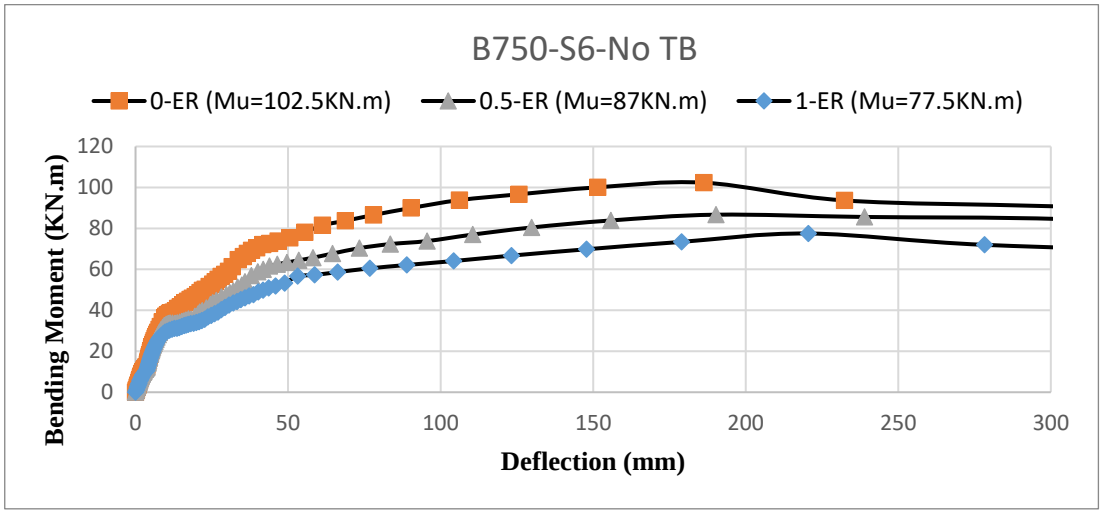

Figure 23.d.B

Beam width 750mm and slab width 4m with transverse beam

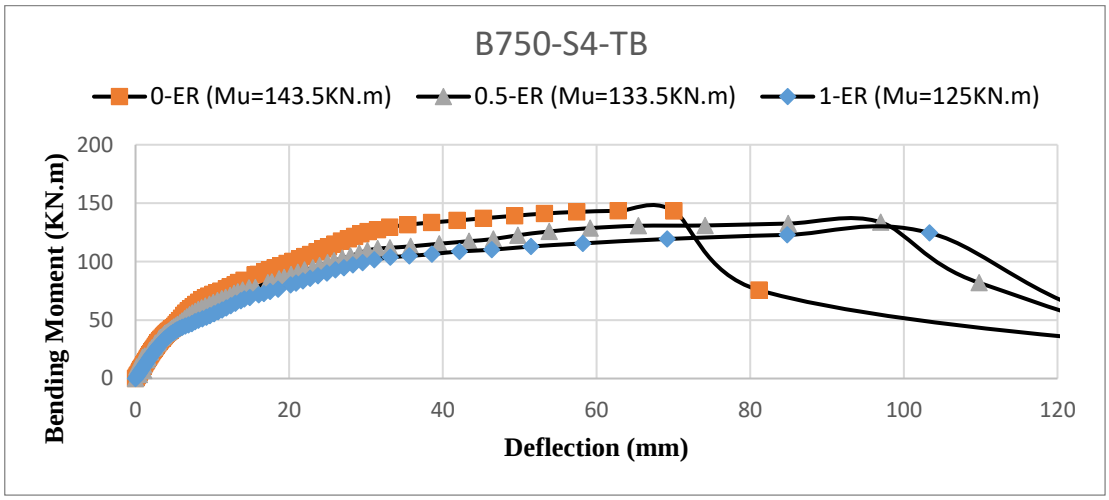

Figure 23.e.B

Beam width 750mm and slab width 5m with transverse beam

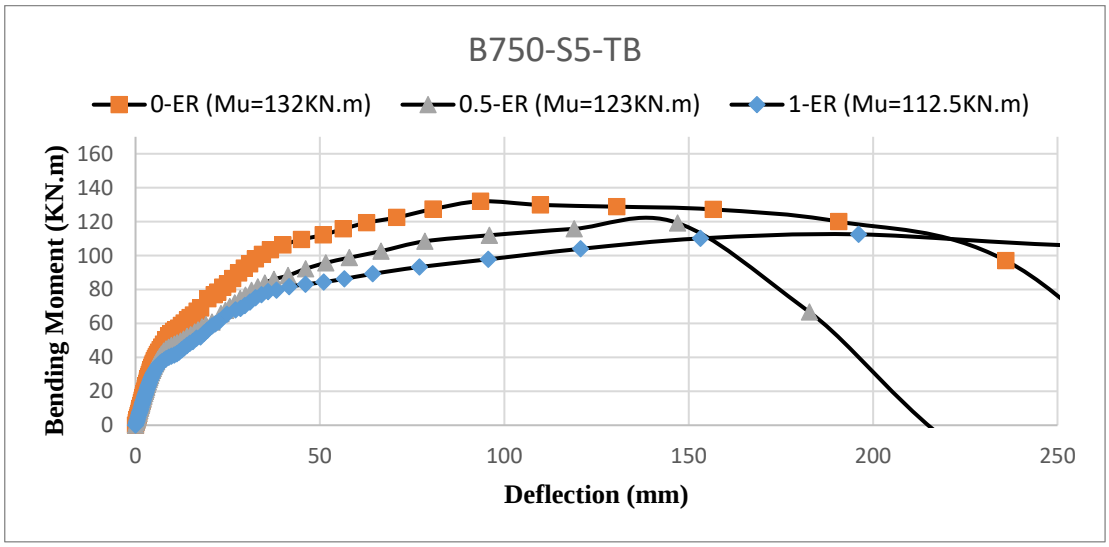

Figure 23.f.B

Beam width 750mm and slab width 6m with transverse beam

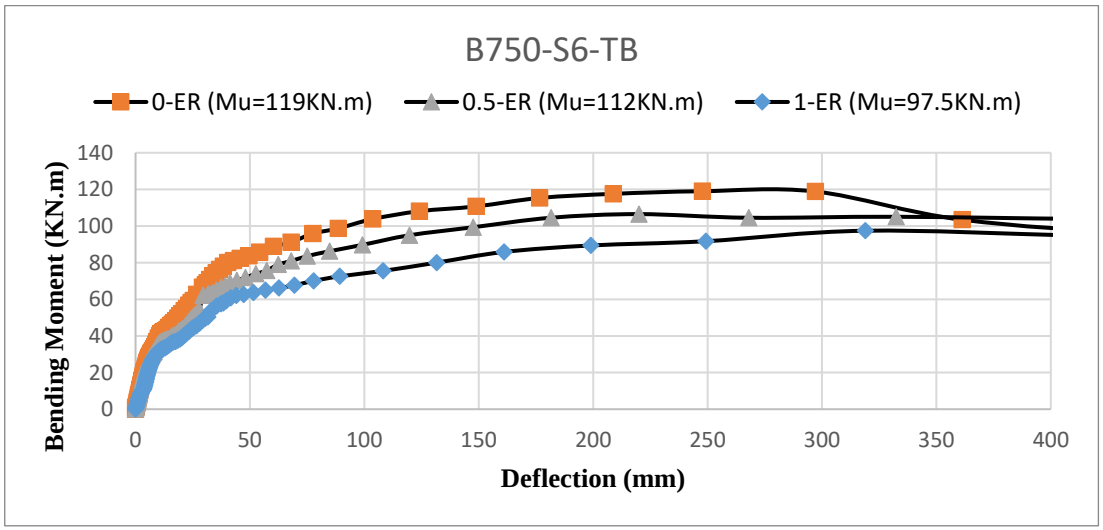

Figure 23.g.B

Beam width 600mm and slab width 4m without transverse beam

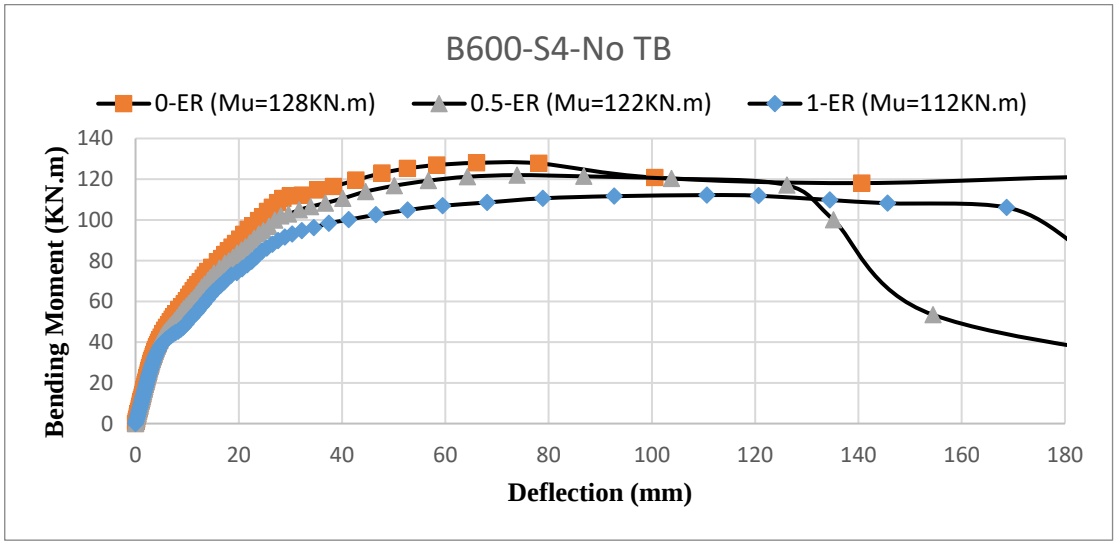

Figure 23.h.B

Beam width 600mm and slab width 5m without transverse beam

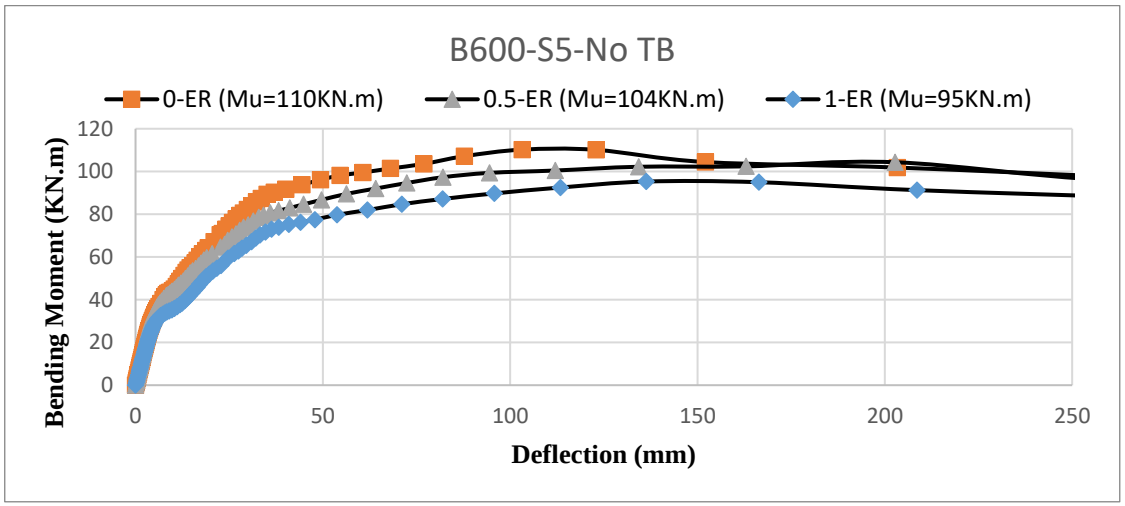

Figure 23.i.B

Beam width 600mm and slab width 6m without transverse beam

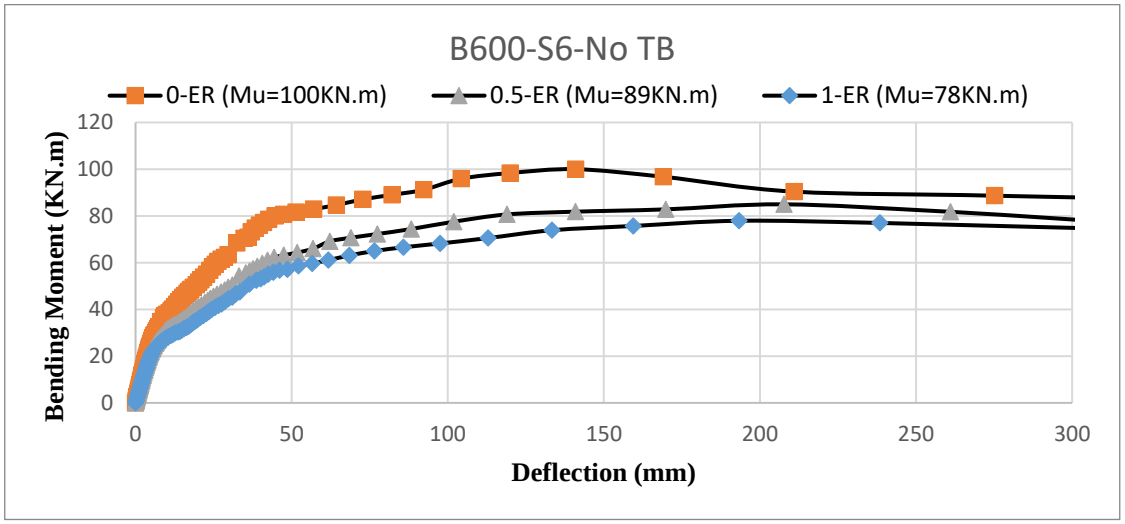

Figure 23.j.B

Beam width 600mm and slab width 4m with transverse beam

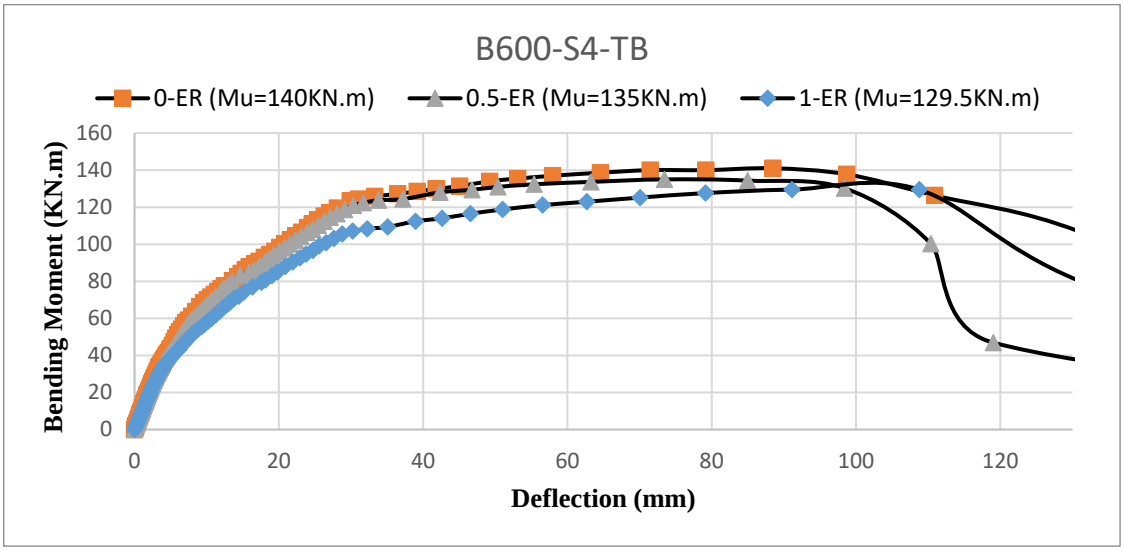

Figure 23.k.B

Beam width 600mm and slab width 5m with transverse beam

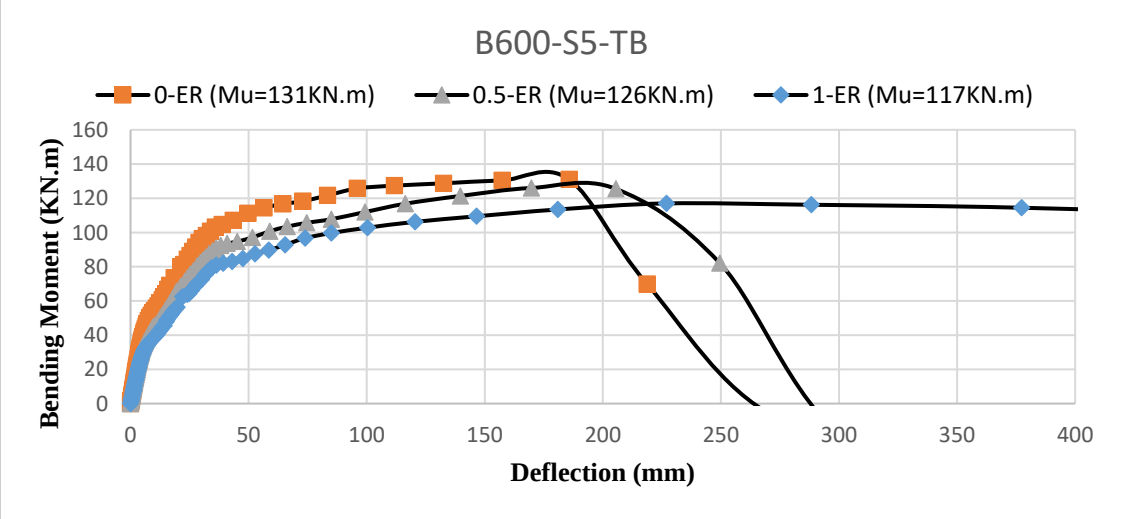

Figure 23.l.B

Beam width 600mm and slab width 6m with transverse beam

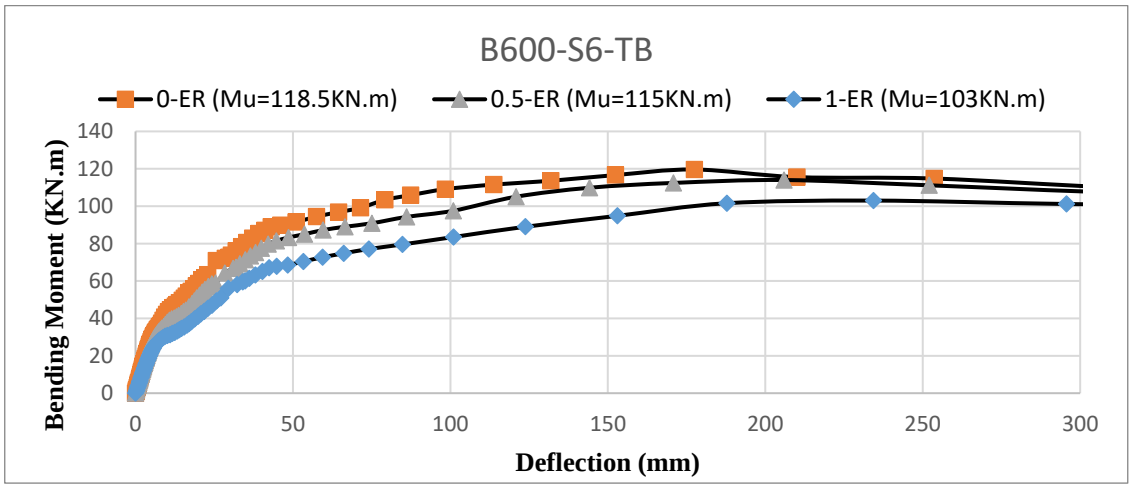

Figure 24.B

Interaction diagram for bending and torsion

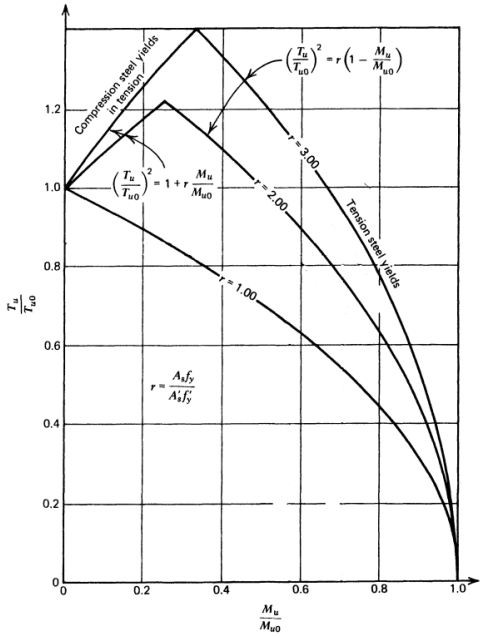

Figure 25.B

Dimenhbb sions of section

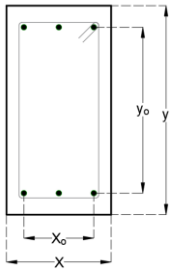

Figure 26.B

Relative Error in all cases

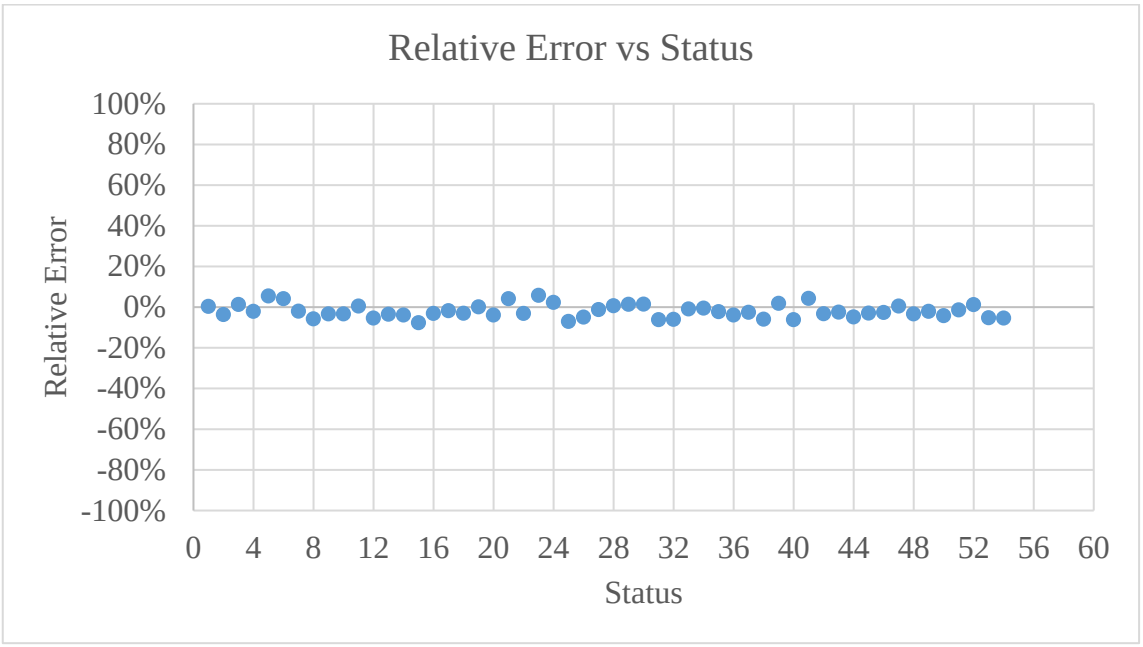

Figure 27.B

Wide beam slab details of example

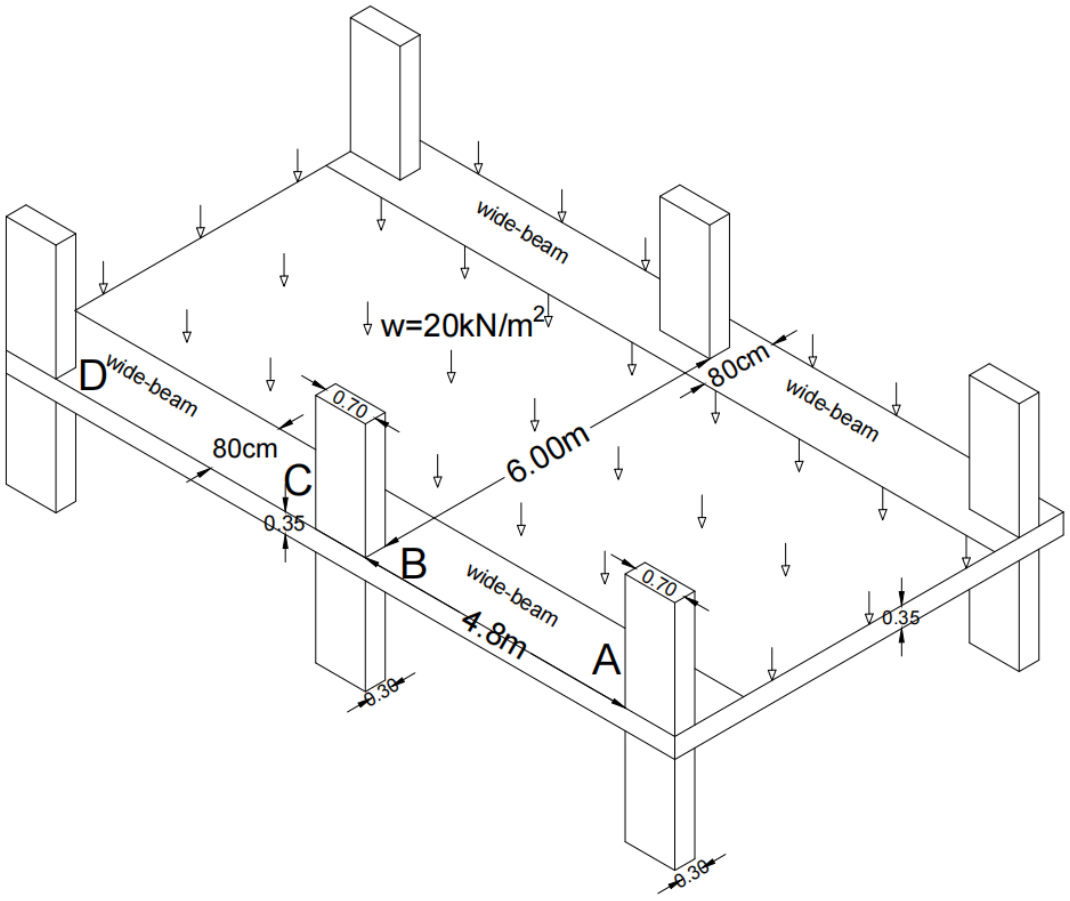

جـامعـــة النجاح الوطنية
كليـــة الدراســـات العليـــا

أثر انحراف مركز الجسر على قدرة تحمل العقد الخرسانية المسلحة ذات الجسور العريضة

إعداد
سليمان غازي عمر

إشراف
د. محمود دويكات
د. منذر دويكات

قدمت هذه الرسالة استكمالا لمتطلبات الحصول على درجة الماجستير في هندسة الإنشاءات، من كلية الدراسات العليا، في جامعة النجاح الوطنية، نابلس– فلسطين.

2022

أثر انحراف مركز الجسر على قدرة تحمل العقد الخرسانية المسلحة ذات الجسور العريضة

اعداد

سليمان غازي عمر

إشراف

د. محمود دويكات

د. منذر دويكات

الملخص

خلفية الدراسة: تعتبر العقد الخرسانية المسلحة بين الاعمدة والجسور أحد العناصر الأكثر أهمية في هياكل الخرسانة المسلحة التي لها تأثير كبير على مسار نقل الاحمال من عنصر إلى آخر. يتم استخدام نوعين من العقد الخرسانية المسلحة في المباني وفقًا لعرض الجسور: عقد تقليدية وعقد ذات الجسور العريضة.

اهداف الدراسة: يقدم نظام اطارات الاعمدة والجسور ذات الجسور العريضة والمخفية العديد من الفوائد على أنظمة الاطارات التقليدية الأخرى. فهي أوفر اقتصاديا، وسهلة البناء، وتوفر مساحة مرنة ومعيقات أقل. هذا النظام هو الأكثر استخدامًا في دول الشرق الأوسط، وبالتالي تم اختياره ليكون موضوع هذه الدراسة. يتكون النظام من بلاطة ذات اعصاب وتحميل باتجاه واحد متجانسة، مدعومة على جسور مخفية وعريضة. علاوة على ذلك، في بعض الحالات، نظرًا للاعتبارات المعمارية، تكون لعقد الاعمدة والجسور العريضة العمود انحرافًا مركزيًا حيث لا يتطابق مركز الجسر العريض مع مركز العمود.

المنهجية: لم يتم فهم السلوك الهيكلي لعقد الاعمدة والجسور العريضة اللامركزية بشكل كامل بسبب النتائج التجريبية المحدودة مقارنة بتلك الخاصة بهياكل الإطارات التقليدية. يركز هذا البحث على تأثير الانحراف المركزي للجسور على قدرة تحمل عقد الاعمدة والجسور العريضة الطرفية الخرسانية المسلحة ضمن إطارات مقاومة العزوم. يستخدم تحليل العناصر المحدودة (FE) باستخدام برنامج FE التجاري المتاح

(ABAQUS) للتحقيق في قدرة تحمل عقد الاعمدة والجسور العريضة الخرسانية المسلحة. تم التحقق من صحة النموذج باستخدام بيانات الاختبارات المنشورة والمتاحة.

النتائج: تُستخدم النتائج لمقارنة التغيير في قدرة عزم الانحناء للجسور مع أو بدون الانحراف حيث تبين ان وجود هذا الانحراف ما بين مركز الجسر ومركز العمود يؤدي الى تقليل قدرة تحمل الجسر للانحناء.

الاستنتاجات: تم تطوير طريقة تحليل للتنبؤ بعزم الالتواء على الجسور العريضة واستخدامها لإيجاد قدرة عزم الانحناء للجسر العريض. الطريقة المقترح مشتق على أساس مبادئ الميكانيكا والاتزان. تم العثور على نتائج النهج لتكون منسجمة مع نتائج طريقة العناصر المحدودة.

الكلمات المفتاحية: الانحراف، الجسر العريض، الجسر الطرفي، العقد ذات الجسور العريضة، انحراف الجسر العريض، قدرة الحمل للانحناء، الالتواء في الجسور الطرفية.